Lignin Patterning in *Cardamine hirsuta* fruit

Inaugural-Dissertation

zur

Erlangung des Doktorgrades

der Mathematisch-Naturwissenschaftlichen Fakultät

der Universität Köln

vorgelegt von

Ilsa Spatz (geb. Schneider)

aus Gelsenkirchen, Deutschland

Köln, Juli 2024

Berichterstatter:	Dr. Angela Hay
(Gutachter)	Prof. Dr. Stanislav Kopriva

Tag der mündlichen Prüfung: 20.09.2024

Contents

Abstract

Seed dispersal is important for plant fitness and adaptations for dispersal are ubiquitous in nature. *Cardamine hirsuta* uses an explosive mechanism for seed dispersal. A key innovation for this trait was the evolution of a polar pattern of secondary cell wall (SCW) deposition in endocarp*b* cells of *C. hirsuta* fruit. To gain genetic insight into this SCW patterning, I conducted a mutant screen. I recovered multiple alleles of known developmental regulators in *C. hirsuta*, indicating that I achieved good genome coverage using EMS as a chemical mutagen. I found that few mutants altered the polar pattern of SCW deposition in endocarp*b* cells. More commonly, I identified mutants with additional, ectopic lignin in endocarp*b* cells. This included several mutants with thick, lignified SCWs in ectopic positions that partially mirrored the endogenous polar pattern. I characterized the ectopic lignin and fruit morphology of two mutants in more detail: *asymmetric leaves1* (*as1*), which encodes a previously described Myb transcription factor, and the newly identified mutant *pat63*. I mapped *pat63* to chromosome 6 using a bulked segregant mapping-by-sequencing approach. I used fine-mapping to further map *pat63* to a position 1.6 cM from a marker located at 7.6 Mb on chromosome 6. I found that *NST3* gene expression was significantly upregulated in fruit valves of *as1* mutants. *NST3* encodes an important transcription factor for secondary cell wall biosynthesis. Using CRISPR/Cas9, I generated knock-out mutants of *NST3* and the paralogous gene *NST1*. I found that both genes control SCW deposition in endocarp*b* cells, since double mutants lacked SCWs. NST1 plays a more important role than NST3, since *nst1* mutants mostly lacked SCW in endocarp*b* cells. *NST3* is expressed in both lignified endocarp*b* cells and non-lignified cells of the fruit valve, and is sufficient to cause ectopic lignin when upregulated in these cells. I also found that strong upregulation of SCW biosynthesis was sufficient to alter the polar pattern of SCW deposition in endocarp*b* cells. In summary, I identified new regulators of endocarp*b* SCW patterning and found that genes known to regulate SCW biosynthesis have an important input into patterning.

Zusammenfassung

Die Ausbreitung von Samen ist wichtig für die Fitness von Pflanzen, und Anpassungen an die Ausbreitung sind in der Natur weit verbreitet. *Cardamine hirsuta* nutzt einen explosiven Mechanismus für die Samenverbreitung. Eine Schlüsselinnovation für dieses Merkmal war die Entwicklung eines polaren Musters der sekundären Zellwand (SCW) in den endocarp*b* Zellen der Frucht von *C. hirsuta*. Um einen genetischen Einblick in diese SCW Muster zu erhalten, führte ich ein Mutantenscreening durch. Ich habe mehrere Allele bekannter Entwicklungsregulatoren in *C. hirsuta* gefunden, was darauf hindeutet, dass ich mit EMS als chemischem Mutagen eine gute Genomabdeckung erreicht habe. Ich stellte fest, dass in nur wenige Mutanten das polare Muster der SCW in den endocarp*b* Zellen verändert war. Häufiger fand ich Mutanten mit zusätzlichem, ektopischem Lignin in endocarp*b* Zellen. Dazu gehörten mehrere Mutanten mit dicken, lignifizierten SCWs in ektopischen Positionen, die das endogene polare Muster teilweise widerspiegelten. Ich charakterisierte das ektopische Lignin und die Fruchtmorphologie von zwei Mutanten genauer: *asymmetric leaves1* (*as1*), das für einen zuvor beschriebenen Myb-Transkriptionsfaktor kodiert, und die neu identifizierte Mutante *pat63*. Ich kartierte *pat63* auf Chromosom 6 mit einem Bulked Segregant Mapping-by-Sequencing-Ansatz. Mit Hilfe der Feinkartierung konnte ich *pat63* an einer Position 1,6 cM von einem Marker auf Chromosom 6 (7,6 Mb) abbilden. Ich stellte fest, dass die Expression des Gens *NST3* in den Fruchtklappen der *as1* Mutanten deutlich erhöht war. *NST3* kodiert für einen wichtigen Transkriptionsfaktor für die sekundäre Zellwandbiosynthese. Mit CRISPR/Cas9 erzeugte ich Knock-out-Mutanten von *NST3* und dem paralogen Gen *NST1*. Ich fand heraus, dass beide Gene die Ablagerung von SCW in endocarp*b* Zellen kontrollieren, da dort den Doppelmutanten SCWs fehlten. NST1 spielt eine wichtigere Rolle als NST3, da den *NST1* Mutanten in den endocarp*b* Zellen meist SCW fehlte. *NST3* wird sowohl in lignifizierten endocarp*b* Zellen als auch in nicht-lignifizierten Zellen der Fruchtklappe exprimiert und reicht aus, um ektopisches Lignin zu verursachen, wenn es in diesen Zellen hochreguliert wird. Ich fand auch heraus, dass eine starke Hochregulierung der SCW-Biosynthese ausreicht, um das polare Muster der SCW in endocarp*b* Zellen zu verändern. Zusammenfassend habe ich neue Regulatoren der SCW-Musterung in endo-

carp*b* Zellen identifiziert und festgestellt, dass Gene, von denen bekannt ist, dass sie die SCW-Biosynthese regulieren, in die Musterung einfließen.

1 General Introduction

1.1 Seed dispersal

Dispersal describes the movement of an individual away from its parent (Nathan, 2006). Seed dispersal is an important phase in a sessile plant's life cycle, and provides critical opportunities to move, in order to reduce competition among seedlings, colonize new habitats or expand a species range (Levin et al., 2003). There are costs and benefits to seed dispersal. It increases plant fitness by influencing reproductive success, but costs the plants to develop specialized morphologies for dispersal and many dispersal strategies have a high rate of seed mortality (Levin et al., 2003; Hamilton and May, 1977). The benefits to dispersal clearly outweigh costs in unstable habitats, but theoretical studies demonstrated that even in stable habitats dispersal is always advantageous (Hamilton and May, 1977).

Seeds can be dispersed either actively or passively, but the most common seed dispersal methods are passive. Plants mostly use external agents for dispersal including wind (anemochory), water (hydrochory), gravity (barochory), or animals (zoochory). More rarely, plants disperse their seeds actively, without any help from an external vector (autochory) (Nathan, 2006; Levin et al., 2003; Pijl, 1982). Methods for active seed dispersal usually rely on mechanical adaptations to generate forces for explosive seed dispersal. Due to the importance and advantages of seed dispersal, it is expected to undergo strong selection pressure (Levin et al., 2003). For these reasons, it is not surprising to find ingenious adaptions for seed dispersal everywhere we look in nature.

1.2 Fruit development

Fruits are an innovation of flowering plants (Angiosperms). The fertilized ovary of a flower develops into a specialized organ called a fruit, which encloses the seed (Ferrándiz et al., 1999). Fruits protect the developing seeds and then aid in dispersing them (Ballester and Ferrándiz, 2017). The huge diversity of fruit morphologies found among flowering plant lineages highlight

the importance of seed dispersal for plant fitness.

The fruit wall of both dry and fleshy fruit is called the pericarp and is comprised of three tissues: the endocarp (inner), mesocarp (middle) and exocarp (outer). The endocarp, which differentiates from the inner ovary layer, can be fleshy, fibrous, or hardened. Fruits with a hard endocarp, stiffened by lignin, are called drupes (Dardick and Callahan, 2014).

The fruit of both the model species *Arabidopsis thaliana* and its relative *Cardamine hirsuta*, are drupes. Like most species in the Brassicaceae family, these plants have pod-like fruit called siliques. The fruit in *A. thaliana* and *C. hirsuta* develop from a gynoecium consisting of two fused carpels. The gynoecium is comprised of a stigma, style, ovary and a base called the gynaphore. The stigma receives pollen, which is transmitted through the style to the ovary, where it penetrates the ovule, resulting in double fertilization: of sperm and egg, to form the embryo, and sperm and central cells, to form the endosperm. After fertilization the gynecium becomes a fruit and seed development and fruit growth begins. At this stage, the parts of the fruit are already formed; the replum, septum, two valves and valve margins, that will differentiate into the dehiscence zone (Figure 1D) (Ferrándiz et al., 1999; Ferrandiz, 2011; Roeder and Yanofsky, 2006).

The fruit valves, or pericarp, comprise the three tissues described earlier: exocarp, mesocarp and endocarp. In *A. thaliana* and *C. hirsuta*, the exocarp is a single cell layer, while the endocarp consists of two layers: an epidermal layer called the endocarp*a*, and a lignified, subepidermal layer called the endocarp*b*. The mesocarp consists of only one cell type in *A. thaliana*, while in *C. hirsuta* the mesocarp has an additional cell type adjacent to the endocarp with smaller, more elongated cells (Figure 1E) (Ferrándiz et al., 1999; Hofhuis et al., 2016).

Fruit development in both *A. thaliana* and *C. hirsuta* starts at stage 14, after fertilization. The fruit starts to elongate rapidly through stage 16, when the sepals and petals abscise from the fruit. The fruit continues to grow until stage 17, which is subdivided into stage 17a, when the fruit reaches its maximum length, and stage 17b, when the fruit reaches its maximum width. In this stage, the cells in the valve margin differentiate into the dehiscence zone, containing two cell layers: a lignified layer and a separation layer containing cells that secrete cell wall

degrading enzymes. The cells of the replum and endocarp*b* layer also lignify during stage 17b. *C. hirsuta* fruit are competent to explode from stage 17b onwards. All three processes: fruit dehiscence, seed abscission and explosive valve coiling, occur simultaneously, resulting in explosive seed dispersal. In contrast to this, *A. thaliana* fruit begin to dry and turn yellow during stages 18 to 20. Fruit dehiscence occurs at stage 19 and by stage 20, the dry fruit tissues can be shattered by any mechanical stimuli, called pod shatter, causing the seeds to fall and disperse (Neumann and Hay, 2019; Roeder and Yanofsky, 2006).
Therefore, the morphology and development of *C. hirsuta* and *A. thaliana* fruit is very similar, but seed dispersal differs dramatically between these two species.

1.3 Explosive seed dispersal in *C. hirsuta*

C. hirsuta uses an explosive mechanism to disperse its seeds. At maturity, the valves detach from the replum along the dehiscence zone and rapidly coil. During this process the seeds are detached and launched by the coiling valves at speeds of more than 10 ms^{-1} (Hofhuis et al., 2016). In this way, the seeds are dispersed over a radius of approximately 2 m around the plant (Figure 1A-C). To power the rapid coiling of the fruit valves, potential elastic energy is stored and rapidly released as kinetic coiling energy, and previous work has described the mechanics of this process (Hofhuis et al., 2016).

By comparing the explosive fruit of *C. hirsuta* with the non-explosive fruit of *A. thaliana*, two key differences were identified. First, the endocarp*b* layer of *C. hirsuta* contains more lignin, which is deposited asymmetrically in the cells (Figure 1E), while it is deposited uniformly in *A. thaliana* endocarp*b* cells. Lignin is a phenylpropanoid polymer deposited in secondary cell walls (SCWs) that confers stiffness and hydrophobicity. Second, the exocarp layer of the valve is under tension (Hofhuis et al., 2016). This was inferred from a simple mechanical experiment where a shallow cut across the exocarp of a *C. hirsuta* fruit valve gaped open, whereas a similar cut across an *A. thaliana* fruit valve remained closed (Hofhuis et al., 2016). From these and other results, we know that exocarp cell contraction puts this cell layer under tension (Hofhuis et al., 2016; Mosca et al., 2024). A combination of live cell imaging and

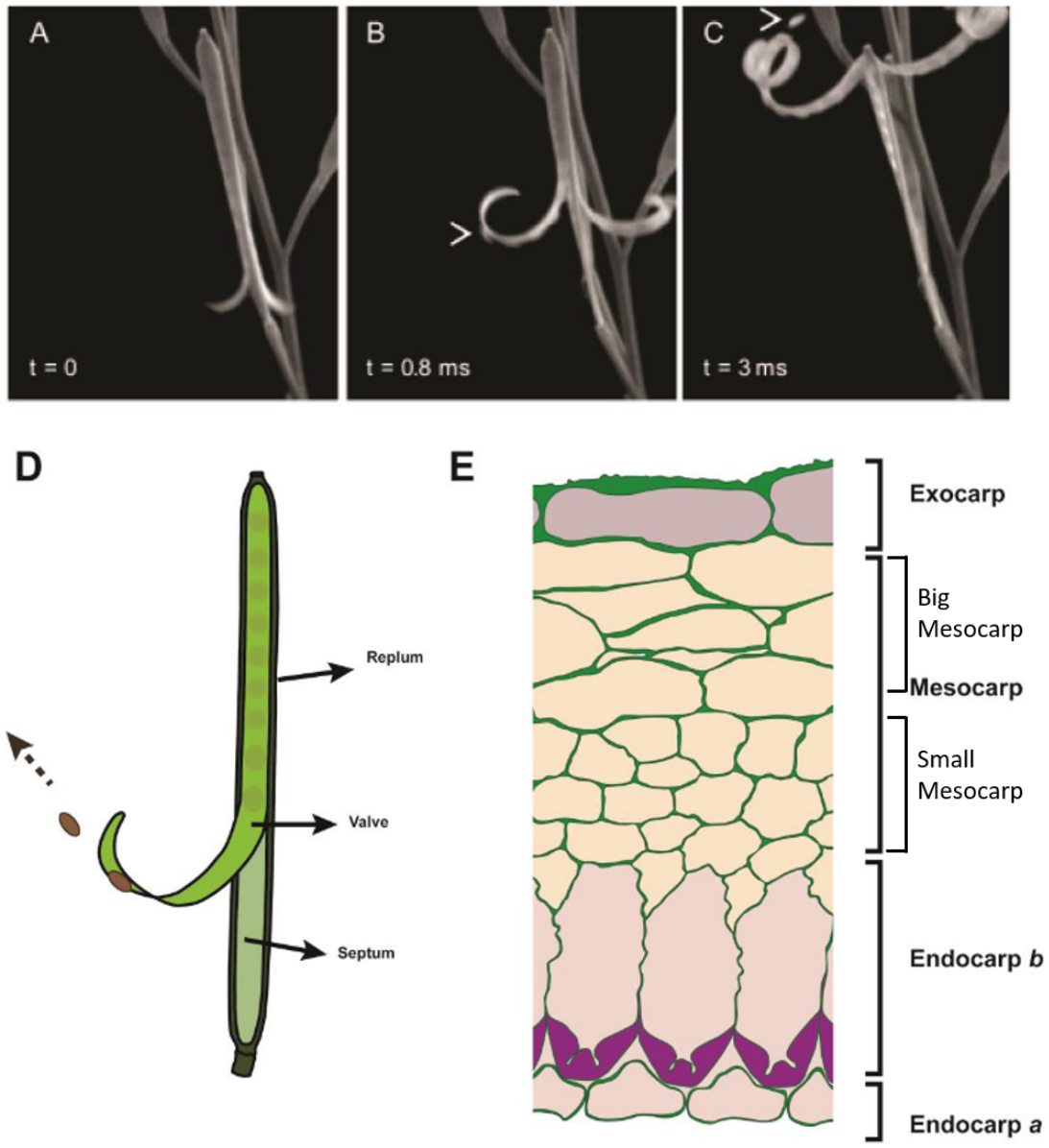

Figure 1. *C. hirsuta* uses an explosive seed dispersal mechanism.
A-C Explosive seed dispersal imaged at 15,000 images per second. The two valves detach from the fruit (A) and coil upwards with the seed at the valves (B). The seed are launched from the valves (C). t: time between frames. Arrows indicate seeds. Images from (Hofhuis et al., 2016). D: Schematic *C. hirsuta* fruit during explosive pod shatter. Image from (Pérez Antón, 2020). E: Schematic cartoon of *C. hirsuta* fruit valve tissue in cross-section. The mesocarp can be subdivided into the big mesocarp, adjacent to the exocarp, and the small mesocarp, adjacent to the endocarp*b* cells. Image from (Pérez Antón, 2020), adapted.

computational modeling were used to describe how microtubule-directed growth patterns and cell wall anisotropy caused exocarp cells to contract and generate pulling force (Mosca et al.,

2024). Therefore, differential contraction of these two valve tissues – the exocarp and the stiff, lignified endocarp*b* – causes the *C. hirsuta* fruit valve to coil.

The geometry of the polar, lignified SCW in *C. hirsuta* endocarp*b* cells is also critical for the explosive nature of valve coiling. Previous work had shown that the endocarp*b* layer, and specifically its SCW geometry, were required for explosive valve coiling. Firstly, a mutant was identified in a screen for less lignified fruit valves that lacked the endocarp*b* cell layer. It was a loss of function allele of the *C. hirsuta* ortholog of the DNA-binding protein BRASSINOSTEROID-INSENSITIVE4 (Hofhuis et al., 2016). The fruit in this mutant were non-explosive, showing that the endocarp*b* layer is required for explosive dispersal.
Secondly, mathematical modeling was used to explicitly describe how the geometry of the lignified endocarp*b* SCW was necessary to rapidly release stored elastic energy in the fruit valve (Hofhuis et al., 2016). This process is analogous to how a toy slap bracelet works: elastic energy is trapped while the whole valve geometry is curved in cross-section. To coil lengthways, the valve must first flatten in cross-section (Figure 2). This flattening is achieved at no energy cost by the endocarp*b* layer widening. The endocarp*b* SCW geometry is key here: the polar deposition of the SCW forms a U-shape with thin hinges at the base that can open. When tension in the valve exceeds a critical level, these hinges are suddenly forced open, causing the endocarp*b* layer to widen, thereby flattening the valve in cross-section, causing sudden coiling of the valve (Figure 2) (Hofhuis et al., 2016). Therefore, the SCW geometry imposes an energy barrier, such that elastic potential energy generated by exocarp cell contraction can be stored. The opening of the hinges overcomes the barrier, and the stored energy is rapidly transformed into kinetic coiling energy. This model predicted that valve coiling would be non-explosive if the endocarp*b* SCW geometry was uniform, rather than polar, in *C. hirsuta* fruit. To test this prediction, Hofhuis *et al.* used a transgenic approach to produce uniformly lignified SCWs and found that the fruit were non-explosive, demonstrating that the geometry of the SCW in endocarp*b* cells is required for explosive release of the stored energy (Hofhuis et al., 2016).

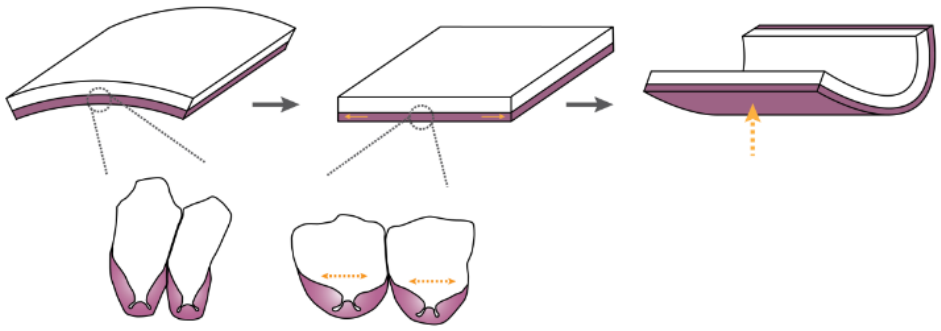

Figure 2. Hinged geometry of SCWs of endocarp*b* cells allows passive flattening of the valves. Schematic depiction of fruit valves and endocarp*b* cells. Left: The valve is curved outwards in cross-section and the U-shape is 'closed'. Middle: Fruit valve with flat cross-section when detached from fruit. U-shape is 'open'. Right: Fruit valves coil. Image from (Pérez Antón, 2020).

Thirdly, phylogenetic comparisons with other species in the Brassicaceae family, showed that the polar SCW geometry of endocarp*b* cells was strictly associated with the trait of explosive seed dispersal (Hofhuis et al., 2016). Species in the *Cardamine* genus had explosive seed dispersal and all of the *Cardamine* species analyzed had a polar endocarp*b* SCW geometry. All other species analyzed had uniformly lignified endocarp*b* SCWs and non-explosive seed dispersal (Hofhuis et al., 2016). Therefore, together with genetics and modeling, these results indicate that the polar SCW geometry of endocarp*b* cells was an important innovation underpinning the evolution of explosive seed dispersal in *Cardamine* (Hofhuis and Hay, 2017).

1.4 Plant cell walls

Cell walls are a feature of all plants and play an important role in cell growth and differentiation (Cosgrove, 2005).

While all plant cells have a primary cell wall, only specialized cell types deposit a secondary cell wall (SCW). Primary cell walls are thin, flexible, highly hydrated layers consisting of cellulose microfibrils, pectin, and hemicellulose, most common xyloglucan, and glycosylated proteins. Cellulose is synthesized at the plasma membrane by cellulose synthase complex, which consists of three isoforms of cellulose synthases (CESA). CESA proteins are transported to the plasma membrane via the secretary pathway. Hemicellulose and pectin are synthesized in

the Golgi apparatus and once secreted into the wall are integrated into it and modified. During expansive cell growth, expansins are important for primary cell walls to yield to turgor pressure. Expansins are non-enzymatic and disrupt the non-covalent linkages between cellulose and hemicellulose residues (Cosgrove, 2005; Endler and Persson, 2011).

Once the phase of expansive cell growth is completed, some specialized cell types deposit a SCW between the primary cell wall and the plasma membrane. In contrast to primary cell walls, SCWs are thick, hydrophobic, non-extensible and resist compression (Cosgrove, 2018). SCWs contain cellulose, but the synthase complexes comprise SCW CESAs, and the most common hemicellulose is xylan rather than xyloglucan, and SCWs contain lignin, but not pectin.

Lignin consists of three different units: H(hydroxyphenyl), G(guaicyl), and S(syringyl) lignin (Barros et al., 2015). The monolignols are synthesized in the cytoplasm via the phenylpropanoid pathway from p-Coumaric acid (Barros et al., 2015), and diffuse through the plasma membrane into the wall down a polymerization-induced concentration gradient (Perkins et al., 2022). In the wall the monolignols are activated by oxidation by phenoloxidases and added end-wise to the lignin polymer (Barros et al., 2015). Phenoloxidases can be laccases or peroxidases. Laccases are the largest subgroup of multicopper oxidases, and have a range of substrates (Reiss et al., 2013). Peroxidases are heme-containing proteins that belong to a large multigenic family. Depending on the cell type different laccases or peroxidases are involved in lignification (Barros et al., 2015).

Secondary cell wall biosynthesis is regulated by a transcription factor pathway that can be divided into three transcription factor tiers. The four master regulators (tier3) are the NAC transcription factors NAC SECONDARY WALL THICKENING PROMOTING FACTOR1 (NST1), NST3, and VASCULAR-RELATED NAC-DOMAIN6 (VND6), VND7. They directly regulate MYB transcription factors (tier2), among them MYB46. Tier2 transcription factors regulate other MYB transcription factors (tier1) that regulate the biosynthesis genes of cellulose, lignin, and hemicellulose. Biosynthesis genes are also regulated by transcription factor of tier3 and tier2 (Kumar et al., 2015).

Specialized cell types that have a SCW that is required for their function, include xylem, the Casparian strip, and endocarp*b* cells of the fruit (Figure 3) (Emonet and Hay, 2022). The lignin in xylem cells imparts rigidity and hydrophobicity, which is important for water transport. Fibers mainly provide mechanical support, and their SCW is uniformly deposited (Figure 3A). Fiber SCW biosynthesis master regulators in Arabidopsis are NST1 and NST3. Vessels and tracheids are involved in water transport, hydrophobicity is provided by the ligninin SCW. The SCW pattern variers. In the primary xylem, derived from the procambium, the SCW has an annular pattern. In the metaxylem, derived from the cambium, the SCW is pitted. The master SCW regulator of the protoxylem is VND7 and of the metaxylem is VND6 in Arabidopsis. In between the SCW pattern can be spiraled, or reticulated-scalariform (Figure 3B) (Emonet and Hay, 2022; Kumar et al., 2015).

Another specialized cell type is the root endodermis with the Casparian strip, a lignified primary cell wall, that provides an apoplastic barrier by forming a band surrounding the endodermal cell (Figure 3C) (Naseer et al., 2012; Emonet and Hay, 2022). Peroxidases are required to lignify the Casparian strip (Rojas-Murcia et al., 2020).

A lignified endocarp cell layer in the fruit valve protects the seeds and aids seed dispersal. In Arabidopsis, the non-polar SCW pattern in endocarp*b* cells is regulated by NST1 and NST3 (Mitsuda and Ohme-Takagi, 2008). In *C. hirsuta* the polar SCW pattern needs three copper-requiring laccases for lignification. Triple *lac4, 11, 17* mutants formed no lignin in the endocarp*b* SCW, showing that LAC4, LAC11, and LAC17 are redundantly required for endocarp*b* lignification (Pérez-Antón et al., 2022). These three laccases co-localized precisely with the polar pattern of lignin in endocarp*b* SCWs. However, when these *C. hirsuta* laccase genes were transferred into *A. thaliana*, they adopted the uniform pattern of lignification found in *A. thaliana* endocarp*b* cells. This result suggested that the polar localization of these *C. hirsuta* proteins is determined in trans by polarity factors present only in *C. hirsuta* and not *A. thaliana* (Pérez-Antón et al., 2022).

In summary, lignocellulosic plant cell walls are of great importance for plant physiology and

development. But they also provide an enormous renewable resource for biofuels, textile, lumber, paper. However, this wall material, especially the lignin, is recalcitrant to degradation, creating a major bottleneck in utilizing this carbon resource. Thus, research efforts to better understand the mechanisms that regulate lignocellulosic cell walls may eventually allow more effective use of plant cell walls as a renewable resource (Sakamoto et al., 2018; Lynd, 2017).

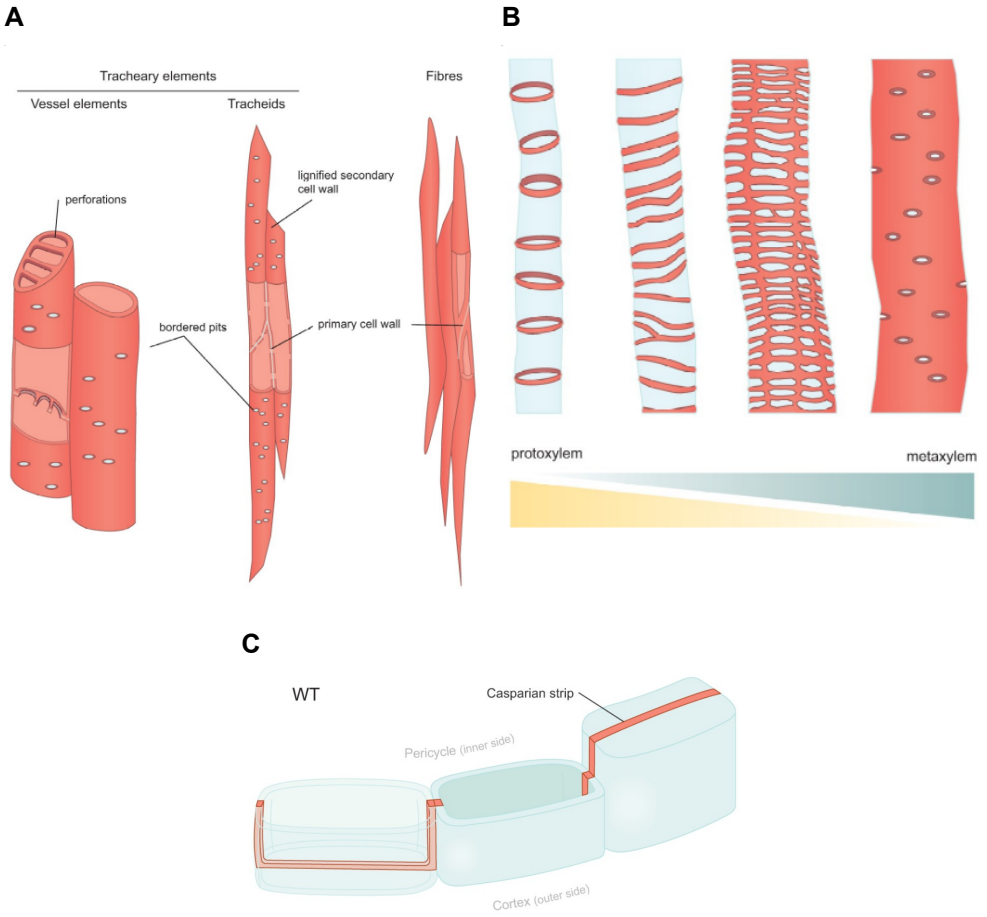

Figure 3. Schematic lignin patterns.
A: Vessel and tracheids transport water and have a bordered pits pattern (red). And fibers have a uniform pattern. B: Xylem cells can have different patterns (red). from left to right: annular, spiraled, reticulated-scalariform, pitted. The pattern changes from protoxylem to metaxylem. C: The Casparian strip has a lignified band (red) in the primary cell wall (blue).
All images from (Emonet and Hay, 2022)

1.5 Thesis aim and experimental objectives

From the perspectives of biomechanics, development and evolution, explosive seed dispersal is a striking trait. Previous work gave a comprehensive understanding of the mechanics underlying this trait and highlighted the importance of the lignified endocarp*b* SCW in this process. The aim of my thesis is to identify the genetic basis for this lignified endocarp*b* SCW pattern. In my thesis project, I used both forward and reverse genetics approaches to identify regulators of the endocarp*b* lignin pattern in *C. hirsuta*. I conducted a mutant screen, generated CRISPR/Cas9 mutants for *NST1* and *NST3* genes, and constructed transgenic lines that upregulated SCW biosynthesis in endocarp*b* cells. All of these approaches yielded genotypes that affected the polar lignin pattern in endocarp*b* cells in *C. hirsuta*. The findings of this work will contribute to a better understanding of SCW patterning and provide a basis to further investigate genetic regulation of the lignified endocarp*b* SCW in explosive fruit of *C. hirsuta* . The experimental objectives of this thesis are:

1. Conduct a forward genetic screen to find mutants with aberrant lignified SCW pattern
2. Characterize in detail two mutants identified in my screen with ectopic lignin (*as1-1* and *pat63*)
3. Characterize *NST1* and *NST3* function by generating CRISPR/Cas9 mutants
4. Generate and characterize feedforward loops of SCW upregulation in endocarp*b* cells

2 Mutant screen for altered endocarp*b* lignin

2.1 Introduction

In the Brassicaceae family, different seed dispersal mechanisms are associated with distinct lignin patterns in the endocarp*b* cells of fruit valves. In the model species *A. thaliana*, fruit release their seeds by a non-explosive mechanism and their endocarp*b* cell layer has a non-polar SCW pattern. By contrast, its close relative *C. hirsuta* disperses its seed explosively. It has polar U-shaped SCW in the endocarp*b* cells that contain more lignin compared to *A. thaliana*. Laccases, involved in lignin deposition, co-localize with the respective lignin patterns in *C. hirsuta* and *A. thaliana* (Pérez-Antón et al., 2022; Hofhuis and Hay, 2017). The mechanism for the patterning is however unknown. Previously, our lab conducted a forward genetic screen for *C. hirsuta* mutants with less lignin in fruit valves. Mutants from this screen improved our understanding of explosive seed dispersal. For example, the *less lignin 2* (*lig2*) mutant lacks the endocarp*b* layer and is non-explosive, indicating the importance of the endocarp*b* layer for this trait (Hofhuis et al., 2016). Another mutant, *less lignin 1* (*lig1*), was identified as *squamosa promoter binding protein-like 7* (*spl7*). While the SCW pattern formed properly, the lignin content was reduced, and so was the seed dispersal range. This mutant showed that laccases are required for endocarp*b* lignification (Pérez-Antón et al., 2022). The specific polar SCW pattern is also necessary for explosive dispersal: in transgenic lines where endocarp*b* cells present a non-polar SCW pattern, the fruit are non-explosive (Hofhuis et al., 2016). Despite these advances, the underlying mechanism for this specific patterning is so far unknown.

Forward and reverse genetics are tools widely used to better understand biological mechanisms. Forward genetic approaches can be used to investigate the function of genes by characterizing a specific phenotype and identifying its genetic basis. On the other hand, in reverse genetics, a target gene is first disrupted, the phenotype then characterized to infer the gene function (Ali Khan et al., 2021). While for reverse genetics the gene of interest must be known and specifically disrupted, forward genetics requires a screening population with random mu-

tations in the genome to find a phenotype of interest. Therefore, forward genetic screen relies on mutagens to generate a mutagenized screening population with a sufficient number of mutations. A commonly used mutagen is ethyl methanesulfonate (EMS). It causes nucleotide alkylation, primarily guanine alkylation, randomly across the genome (Snyman et al., 2021). This causes a mis-pairing with thymine instead of cytosine during DNA replication and repair. Consequently, most EMS mutations are G/C to A/T substitutions (Coulondre and Miller, 1977). Although possible, insertion and deletions (indels) and chromosomal breaks happen less frequently (Snyman et al., 2021). In order to observe recessive mutations, the mutagenized seed give rise to (M_1) plants, which are selfed and M_2 seed collected. The M_2 generation is then screened for a phenotype of interest. Since only 25 % of the progeny carries the recessive homozygous mutation of the original M_1 plant, a sufficient number of M_2 plants need to be screened. By searching for specific phenotypes, genes involved in biological processes related to this phenotype are identified. In this way, no assumptions are made about possible genes involved in the process (Snyman et al., 2021).

In this chapter, I applied the EMS forward genetic screen approach to identify *C.hirsuta* mutants with aberrant SCW pattern in endocarp*b* cells. Such mutants can give insights into processes regulating the SCW pattern formation. In addition to SCW pattern defect, some mutants showed well recognizable traits of known mutants in *A. thaliana* and *C. hirsuta*. I could identify alleles of: *FRUITFULL* (*FUL*), *ASYMMETRIC LEAVES 1* (*AS1*) and *BREVIPEDICELLUS* (*BP*) (also known as *KNOTTED1-LIKE in ARABIDOPSIS THALIANA 1* (*KNAT1*)). These mutants are described in detail in this chapter.

2.1.1 Fruit patterning: *FRUITFULL* and *INDEHISCENT*

FRUITFULL is a MADS-box transcription factor, necessary for fruit valve differentiation in *A. thaliana*. The fruit consists of two valves that are joined to the replum on each side. The boundary region is called the valve margin. In that region forms the dehiscence zone, which

consists of two cell types: the separation layer and the lignified layer (Ferrándiz et al., 2000). In *A. thaliana* and *C. hirsuta ful* mutants, the valve cells fail to differentiate and elongate. Instead the cells differentiate into cell types found in the valve margin dehiscence zone and form a valve-like structure between the repla. In *A. thaliana ful* mutants, the valve-like structure is formed by cells identical to lignified layer cells of the dehiscence zone. In contrast, the valve-like structure in *C. hirsuta ful-1* consists of cells typical of the separation layer (Gu et al., 1998; Galstyan et al., 2021). Constitutive expression of *FUL* in *A. thaliana* caused the conversion of the valve margin and the outer replum cells into valve cells. Due to the lack of dehiscence zone, the fruit are indehiscent (Ferrándiz et al., 2000). Therefore, FUL negatively regulates genes involved in valve margin differentiation. These genes include *SHATTERPROOF1* (*SHP1*) and *SHP2* (Ferrándiz et al., 2000).

Another important gene involved in valve margin differentiation is *INDEHISCENT* (*IND*), an atypical bHLH protein, which is also negatively regulated by FUL. IND promotes the differentiation of the separation and the lignified layers in the valve margin. In *A. thaliana ind* mutant, the lignified layer and the separation layer are both missing, while constitutive expression of *IND* phenocopies the *ful* phenotype (Liljegren et al., 2004). FUL promotes valve differentiation by negative regulation of valve margin genes (Figure 4) (Ferrándiz et al., 2000; Liljegren et al., 2004). Similarly, the homeodomain protein REPLUMLESS (RPL) (also known as PENNYWISE (PNY), BELLRINGER (BELL1)) promotes replum differentiation by negative regulation of the valve margin genes *SHP1* and *SHP2*. In *rpl* mutant, replum cells have been replaced by valve margin cells, and valve margin genes are ectopically expressed in that region (Roeder et al., 2003). RPL interacts with the homeodomain protein BP in the replum and BP promotes *RPL* expression (Alonso-Cantabrana et al., 2007).

BP and RPL also regulate together internode patterning in Arabidopsis inflorescence. Loss of *BP* or *RPL* results in an aberrant internode length and downward pointing siliques (Smith and Hake, 2003; Khan et al., 2011).

AS1, a MYB-domain transcription factor, acts in a complex with AS2 to repress *BP* expression in leaf primordia in *A. thaliana* and *C. hirsuta* (Byrne et al., 2000; Hay and Tsiantis, 2006). *C.*

hirsuta as1 mutant leaves show close initiation of leaflets along a compressed proximo-distal axis and additional leaflets (Hay and Tsiantis, 2006). Functions and interactions of BP and AS1 will be described in further detail in Chapter 3.1.

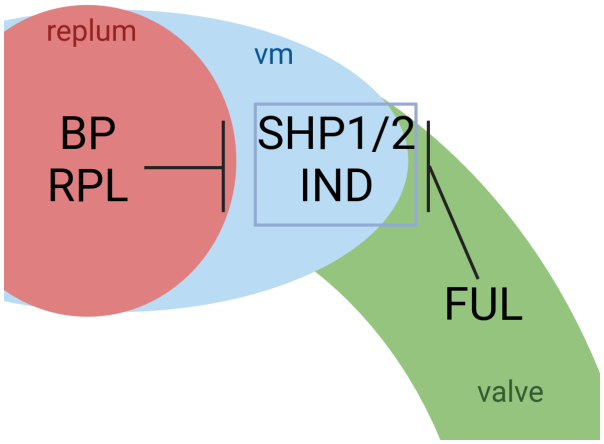

Figure 4. Schematic overview of fruit marker gene expression in *A. thaliana*. *BP* and *RPL* are expressed in the replum and negatively regulate valve margin genes, *SHP1*, *SHP2*, and *IND*. *FUL* is expressed in the valve and negatively regulates the valve margin genes. The valve margin genes promote differentiation of valve margin cell types.

In summary, I generated and screened an EMS mutagenized forward genetic screening population to look for mutant involved in SCW patterning. I collected several interesting mutants. And identified alleles of *ful*, *as1*, and *bp*. The screen provides a first insight into the mechanisms of SCW patterning in endocarp*b* cells.

2.2 Results

2.2.1 Summary of screen - gain and loss of lignin mutants

In order to find genes involved in patterning mechanisms of the endocarp*b* SCW, I conducted a forward genetic screen. For this, I mutagenized approximately 1700 *C. hirsuta* seeds with 0.3 % ethyl methane sulfonate (EMS) overnight. Of the sowed seeds 1181 M_1 germianted, I allowed these plants to self, and collected M_2 seed from individual plants. Approximately 5 % of the M_1 plants were completely sterile (54 plants) and other plants produced only a few seeds that were collected. In total, I collected M_2 seed from 1127 individual M_1 plants. I also sowed additional M_1 seeds and collected M_2 seed in pools of up to 5 M_1 plants per pot. In total, I collected 112 M_2 seed pools from these M_1 plants. For my project, I screened 500 of the 1127 M_2 families collected from individual M_1 plants, sowing 36 to 54 seeds per family when possible. For families with less seed than this, I sowed all available seed. Due to germination and fertility issues, not every seed produced a plant that was screened. Screening consisted of morphological observation, including dehiscence of mature fruit, and examination of the endocarp*b* lignin pattern of hand-cut fruit sections at stage 17b by autofluorescence under UV light (Figure 5).

I focused my screening on aberrations of the endocarp*b* lignin pattern, but I also recorded fruit morphology phenotypes. I did not collect seed from every plant that I recorded, especially for redundantly occurring phenotypes. In total, I collected 382 M_2 families with phenotypes affecting the endocarp*b* lignin pattern, fruit morphology, or other interesting phenotypes, like aberrant cell size or morphological changes in the fruit. It is likely that not all collected lines have a heritable genetic basis for their phenotype. Given the large number of lines that I collected, some phenotypes could be caused by the stress of genetic load due to the EMS mutagenesis, or the stress of crowded growing conditions. All mutants originating from this screen, regardless of their phenotype, were called *lignin pattern* (*pat*) and the M_2 family number of the mutant. In total, I screened fruit from 6643 fertile plants from 500 M_2 families derived from individual M_1 plants, with an additional 1197 plants being sterile.

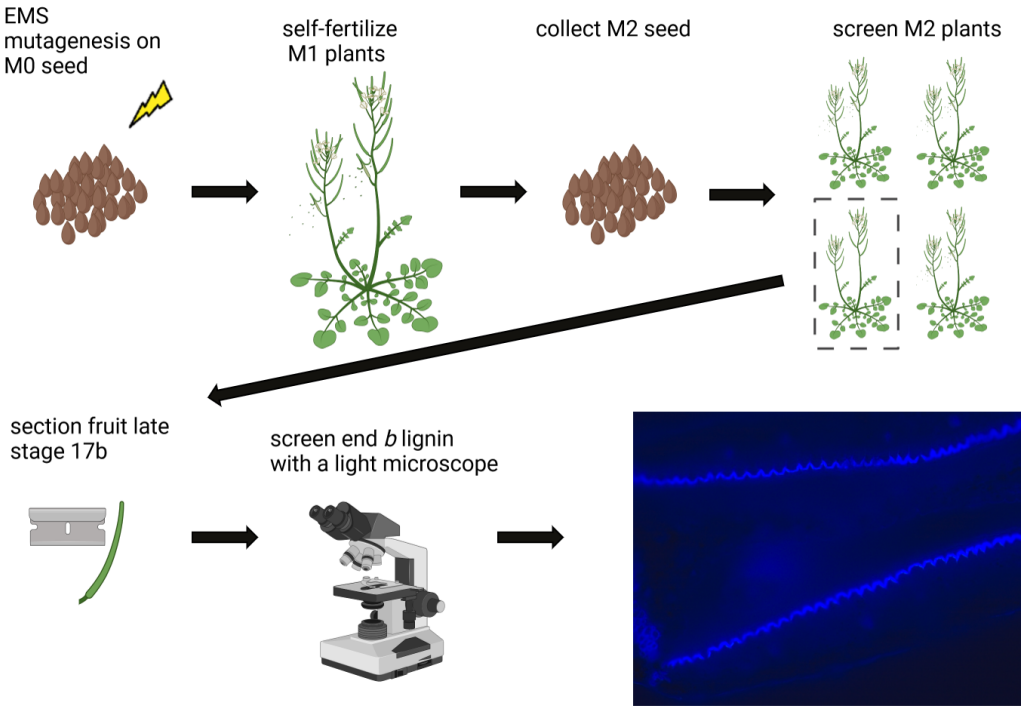

Figure 5. Schematic overview of EMS mutagenesis and screen. *C. hirsuta* seed were mutagenized with EMS (M_0), sown to give rise to M_1 plant. The M_1 plants were self-fertilized individually and their M_2 seed collected, such that each M_1 plant gave rise to one M_2 family. From each M_2 family 36 - 54 seed were sown in order to identify segregating homozygous recessive mutants. From each M_2 plant, a mature stage 17b fruit was hand-cut and the endocarp*b* lignin pattern observed by autofluorescence under UV light using a compound microscope.

I classified the collected mutants into four main phenotypic categories (Table 1). The most important categories were gain of lignin, with 527 mutants, and loss of lignin, with 87 mutants (Figure 6A, 6B). Furthermore, I collected 41 mutants with fruit morphology phenotypes and 10 mutants with aberrant cell size in the valve (Figure 6C). Mutants were listed in all categories they showed characteristics for, thus some mutants were listed in more than one category (Figure 6D).

Table 1. Phenotypic mutant categories observed in forward genetic screen

Mutant Category	Groups	Number of M_2 plants
gain		**527**
	ectopic lignin endocarp*b* thin	458
	ectopic lignin endocarp*b* thick	52
	ectopic lignin mesocarp thin	30
	ectopic lignin mesocarp thick	2
	stronger endogenous lignin	24
loss		**87**
	gaps (endocarp*b* cells without lignin)	25
	less endogenous lignin	62
cell size		**10**
	cell size in endocarp*b*	4
	cell size in mesocarp	6
phenotype fruit		**41**
	bukly	8
	twist	4
	repla	7
	other (e.g. *ful*, *bp*)	22

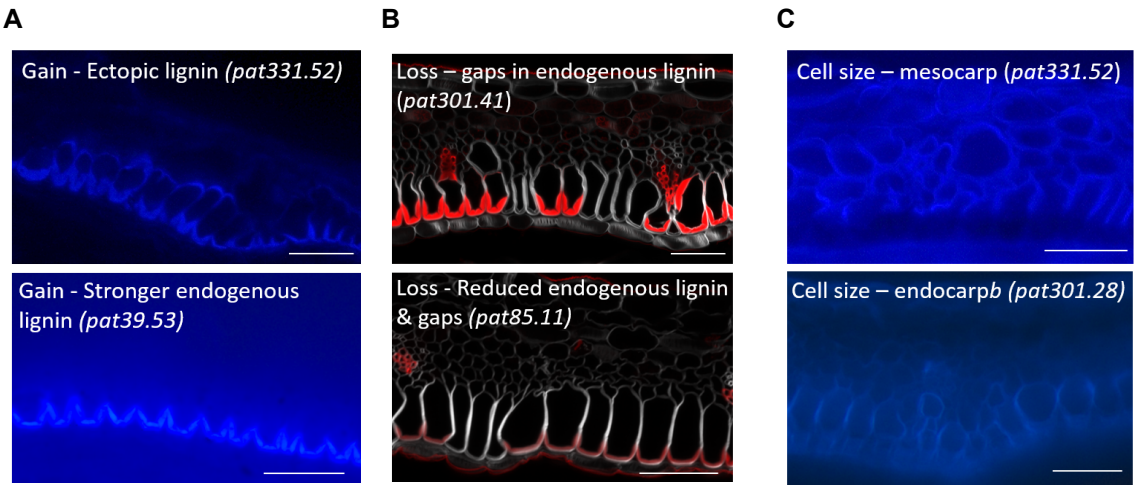

Figure 6

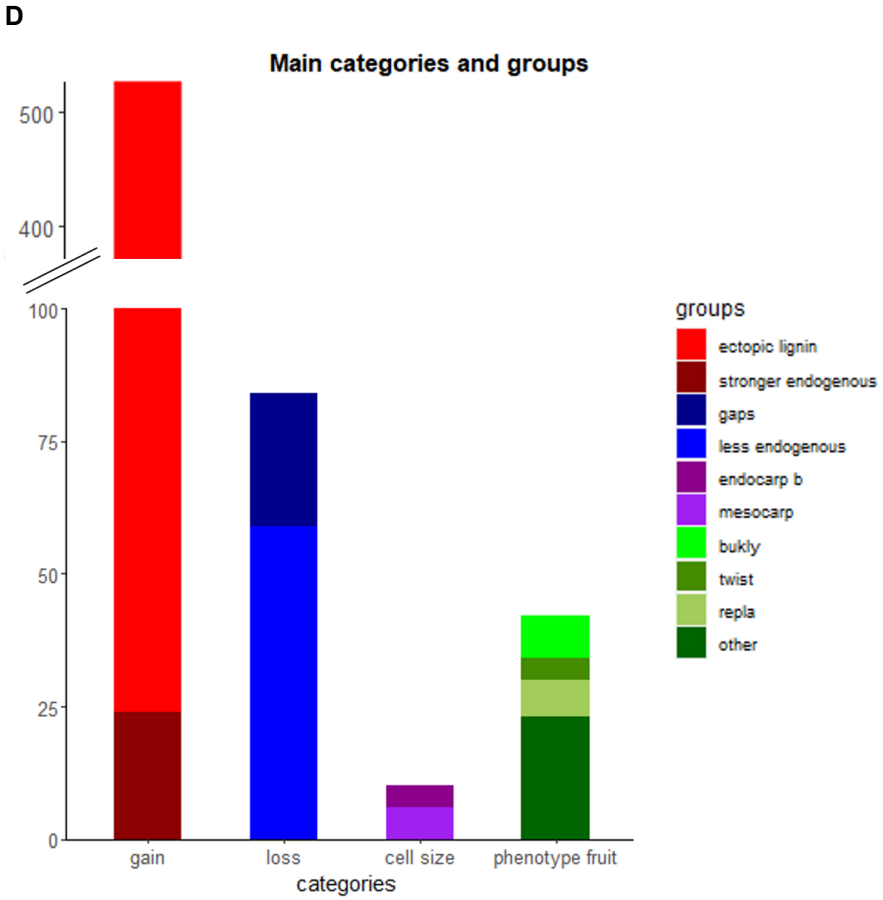

Figure 6. Barplot of the four main categories I choose for the collected mutants from the EMS mutant screen and exemplary images for some the categories.
A: Exemplary images of 'gain' category. Ectopic lignin in endocarp*b* cells and stronger endogenous lignin. Hand-cut, lignin aufofluorescence (blue). Scale bar 50 μm. B: Exemplary images of 'loss' category. Gaps (missing SCW in individual cells of the endocarp*b* layer) and in this mutants also ectopic lignin in endocarp*b* cells, and reduced endogenous SCW formation in endocarp*b* cells and gaps. Vibratome sections, lignin stained with Basic Fuchsin (red) and cellulose stained with Calcofluor White (gray). Scale bar 50 μm. C: Exemplary images of 'cell size' category. Aberrant cell size in mesocarp layer and in endocarp*b* cells. Hand-cut, cellulose stained with Calcofluor White (blue). Scale bar 50 μm. D: The barplot shows the four main categories, zoomed plot on the left. 'Gain' refers to gain of lignin mutants consisting of 527 mutants, with 503 mutants with 'ectopic lignin' (red) and 24 mutants with 'stronger endogenous' lignin (darkred). 'Loss', with 87 mutants, contains mutants that have subjectively less lignin compared to wild type. This category comprises 62 'reduced endogenous' lignin mutants (blue) and 25 mutants with 'gaps' (darkblue), some endocarp *b* cells without lignin. 'phenotype fruit' refers to 41 mutants in which the morphology of the fruit and inflorescence is aberrant from the wild type morphology. 'Cell size' contains 10 mutants in which subjectively the cell size of either endocarp*b* (purple) or small mesocarp cells (lilac) in the valve is aberrant from wild type.

Gain-of-lignin mutants were further divided into ectopic lignin, with 503 mutants, and increased endogenous lignin, with 24 mutants (Figure 6). The type of ectopic lignin was subjectively divided into 'thin' and 'thick' ectopic lignin. 477 mutants had ectopic lignin in endocarp*b* cells, of which 52 had thick ectopic lignin and 458 had thin ectopic lignin (Figure 7A, 7C). An additional 32 mutants had ectopic lignin in small mesocarp cells of the valve, of which 30 mutants had thin ectopic lignin and 2 mutants had thick ectopic lignin (Figure 7A, 7B). Mutants that had ectopic lignin in both locations or both types of ectopic lignin were counted in both categories. The thick ectopic lignin in small mesocarp cells appeared to recapitulate the endocarp*b* lignin pattern in an ectopic position. I did not observe ectopic lignin in large mesocarp cells of the valve.

In endocarp*b* cells I categorized the position of ectopic lignin in the cell. The cell wall with endogenous lignin, facing the adaxial side of the valve, was named the adaxial wall. The opposite wall, which is non-lignified and faces the abaxial side of the valve, was named the abaxial wall (Figure 8A). The endogenous lignin pattern also extends partly up the lateral cell walls. Ectopic lignin occurring in the lateral walls and having contact with the endogenous lignin was termed 'lateral' (Figure 8A). Ectopic lignin that was found on the abaxial or lateral wall, but without connecting to the endogenous lignin, was termed 'abaxial' (Figure 8A). Ectopic lignin going around the whole normally non-lignified cell wall was termed 'whole' (Figure 8A). Ectopic lignin in the lateral walls of endocarp*b* cells was the most common category, with 372 mutants (Figure 8B). Given the prevalence of this phenotype, selfed seed was not collected from all of these mutants. Ectopic lignin at the abaxial side occurred in 61 mutants (Figure 8B). And whole cell wall was ectopically lignified in 70 mutants (Figure 8B). Interestingly, the thick ectopic lignin in endocarp*b* cells recapitulated the endogenous pattern of lignin in a mirrored position (Figure 7C). Specifically, the precise pattern of lignified SCW in the endogenous position on a lateral wall tended to be mirrored on the opposite (abaxial) side of the same wall (Figure 7C, 8A). One mutant with this phenotype is *pat63*, which I investigate in more detail in chapter 3. In all 52 mutants with thick ectopic lignin in endocarp*b* cells, the thick ectopic lignin localized in this way on the abaxial side of the cell.

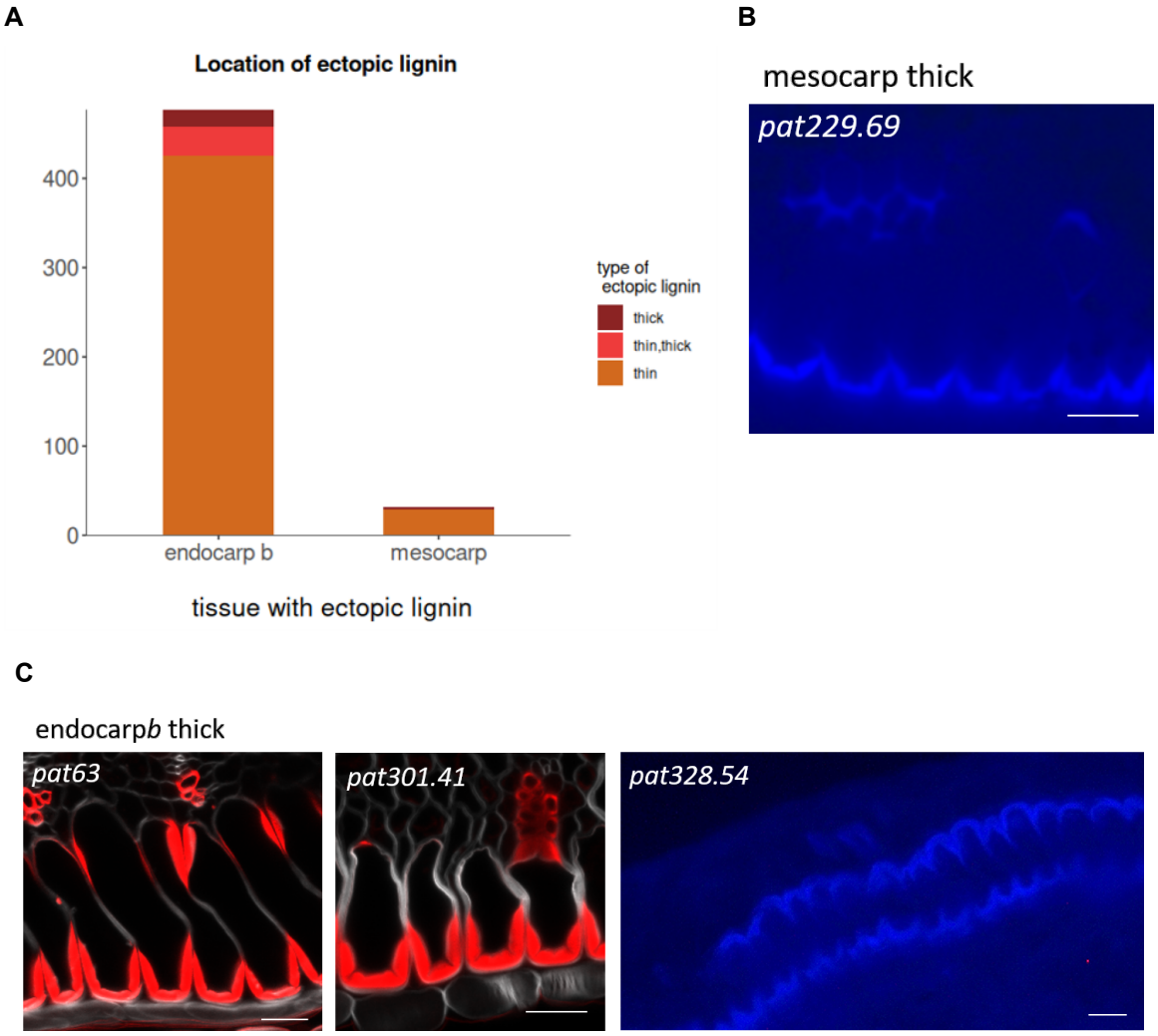

Figure 7. Thin and thick ectopic lignin in endocarp*b* and small mesocarp cells.
A: Barplot of tissue location of ectopic lignin, in endocarp*b* or small mesocarp cells and type of ectopic lignin. In total 477 mutants had ectopic lignin in endocarp*b* cells. 425 mutants had thin ectopic lignin and 19 mutants had thick ectopic lignin. In 33 mutants thin and thick ectopic lignin was observed. 32 mutants were observed to have ectopic lignin in small mesocarp cells. 30 mutants thin ectopic lignin and 2 mutants thick ectopic lignin. B: Exemplary images of thick ectopic lignin in small mesocarp cells. The pattern resembles endogenous endocarp*b* lignin. Hand-cut, lignin autofluorescence (blue). C: Exemplary images of thick ectopic lignin in endocarp*b* cells that mirrors one rod of the endogenous SCW pattern. In *pat63* only one rod is mirrored. In *pat301.41* two connecting rods are mirrored. In this mutant also gaps occur. In *pat328.54* the U-shape is mirrored. *pat63* and *pat301.41* vibratome section, lignin stained with Basic Fuchsin (red) and cellulose stained with Calcofluor White (gray). Scale bar 20 μm *pat328.54* hand-cut, lignin autofluorescence (blue).

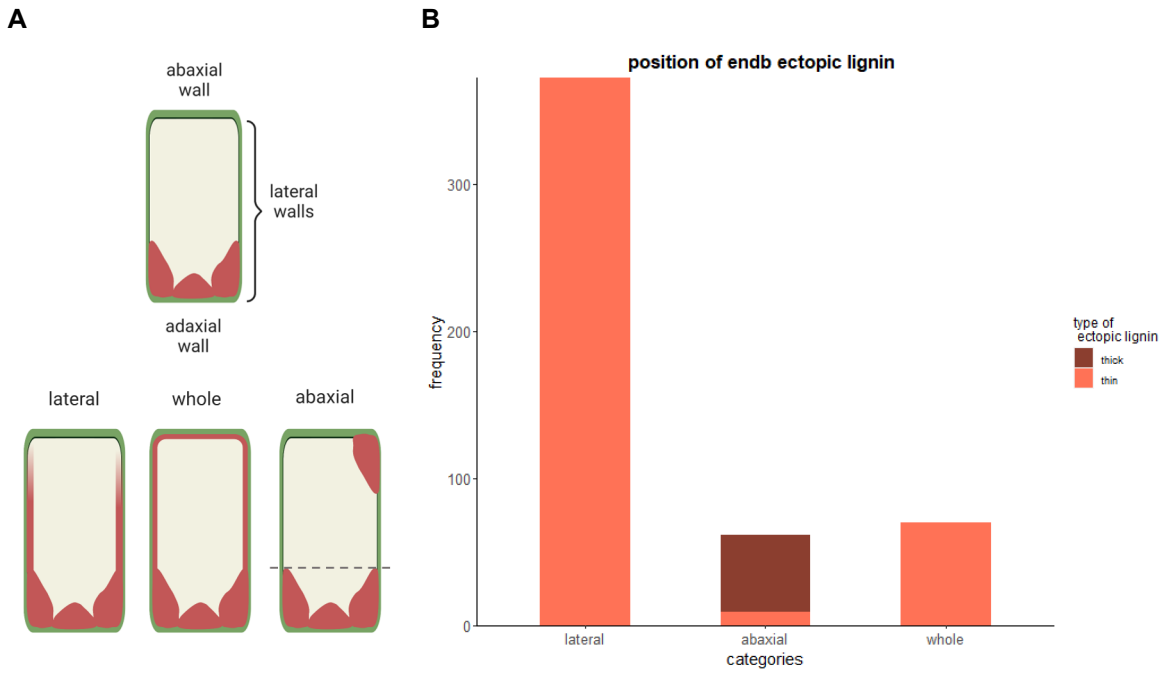

Figure 8. Thin and thick ectopic lignin in endocarp*b* and small mesocarp cells.
A: Schematic overview of the labeling of the walls of endocarp*b* cells and positions of ectopic lignin. Adaxial wall describes the wall with endogenous lignin. The opposite wall, which is completely non-lignified, was named the abaxial wall. The lateral walls are partly lignified. Ectopic lignin occurring in the lateral walls and having contact with the endogenous lignin was termed ‘lateral’. Ectopic lignin that was found on the abaxial or lateral wall, but without connecting to the endogenous lignin, was termed ‘abaxial’. B: Barplot of the positions of ectopic lignin in endocarp*b* cells. In 372 mutants it localizes lateral, in 61 mutants abaxial. And in 70 around the whole endocarp*b* cells. In lateral and whole only thin ectopic lignin localizes. Abaxial localization is in 9 mutants thin and in 52 mutants thick.

Loss of lignin mutants show defects in endocarp*b* lignin, including reduced lignification or gaps in the endocarp*b* cell layer with unlignified cells. Mutants that had both gaps and reduced lignin were listed in both categories. 62 mutants had reduced lignification and 25 mutants had gaps (Table 1). Two additional mutants, *pat162.34* and *pat477.11*, were included in this class, but they lacked lignin in the valve margin, rather than the endocarp*b*. Based on their phenotype, these two mutants are defective in fruit patterning, and are described further with other fruit patterning mutants in chapter 2.2.2. The category of gap mutants is quite variable, so I will describe four gap mutants to illustrate the variability (Figure 9). Mutant *pat158.8* displays a wild-type lignified SCW pattern in most endocarp*b* cells, but is interrupted by gaps of several cells in which the complete SCW is missing, including lignin and cellulose (Figure 9A). In mutant *pat295.51*, most cells completely lack a SCW, including lignin and cellulose, but contain a few cells with a wild-type lignified SCW pattern (Figure 9B). Mutant *pat301.41* is similar to mutant *pat158.8*, with a wild-type lignified SCW pattern in most endocarp*b* cells, interrupted by gaps of several cells in which the complete SCW is missing. However, it differs from *pat158.8*, because it also shows ectopic endocarp*b* lignin and aberrant cell sizes in endocarp*b* and small mesocarp cells (Figure 9C and 9D). The ectopic lignin ranges from thin to thick, always on the abaxial wall, with thick ectopic lignin mirroring the endogenous pattern of lignin on the abaxial wall (Figure 9D). The endocarp*b* cell layer in mutant *pat229.29* is completely different to wild type as cell size is reduced and lignified cells have a uniform, non-polar pattern of lignin (Figure 9E). These lignified cells are interrupted by gaps of several cells in which the complete SCW is missing (Figure 9E).

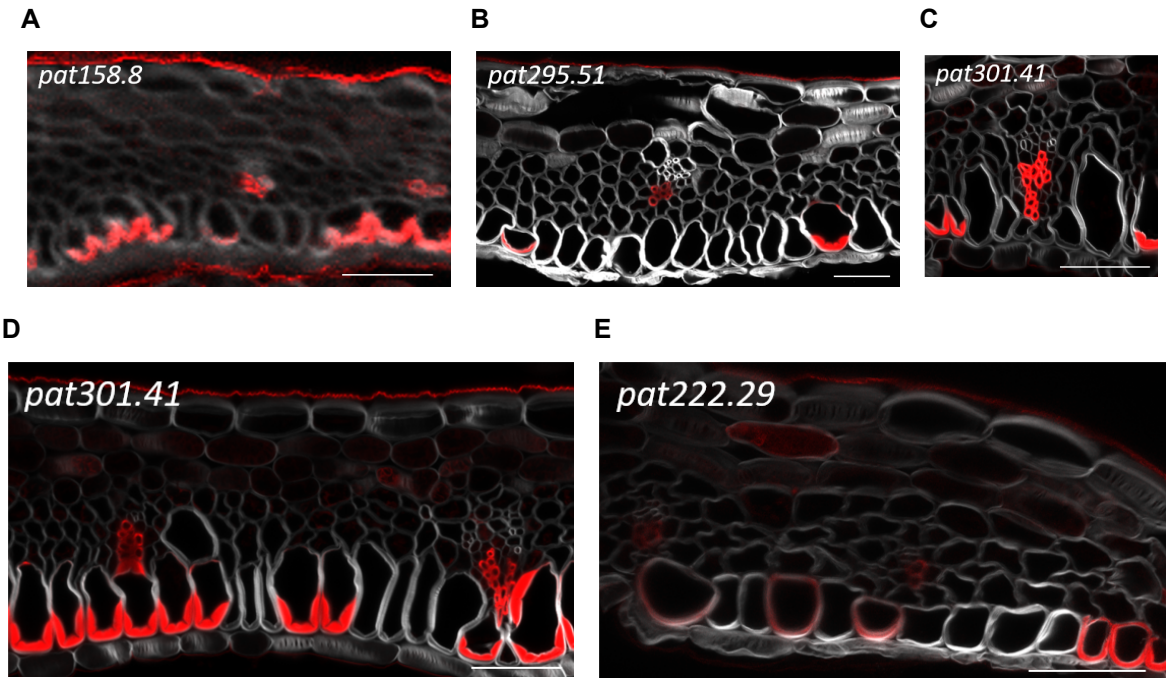

Figure 9. Examples of mutants from the category 'gap'. A: Mutant *pat158.8* displays endogenous SCW pattern in most endocarp*b* cells,and some cells without SCW (gaps). B: Mutant *pat295.51* has mostly endocarp*b* cells lacking SCW and the other cells have the endogenous SCW pattern. C and D: Mutant *pat301.41* has mostly endocarp*b* cells with endogenous lignin and some without (D). Additionally, ectopic lignin ranging from thin lignin to mirroring ectopic lignin in endocarp*b* cells occurs (D), and some cells in the endocarp*b* and small mesocarp differ in size (C). E: Mutant *pat222.29* has endocarp*b* cells without SCW and the cells with have a non-polar lignin pattern instead of a polar pattern. Mutants 158.8 and 222.29 were imaged by another student Ioannis Zafeiriou, who is further characterizing these mutants. Lignin stained with Basic Fuchsin (red), cellulose stained with Calcofluor White (gray). Scale bar 50 μm.

I identified additional fruit mutants that did not directly address the question of endocarp*b* lignin deposition and patterning, but are of general interest, and classified them in the categories 'cell size' and 'phenotype fruit'. Compared to the gain-of-lignin category, only a few mutants were collected here, 10 cell size mutants and 41 mutants for phenotype fruit (Figure 6D). Whole fruit development was affected in the fruit phenotype class, while cell size mutants were affected only in the development of endocarp*b* or small mesocarp cells in the valve. I further divided fruit phenotype mutants into 4 groups (Table 1). Fruit that did not have a smooth surface were classified as 'buckled' (8 mutants) and fruit that were curved and twisted were classified as 'twisted' (4 mutants). Fruit with supernumerary repla belonged in the group 'repla' (7 mutants), exception is one mutant with only one replum. And additional mutants that did

not belong in one of these three groups were simply classified as 'other' (22 mutants). This group included mutants that were similar to previously cloned mutants; for example, *bp* and *ful* mutants, or mutants with fruit that appeared subjectively more or less stiff than wild type. I did not use explosive coiling of the valves as a phenotype in my screening. Similar to previous screens (Hofhuis et al., 2016), I found that reduced coiling was either associated with another phenotype; for example, loss of endocarp*b* lignin, or influenced by general growth defects with either a genetic or an environmental basis. Therefore, mutants that I identified here can be accurately phenotyped for valve coiling in future studies.

2.2.2 Fruit patterning mutants - *fruitfull* and valve margin mutants

Among the mutants in the phenotype fruit category, I identified four new alleles of the *FRUITFULL* (*FUL*) MADS-box gene (*ful-2, -3, -4* and *-5*). I suspected that these mutants could be *ful* alleles based on their conspicuous fruit phenotype, in which the valve is replaced by valve margin tissue. This fruit phenotype had been previously described for the *ful-1* allele in *C. hirsuta* (Galstyan et al., 2021). I confirmed that all four mutants had mutations in the *FUL* gene by Sanger sequencing (Figure 10A). The published *ful-1* allele contains a point mutation in exon 5, leading to a premature stop codon (Galstyan et al., 2021) (Figure 10A). The *ful-2* allele contains a point mutation in the first nucleotide of the first intron, which changes the splice donor site, resulting in alternative splicing whereby 31 nucleotides are omitted, causing a frameshift that leads to a premature stop codon in exon 3 (Figure 10A). The *ful-3* and *ful-4* alleles contain point mutations that directly lead to premature stop codons in exon 3 and exon 4, respectively (Figure 10A). In *ful-5*, a missense point mutation causes an amino acid substitution in exon 2 (Figure 10A). I also performed an allelism test by crossing one of my new mutants (*ful-2*) with the existing *ful-1* mutant (Galstyan et al., 2021). The resulting F_1 plants from this cross had the same fruit phenotype as both parents (Figure 10B), indicating that they are alleles of the same gene.

At the scale of the whole fruit, all *ful* mutants had transparent tissue in place of the normal valves, which was narrow in width, making the whole fruit narrower than wild type, and re-

vealed the underlying seeds (Figure 10B). I measured fruit length in the identified *ful* alleles and showed the *ful* alleles were significantly reduced in length compared to wild type (Figure 11). But the fruit length also was significantly different between the *ful* alleles, except for *ful-2* and *ful-4*, which were the shortest. *ind* had a similar fruit length to wild type (Galstyan et al., 2021) (Figure 11). And *ful-2;ind* partially rescued the reduced fruit length of *ful-2* (Figure 11).

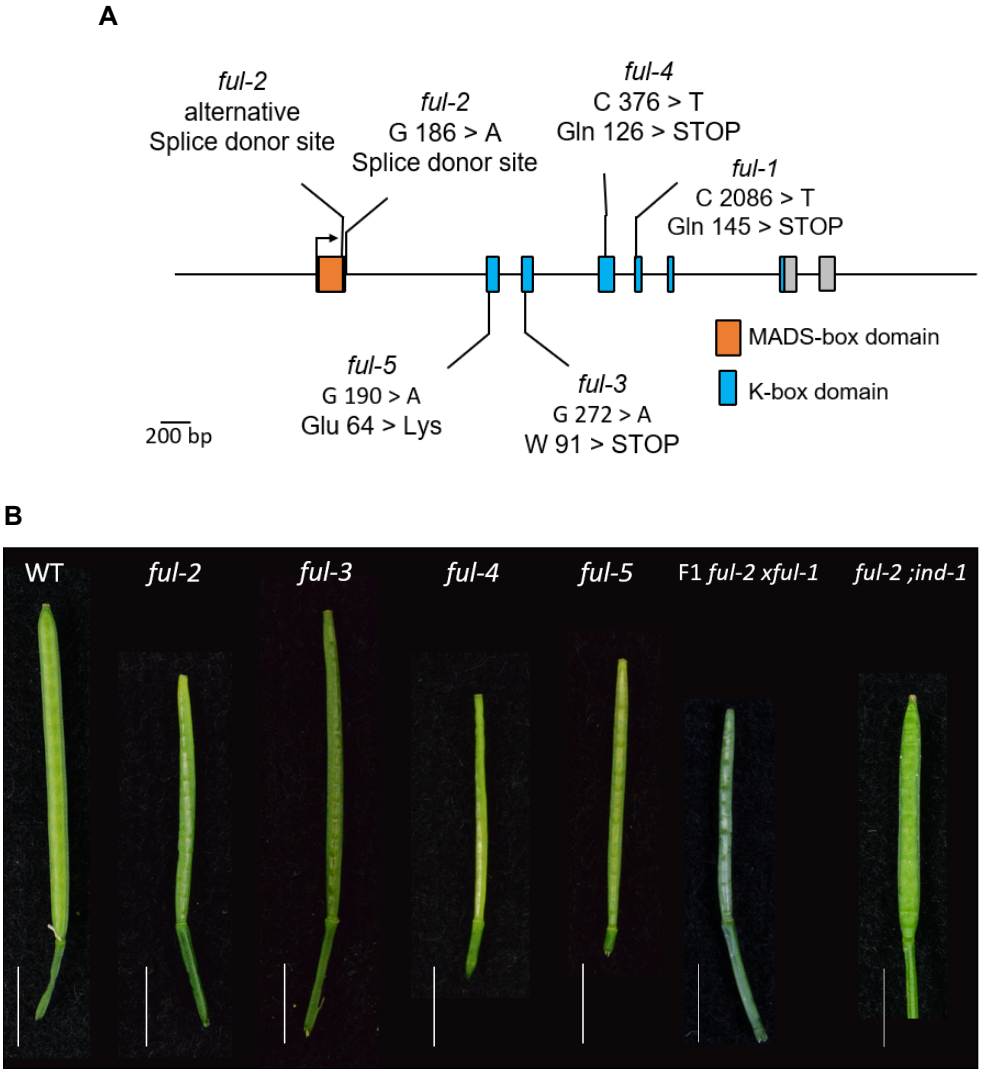

Figure 10. The identified *ful* alleles in *C. hirsuta*. A: Gene model with the mutations of the *ful* alleles, the nucletoide positions always include the intron regions. In *ful-2* a guanin (G) changes to adenin (A) at nucleotide position 186, which is the first nucleotide of the first intron. This causes an alternative splice donor site, leading to loss of 31 nucleotides and a frameshift that causes a premature stop codon at nucleotide position 282. In *ful-3* a guanin to adenin point mutation at 272 nucleotide causes a premature stop codon at amino acid 91. In *ful-4* a cytosin (C) to thymin (T) point mutation at 376 nucleotide causes a premature stop codon at amino acid 126. In *ful-5* a guanin to adenin point mutation at 190 nucleotide causes a missense mutation that changes amino acid 64 from negatively charged glutamic acid (Glu) to the positively charged lysin (Lys). B: Images of the mature fruit of wild type, the identified *ful* alleles and the fruit of the allelism test of *ful-1* and *ful-2* (F_1 *ful-1x x ful-2*). The reduced width of the 'valve' structure is visible for all four mutant alleles and the F_1 *ful-1x x ful-2* fruit. Scale bar 5 mm.

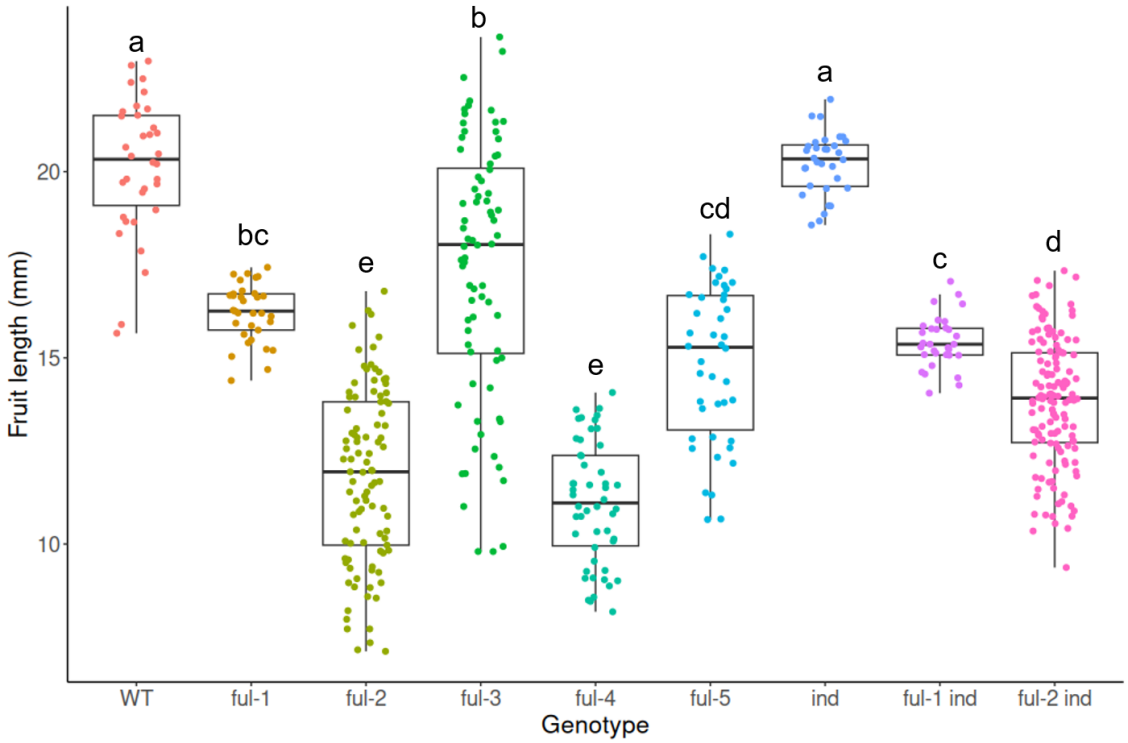

Figure 11. Boxplot of fruit length of wild type *ful-1, ful-2, ful-3, ful-4, ful-5, ind, ful-1;ind* and *ful-2;ind*. The means are the following: wild type 20.12 mm, *ful-1* 16.22 mm, *ful-2* 11.82 mm, *ful-3* 17.41 mm, *ful-4* 11.12 mm, *ful-5* 14.84 mm, *ind* 20.22 mm, *ful-1;ind* 15.43 mm, *ful-2;ind* 13.82 mm. Different letters denote statistically significant differences ($p < 0.05$) between means based on ANOVA (Tukey's HSD). n fruit: wild type 34, *ful-1* 64, *ful-2* 232, *ful-3* 76, *ful-4* 50, *ful-5* 42, *ind* 198, *ful-1;ind* 31, *ful-2;ind* 135. Wild type, *ful-1*, *ind*, *ful-1;ind* data from (Galstyan et al., 2021).

At the cellular scale, I stained fruit cross-sections with Basic Fuchsin to visualize lignin, and Calcoflour White to visualize cellulose. I compared wild-type valves with the transparent tissue replacing valves in each of the *ful* alleles. I concluded that this transparent tissue has valve margin identity, similar to the interpretation for other *ful* mutants in both *C. hirsuta* and *A. thaliana* (Galstyan et al., 2021; Gu et al., 1998; Ferrándiz et al., 2000). Valve margin cells are small and comprise two different cell types that differentiate to form the dehiscence zone: lignified and separation layer cells (Galstyan et al., 2021). In comparison, the valve contains various cell types of different sizes, including exocarp, large and small mesocarp cell layers, vascular bundles with lignified xylem cells, endocarp*a* cells and lignified endocarp*b* cells (Figure 12A). The transparent tissue in *ful* fruit mostly comprised small, non-lignified cells, similar to separation layer cells from the valve margin (Figure 12B). Valve cell types were missing from *ful* fruit (Figure 12B). This supports the idea that valve identity has been replaced by valve margin identity in *ful* mutants.

Interestingly, the phenotype of *ful-5* appears somewhat weaker in comparison to the other three alleles. This fits with the fact that the amino acid substitution in *ful-5* is also a weaker lesion than the premature stop codons in the other three alleles (Figure 10A). In the transparent tissue of *ful-5* fruit, I observed larger cells in the outer layer, similar to wild-type exocarp cells, and lignified cells that resemble xylem cells in the position of wild-type vascular bundles (Figure 12B). Therefore, *ful-5* fruit appear to retain some valve identity. I also observed many lignified cells that resemble lignified layer cells of the valve margin (Figure 12B).

The phenotypes of *ful-2, ful-3* and *ful-4* alleles were very similar and mostly comprised one cell type, which resembled small, separation layer cells of the valve margin (Figure 12B). I also observed small, lignified cells in these alleles, but it is difficult to conclude whether these cells have the identity of lignified layer cells of the valve margin, or xylem cells. Future work can distinguish between these two possibilities.

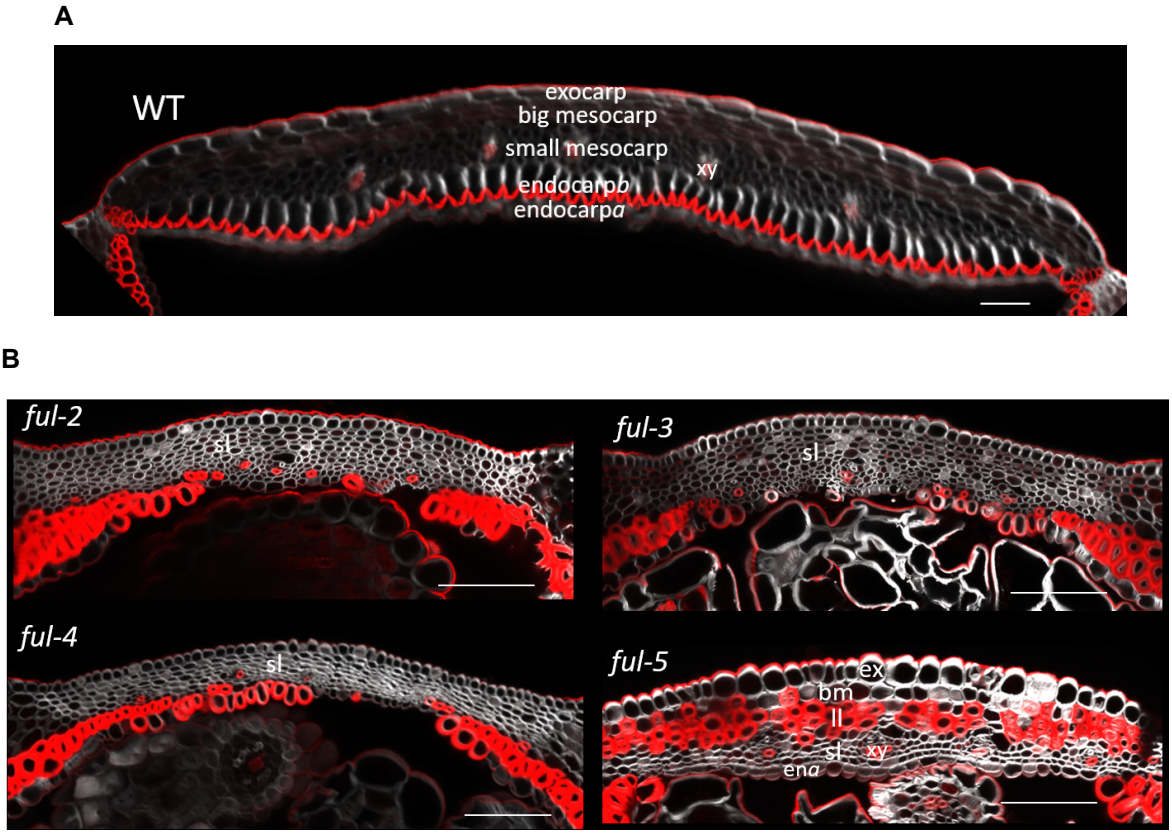

Figure 12. The identified *ful* alleles in *C. hirsuta*. A: Image of labeled wild type valve. The valve contains various cell types of different sizes, including exocarp, large and small mesocarp cell layers, vascular bundles with lignified xylem cells (xy), endocarp*a* cells and lignified endocarp*b* cells. Scale bar 50 μm. B: Confocal images of the 'valve' of the four *ful* alleles. The differentiated valve cell types are missing. *ful-2, ful-3* and *ful-4* alleles mostly comprise of one cell type, that resembles separation layer cell (sl). *ful-5* seems to retain some valve identity. Larger cells in the outer layer are similar to wild-type exocarp cells (ex), and lignified cells that resemble xylem cells (xy). Cell beneath the exocarp cells have a similarity to big mesocarp cells (bm) and the inner epidermal cells have similarity to endocarp*a* cell (ena). Lignified cells resemble lignified layer cells (ll) of the valve margin. And small cells resemble separation layer cells (sl) of the valve margin. Lignin stained with Basic Fuchsin (red) and cellulose stained with Calcofluor White (gray). Scale bar 50 μm.

A key function for the MADS-domain transcription factor FUL in fruit patterning, is to negatively regulate valve margin genes, such as *INDEHISCENT* (*IND*) (Liljegren et al., 2004; Galstyan et al., 2021). *IND* encodes a bHLH transcription factor that is a master regulator of valve margin identity and *ind* mutants in both *A. thaliana* and *C. hirsuta* have indehiscent fruit because they lack a valve margin (Liljegren et al., 2004; Galstyan et al., 2021). To test to what extent the fruit phenotype of *ful-2* is caused by ectopic *IND* expression in the valve, I crossed *ful-2* with the published *ind-1* mutant (Galstyan et al., 2021) to generate double

mutants. Cross-sections of *ful-2;ind-1* double mutant fruit showed the absence of a valve margin, similar to *ind-1* (Figure 13A). The loss of valve identity in *ful-2* (Figure 12B) was partially rescued in *ful-2;ind-1* (Figure 13B). I observed cells in the double mutant that resembled exocarp, large and small mesocarp cells, endocarp*a* cells and vascular bundles similar to wild type valves (Figure 13B). I also observed endocarp*b* cells with polar lignification, similar to wild type, but these cells were smaller than wild type and most cells in this layer were non-lignified (Figure 13B). Fruit length in the *ful-2;ind-1* double mutant was also partially rescued, as the double mutant was significantly longer than *ful-2*, but significantly shorter than wild type and *ind-1* (Figure 10B and 11). Taken together, these results indicate that ectopic *IND* expression contributes to the loss of valve identity in *ful-2*, and the small valve margin cells that replace the valve in *ful-2* contribute to the reduction in fruit length.

Two mutants that I identified in the loss-of-lignin class had loss of lignified cells in the valve margin, rather than the endocarp*b*. Mutant *pat162.34* had indehiscent fruit, therefore, I sequenced the *IND* locus and identified a G to A point mutation at nucleotide position 347 in exon 1. This causes a substitution of amino acid 116 from Serine to Asparagine. Future work will be needed to verify whether this mutation is causal for the phenotype. The valve margin is not so obviously lacking in mutant *pat162.34*, in comparison to *ind-1* (Figure 13A). This may indicate that *pat162.34* is a weaker allele of *ind*, or that differentiation processes, rather than cell fate specification, are defective in this mutant.

The second mutant, *pat477.11*, had fruit that could still dehisce along the valve margin. In agreement with this, the valve margin had small, separation layer cells like wild type, but mostly lacked lignified cells at the valve margin (Figure 13A). In addition, the endocarp*b* cells in this mutant had thin ectopic lignin surrounding the whole cell (Figure 13B).

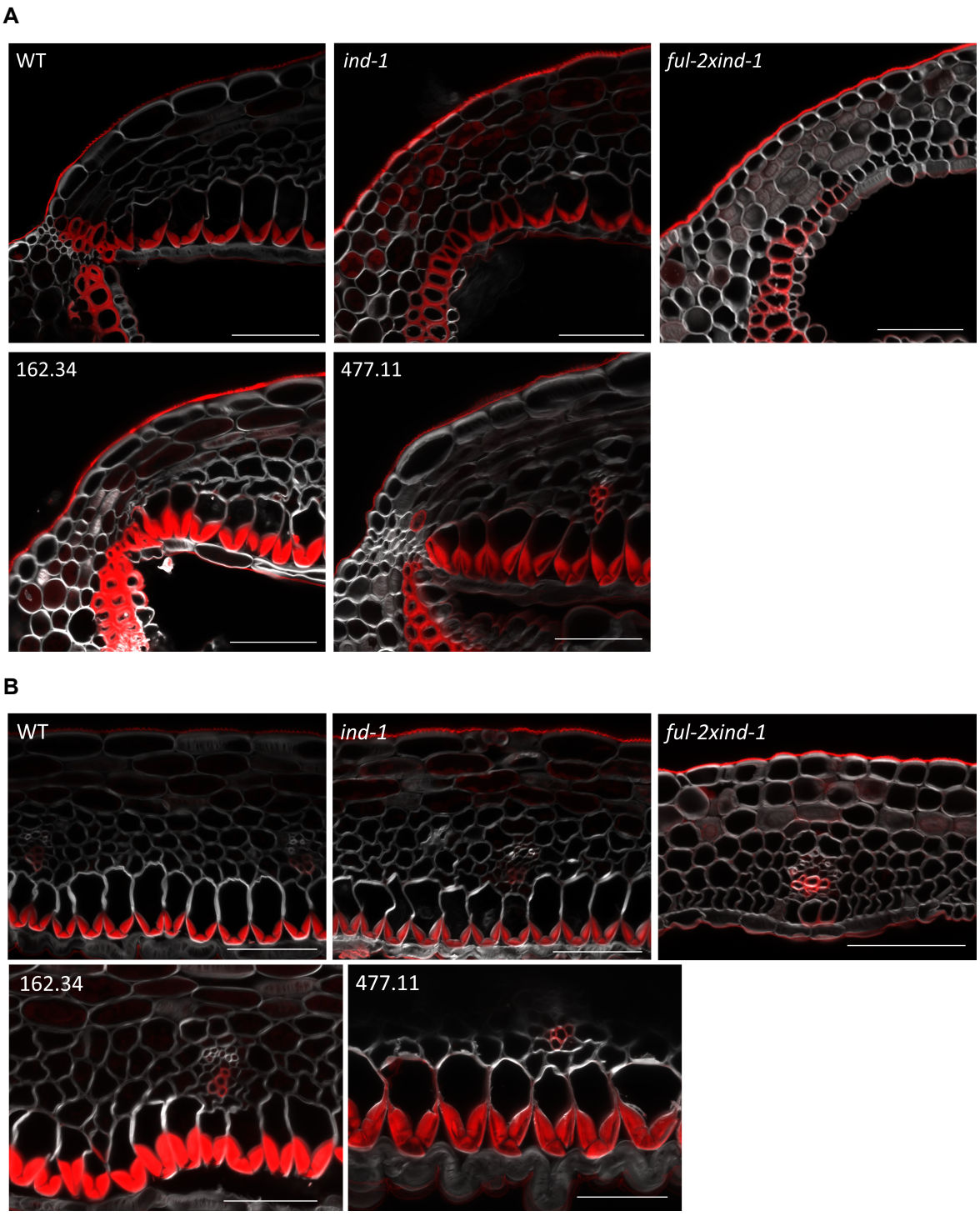

Figure 13. Valve margin (A) and valve (B) confocal images of wild type, *ind-1*, *ful-2;ind-1*, and mutant *pat162.34* and *pat477.11*. A: In *ind-1* and *ful-2;ind-1* the valve margin cell types are completely missing. In *pat162.34*, separation layer and SCW in lignified layer are missing. In *pat477.11*, SCW in lignified layer is missing, but the cell types appear to differentiate similar to wild type. B: Endocarp*b* SCW is similar to wild type in *ind-1*, *pat162.34*, and *pat477.11*. Latter has thin while ectopic lignin. In *ful-2;ind-1* valve cell types are resuced, except for endocarp*b* cells, which are smaller and mostly non-lignified. Cross-sections of fruit stage 17b, fixed and lignin stained with Basic Fuchsin (red), cellulose stained with Calcofluor White (gray). Scale bar 50 μm.
Fruit image and fruit length plot in Figure 10B and 11.

2.2.3 Multiple *as1* and *bp* alleles identified in the mutant screen

Among the mutants in the 'other' category of fruit phenotypes, I identified two new alleles of the *ASYMMETRIC LEAVES1* (*AS1*) Myb gene (*as1-2* and *-3*). I suspected that these mutants (*pat247.68* and *pat310.29*) could be *as1* alleles based on their conspicuous leaf phenotype. In *C. hirsuta*, the leaf phenotype of *as1-1* had been previously described as having reduced rachis length and aberrant leaflet positioning (Rast-Somssich et al., 2015) (Figure 14B). I confirmed that the new mutants had mutations in the *AS1* gene by Sanger sequencing. The published *as1-1* allele contains a point mutation at nucleotide 508, causing a premature stop codon at amino acid 170 (Hay and Tsiantis, 2006) (Figure 14A). The *as1-2* allele has a C to T point mutation at nucleotide 199, causing a premature stop codon at amino acid 67 (Figure 14A). The *as1-3* allele has a G to A point mutation at nucleotide 21, causing a premature stop codon at amino acid 7 (Figure 14A). These mutations identified in *AS1* are likely to cause the leaf phenotypes of *as1-2* and *as1-3*, however further evidence from an allelism test or transgenic complementation, would be required to confirm this.

Interestingly, all *as1* alleles had a fruit phenotype in addition to the leaf phenotype. Of particular interest, I observed ectopic lignin in endocarp*b* cells of all *as1* alleles. For this reason, I investigate these *as1* mutants in more detail in chapter 3.

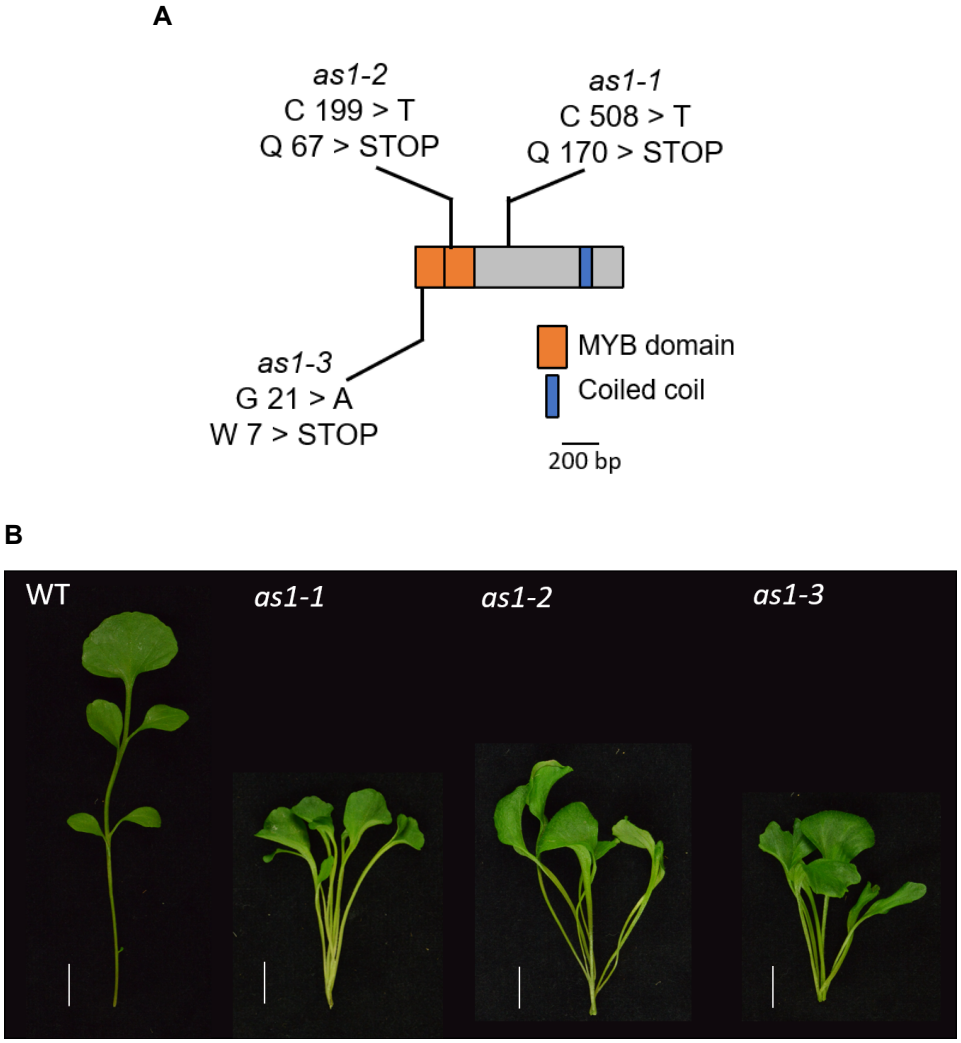

Figure 14. Two new *as1* alleles were identified in the mutant screen. A: Gene model of *AS1*, all nucleotides given without introns. *as1-1* is an already published mutant with a point mutation from cytosine (C) to thymine (T) at nucleotide 508, causing a premature stop codon at amino acid 170 (Hay and Tsiantis, 2006). I identified *as1-2*, with a cytosine to thymine point mutation at 199 nucleotides, causing a premature stop codon at amino acid 67. And I also identified *as1-3* with a guanine (G) to adenine (A) point mutation at nucleotide 21, causing a premature stop codon at amino acid 7. B: Leaf phenotypes of WT, *as1-1*, *as1-2*, and *as1-3*. The *as1* alleles leaves have a reduced rachis and aberrant leaflet initiation. Scale bar 1 cm.

In the 'other' category of fruit phenotypes, I also identified two new alleles of the *BREVIPEDICELLUS* (*BP*) KNOX1 homeobox gene (*bp-2* and *-3*). I suspected that these mutants (*pat12* and *pat366*) could be *bp* alleles based on their conspicuous downward-pointing fruit (Figure 15B). The reduced plant stature, disrupted inflorescence architecture and altered fruit orientation of *bp* mutants had been previously described in *A. thaliana* and *C. hirsuta* (Venglat

et al., 2002; Rast-Somssich et al., 2015). I confirmed that the new mutants had mutations in the *BP* gene by Sanger sequencing. The *bp-2* and *bp-3* alleles contain different point mutations that directly lead to premature stop codons in exon 3 (Figure 15A). The *bp-1* allele has a point mutation causing a premature stop codon at the beginning of the second intron (Rast-Somssich et al., 2015). Again, it is likely that these mutations identified in *BP* are likely to cause the mutant phenotypes of *bp-2* and *bp-3*, however further evidence from allelism test or transgenic complementation, would be required to confirm this.

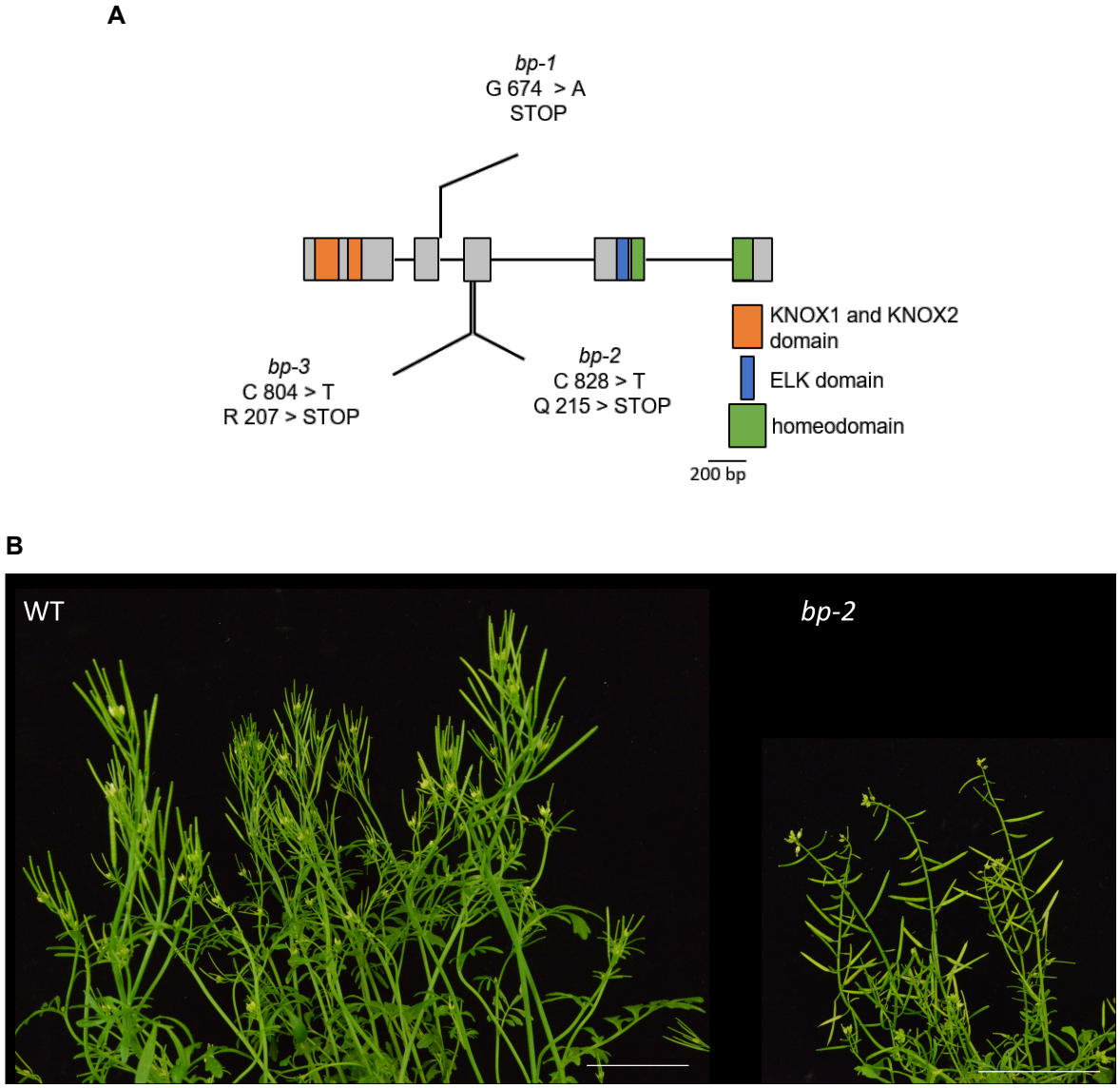

Figure 15. Two new *bp* alleles were identified in the mutant screen. A: Gene model of *BP*, all nucleotides given with introns. *bp-1* is an already published mutant with a point mutation from guanine (G) to adenine (A) at nucleotide 674, causing a premature stop codon at amino acid 170 (Hay and Tsiantis, 2006). I identified *bp-2*, with a cytosine (C) to thymine (T) point mutation at 828 nucleotides, causing a premature stop codon at amino acid 215. And I also identified *bp-3* with a cytosine (C) to thymine (T) point mutation at nucleotide 804, causing a premature stop codon at amino acid 207. B: Inflorescence phenotype of WT and *bp-2*. *bp-3* was not imaged but showed the same phentoype of downward pointing siliques. Scale bar 5 cm

2.3 Discussion

In summary, I screened 500 M_2 families that yielded 382 interesting mutants. The fact that I isolated two or more alleles for three separate genes, suggests that I achieved good genome coverage with my EMS mutant population. The 5 % sterility rate that I observed in the M_1 generation is another indicator that the EMS mutagenesis was efficient (Mesken and van der Veen, 1968).

My screen was searching for changes in the lignin pattern. However, the endogenous lignin pattern in endocarp*b* cells was rarely disrupted. Instead, I mostly identified mutants with ectopic lignin. An interesting class of these mutants were those with thick ectopic lignin, deposited on the opposite side of the cell, mirroring the endogenous lignin pattern. This suggests that both the adaxial and abaxial sides of the cell are competent to form this SCW pattern. But that there are polarity determinants that specify the adaxial side of the cell as the site where the SCW should be deposited. Specification could be determined by activators that mark the site of SCW deposition. Or repressors could mask the sites where SCW is not deposited. Or a boundary could specify the difference between SCW deposition or not. I will explore these possibilities further in my general discussion section.

I identified many mutants with thin ectopic lignin and stopped collecting these mutants once it became apparent that this phenotype was so frequent. Given its frequency, it is likely that this phenotype has both genetic and non-genetic causes. It could be stress-induced, from the genome caused by mutagenesis, and from the environment caused by large-scale growing conditions. The thin ectopic lignin occurred on walls in lateral and abaxial positions in endocarp*b* cells. It was difficult to distinguish whether this lignin was deposited in primary cell walls or associated with thin ectopic SCW deposition. Typically, lignin occurs in SCWs, but lignin can also occur in primary cell walls. A good example is the Casparian strip in roots. This consists of a localized band of lignin impregnation in the primary cell wall of root endodermal cells, forming an apoplastic barrier (Naseer et al., 2012; Rojas-Murcia et al., 2020). Also, in dark-grown maize coleoptile and aspen cell cultures, lignin can be found in PCWs (Muese et al., 1997; Christiernin et al., 2005). Therefore, it is possible that this thin ectopic lignin is

deposited in the primary cell wall in response to stress. The exact localization could be determined by transmission electron microscopy.
The only other cell type in the fruit valve where I found ectopic lignin was in small mesocarp cells. This either recapitulated the polar endocarp*b* pattern, suggesting a cell fate change, or initiated ectopically in cell corners. This could suggest that this mesocarp cell type, adjacent to the endocarp*b*, and found in *C. hirsuta* but not *A. thaliana* fruit valves, has a higher susceptibility to ectopically lignify.

Mutants with reduced lignin can give further insights into the genes involved in endocarp*b* SCW lignification. These could include genes required to specify endocarp*b* cell fate, or control SCW biosynthesis, or control lignification. My screening method was optimized for SCW pattern changes, and while gaps are easy to spot with this method, reduced amounts of lignin are harder to identify. Therefore, future work to identify endocarp*b* lignification mutants may benefit from a different screening method.
In the gap mutants, the cells that lack lignin always lack the complete SCW. Therefore, these mutants may define genes that activate SCW biosynthesis. The stochastic nature of this phenotype is intriguing. It may suggest redundancy amongst genes controlling this process, such that higher order mutants will be required to see complete loss of function. Within the gap mutant class, I highlight mutant *pat222.29* as being of special interest to further characterize and identify the causal mutation. This is because the mutant has defects not only in SCW biosynthesis but also in SCW patterning. This was the only mutant I recovered from the screen where the endocarp*b* SCW pattern was changed from polar to uniform. I had expected to identify more mutants with a uniform SCW pattern in my screen. *A priori*, I thought that a uniform SCW, such as found in Arabidopsis endocarp*b* cells, could represent a default state. However, this was not the case and the phenotype of *pat222.29* was an exception.

In my screen I identified new alleles of the important fruit patterning genes *FRUITFULL* (*FUL*) and *INDEHISCENT* (*IND*), as well as the *BREVIPEDICELLUS* (*BP*) and *ASYMMETRIC LEAVES1* (*AS1*) genes. Isolating multiple alleles of multiple genes is a good indication that I

achieved reasonable genome coverage in my screen.

I identified four new alleles of the MADS box-encoding gene *FUL*. Similar to *C. hirsuta ful-1*, the valve was converted to valve margin identity in all of these new alleles. In three alleles (*ful-2*, *ful-3* and *ful-4*) the cells in the ectopic valve margin mostly had the identity of separation layer cells (Galstyan et al., 2021). However, in *ful-5*, these cells had mostly the identity of lignified layer cells. This is more similar to the phenotype of strong *ful* alleles in *A. thaliana* (Ferrándiz et al., 2000; Gu et al., 1998). Interestingly, *ful-5* is a weaker allele compared to the other four *C. hirsuta ful* alleles. It has a missense point mutation while the other mutants have premature stop codons. This suggests that FUL has a similar function in both *C. hirsuta* and *A. thaliana* to specify valve fate by restricting valve margin fate. However, the consequence of losing FUL differs between species. In *A. thaliana ful* mutants, lignified cell types differentiate, while separation layer cell types differentiate in *C. hirsuta*.

To further investigate *FUL* function in *C. hirsuta*, I crossed *ful-2* with an allele of *IND*, which is a bHLH-encoding gene that regulates valve margin fate in both *A. thaliana* and *C. hirsuta* (Ferrándiz et al., 2000; Liljegren et al., 2004; Galstyan et al., 2021). In *ind-1;ful-2* fruit, valve cell fate was mostly restored, supporting the idea that FUL specifies valve fate by restricting *IND* gene expression to the valve margin. Mutant alleles of *IND* are indehiscent and lack both cell types of the valve margin in both *A. thaliana* and *C. hirsuta* (Liljegren et al., 2004; Galstyan et al., 2021). In the indehiscent mutant *pat162.34*, where I identified a missense mutation in *IND*, the valve margin looks somewhat different to this. It lacks a separation layer, but differentiates cells similar to lignified layer cells that lack SCW. This may suggest a weak *ind* phenotype, but this needs to be confirmed by allelism tests or transgenic complementation. In contrast to this, mutant *pat477.11* has a valve margin with a separation layer and cells with a SCW that lack lignin, but these fruit are dehiscent, although the valves detach with reduced coiling. As the three mutants described here all lack lignification in the valve margin, yet show different dehiscence, this suggests that the separation layer might play a more important role than the lignified layer in dehiscence in *C. hirsuta* fruit.

The new alleles of *as1* that I identified had the well described leaf phenotype (Rast-Somssich

et al., 2015), and the enlarged replum phenotype described in *A. thaliana as1* fruit (Alonso-Cantabrana et al., 2007). In my screen, I also observed ectopic lignin in the endocarp*b* of *as1* fruit valves. Therefore, the next chapter will focus on the fruit phenotypes and ectopic endocarp*b* lignin in *C. hirsuta as1*, as well as mutant *pat63*.

3 Characterization of ectopic lignin mutants *as1* and *pat63*

3.1 Introduction

In the previous chapter I identified *as1* alleles in my mutant screen. In this chapter I will characterize loss of *AS1* in *C. hirsuta* in regard to the fruit and ectopic lignin in the endocarp*b* layer. So far, *AS1* is well characterized as a negative regulator of three *KNOTTED1-like homeobox* (*KNOX*) class I genes and as an adaxial polarity marker.

AS1 interacts with AS2 to negatively regulate expression of three *KNOX* class I genes, *BREVIPEDICELLUS* (*BP*), *KNOTTED1LIKE in ARABIDOPSIS THALIANA 2* (*KNAT2*), and *KNAT6*, restricting their expression to the meristem. The *KNOX1* genes are involved in meristem maintenance in the shoot apical meridtem (SAM), from which lateral organ primordia initiate. Another *KNOX1* gene is *SHOOTMERISTEMLESS* (*STM*), which negatively regulates *AS1* (Scofield et al., 2014). In leaf development, AS1 acts as an adaxial polarity regulator (Xu et al., 2003). The function of AS1 to repress *BP* is conserved in the fruit. AS1 is expressed in the valve and restricts *BP* expression to the replum in *A. thaliana*. Loss of *AS1* in *A. thaliana* causes fruit repla to be enlarged. Specifically, the outer epidermis of the repla contains more cells compared to wild type. On the other hand, valves are reduced in width and the number of their outer epidermal cells was lower. Lignification pattern in the valve was not affected in *A. thaliana as1* mutants. Double knockout mutant *as1;bp* partially rescued the *as1* phenotype. And constitutive expression of *BP* phenocopied the *as1* fruit. (Alonso-Cantabrana et al., 2007). AS1 phenotypes are often *BP*-dependent (Rast-Somssich et al., 2015; Alonso-Cantabrana et al., 2007).

The impact of BP on lignin deposition has been studied in *A. thaliana* vasculature. In the hypocotyl and the root, the centrally located procambium differentiate into xylem and phloem during primary xylem formation. The vessel cells are surrounded by parenchymatic non-lignified cells. Upon flowering, the secondary xylem formation begins and vessel and lignified

fiber cells differentiate then radially. *BP* is expressed in developing xylem fibers and in the cambial zone, a continuous vascular ring between phloem and xylem. Loss of *BP* causes reduced xylem fiber formation in xylem II. Furthermore, SCW-related genes are significantly downregulated, including the SCW master regulators *NST1* and *NST3* in hypocotyl of the double mutant of *bp* with a weak *stm* allele. BP promotes fiber formation by transcriptional repression of *BLADE-ON-PETIOLE 1* (*BOP1*) and *BOP2*, which repress fiber formation (Liebsch et al., 2014; Woerlen et al., 2017). The repressive interaction also occurs for the inflorescence stem architecture (Khan et al., 2011). In contrast, in the stem, primary vasculature is organized in individual bundles, each with its own fascicular cambium. During secondary growth, fibers differentiate in the interfascicular region. *bp* mutants showed premature lignification of the interfascicular region and vascular bundle differentiation in the stem, and constitutive *BP* expression repressed interfascicular fiber lignification. BP directly binds to the promoters of a handful of genes playing a role in the phenylpropanoid pathway (Mele et al., 2003). Therefore, BP is able to regulate lignin and impact fiber differentiation. However, the type of regulation, positive or negative, seems to be dependent on other factors (Liebsch et al., 2014; Felipo-Benavent et al., 2018).

In the previous chapter, I identified mutants with aberrant SCW pattern in endocarp*b* cells. Among them *pat63*, which has thick ectopic lignin on the abaxial side of endocarp*b* cells. *as1-1* mutant show similar ectopic lignin on the abaxial side and fruit morphology (Hay and Tsiantis, 2006). In this chapter I characterized ectopic lignin and fruit morphology of *as1-1*, *as1-3*, and *pat63* mutants.

3.2 Results

3.2.1 Comparing of *as1-3*, *as1-1*, and *pat63*

In my mutant screen I identified several mutants with thick ectopic lignin on the abaxial side of endocarp*b* cells that partially mirrors the endogenous lignin pattern (chapter 2.2.1). Since this phenotype may give some insight into endocarp*b* SCW patterning, I further investigated such mutants. I observed this phenotype in the two alleles of *as1* that I isolated and in the *pat63* mutant. I selected my newly isolated *as1-3* allele to study, as it is predicted to be the strongest allele (chapter 2.2.3, Figure 14A). I also selected the previously described allele *as1-1* (Hay and Tsiantis, 2006) to compare with *as1-3* and *pat63*.

Ectopic endocarp*b* lignin

To compare the ectopic endocarp*b* lignin between the three mutant alleles, I quantified this phenotype (Figure 16. For this, I counted the number of endocarp*b* cells with ectopic lignin in the entire valve and divided it by the total number of endocarp*b* cells in that valve. I tested the statistical significance of difference between genotypes by performing ANOVA and Tukey post-hoc tests using R. The *as1-1* and *pat63* mutants have a significant increase of endocarp*b* cells with ectopic lignin compared to wild type (Figure 16B, left plot). Fruit valves of *as1-1* had a mean of 85.80 % of all endocarp*b* cells having ectopic lignin, and in *pat63* valves, a mean of 67.33 % of endocarp*b* cells had ectopic lignin. Although *as1-3* valves had a higher proportion of endocarp*b* cells with ectopic lignin than wild type (mean of 2.17 % compared to 0.45 %), this difference was not statistically significant by ANOVA (Figure 16B, left plot). When this data was compared using a Student's t-test, the p-value was 0.021, suggesting that the difference in ectopic lignin between *as1-3* and wild type was statistically significant (Figure 16B, left plot).

To further characterize the ectopic lignin in endocarp*b* cells, I subjectively categorized two types: thin and thick. I also distinguished the position where the ectopic lignin was observed in endocarp*b* cells: ectopic lignin that has contact with the endogenous lignin and occurs at

the lateral walls was termed 'lateral', while ectopic lignin on the opposite side of the cell, not connected to the endogenous lignin, was called 'abaxial' (see Figure 8A in chapter 2.2.1). In *as1-1* valves, a mean of 83.06 % of endocarp*b* cells had thin ectopic lignin and this almost always localized in a lateral position (Figure 16B, middle plot). Thick ectopic lignin was observed in a mean of 7.45 % of endocarp*b* cells in *as1-1*, and this localized in an abaxial position (Figure 16B, right plot). According to ANOVA testing, the amount of thin ectopic lignin in *as1-1* was significantly different from all other genotypes, while the amount of thick ectopic lignin was not significantly different to wild type and *as1-3*. However, when using a Student's t-test to compare the data, I obtained a p-value of $3.062e^{-05}$, which indicates a significant difference between the amount of thick ectopic lignin in *as1-1* compared to wild type. In fruit valves of *pat63*, the majority of both thin and thick ectopic lignin localized to abaxial positions in endocarp*b* cells (Figure 16C). The proportion of endocarp*b* cells with thick ectopic lignin (mean of 40.76 %) was higher than cells with thin ectopic lignin (mean of 24.91 %) in *pat63* valves. According to ANOVA testing, the amount of thin ectopic lignin was significantly different form wild type and *as1-1*, and the amount of thick ectopic lignin was significantly different from all genotypes. In *as1-3* valves, the majority of ectopic lignin localized in an abaxial position and a mean of 0.42 % of endocarp*b* cells had thin ectopic lignin and 1.75 % of endocarp*b* cells had thick ectopic lignin (Figure 16C). Neither of these values were significantly different to wild type by ANOVA. However, when using a Student's t-test to compare the data, I obtained a p-value of 0.046, indicating that the amount of thick ectopic lignin in *as1-3* was significantly different to wild type. In summary, *as1-1* had mostly thin ectopic lignin in lateral positions, while *pat63* had mostly thick, but also thin, ectopic lignin in abaxial positions of endocarp*b* cells. Valves of *as1-3* had mostly thick ectopic lignin in abaxial positions, but had less ectopic lignin than the other genotypes. A clear result from this analysis is that thick ectopic lignin always localizes to abaxial positions, mirroring the position of endogenous lignin on the adaxial side of endocarp*b* cells.

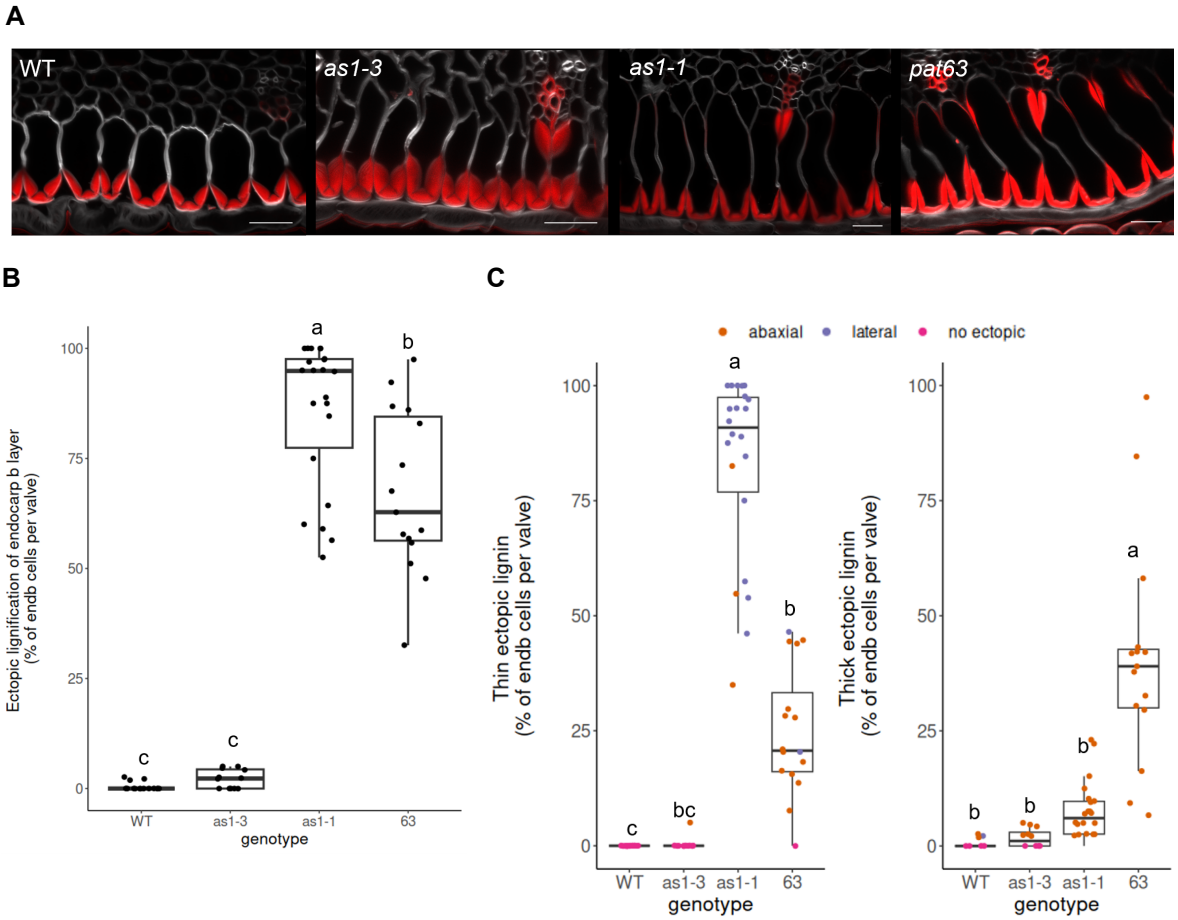

Figure 16. Lignin quantification of *as1-3*, *as1-1* and *pat63*. *as1-1* and *pat63* have significantly increased ectopic lignin. While *as1-1* has mostly thin lateral ectopic lignin, *pat63* has mostly thick abaxial ectopic lignin.
A: Confocal images of wild type, *as1-3*, *as1-1*, and *pat63* fruit stage 17b. Lignin stained with Basic Fuchsin (red) and cellulose stained with Calcofluor White (gray). Scale bar 20 μm.
B: Quantification of ectopic lignin in wild type, *as1-3*, *as1-1* and *pat63*. Endocarp*b* cells with ectopic lignin divided by endocarp*b* cells. The means are the following: wild type 0.45 %, *as1-3* 2.17 %, *as1-1* 85.80 %, and *pat63* 67.33 %. C: Two plots of endocarp*b* cells with thin and thick ectopic lignin divided by endocarp*b* cells. Colors according to ectoic lignin position, abaxial (orange), lateral (purple). The means are the following for thin: wild type 0.00 %, *as1-3* 0.42 %, *as1-1* 83.06 %, and *pat63* 24.91 %. The means for thick are the following: wild type 0.39 %, *as1-3* 1.75 %, *as1-1* 7.45 %, and *pat63* 40.76 %. Different letters denote statistically significant differences ($p < 0.05$) between means based on ANOVA (Tukey's HSD). n valves: wild type 18, *as1-3* 12, *as1-1* 79, *pat63* 30.

All of the imaging and quantifications of ectopic lignin presented so far, were from cross-sections through the fruit (Figure 16A). However, when observing the ectopic lignin in surface views of freshly peeled valves, I noticed that the thick ectopic lignin is not continuous along the entire length of these long endocarp*b* cells (Figure 17). Because of this, my quantifications are likely to under-estimate the proportion of endocarp*b* cells with thick ectopic lignin, since

this will depend on the position along the cell where the cross-section was made. Future work to image and analyze endocarp*b* cells in 3-dimensions, rather than 2-dimensions, will address this issue.

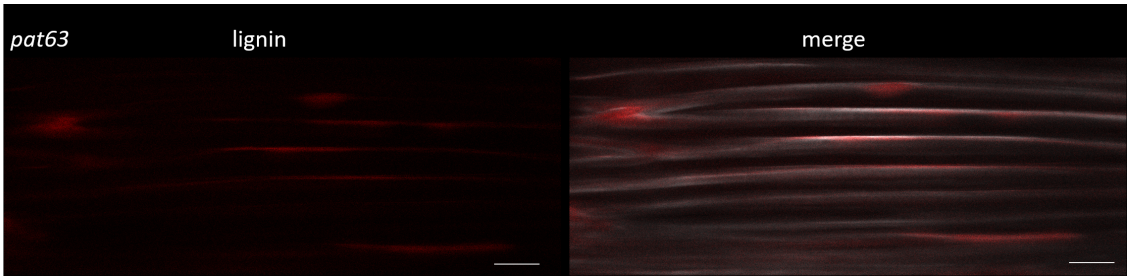

Figure 17. Exemplary confocal image of *pat63* of a peeled off valve stage 17b. Showing that thick ectopic lignin is not uniform along endocarp*b* cells. Lignin stained with Basic Fuchsin (red), cellulose stained with Calcofluor White (gray). Scale bar 50 μm

Replum width

In *A. thaliana*, *as1* mutants have been described as having a broadened replum (Alonso-Cantabrana et al., 2007). To analyze this phenotype in *C. hirsuta*, I measured the replum width of *as1-1, as1-3* and *pat63*. I took my measurements from images of fruit cross-sections, taking the width across the replum at the point closest to the valve margin. I found that all three mutants had an enlarged replum that was significantly wider than wild type (Figure 18). Both *as1* alleles had very broad repla. The stronger *as1* allele, *as1-3*, had the broadest replum and was significantly different to the other three genotypes, with a mean of 720.11 μm (Figure 18B). The replum of *as1-1* had a mean of 648.81 μm (Figure 18B). The replum morphology in both *as1* alleles differed markedly from wild type. In particular, the lignified edges of the repla that connect to the valve margin, are considerably extended in *as1-3* and *as1-1* (Figure 18A). The replum morphology of *pat63* is similar to wild type (Figure 18A). However, the *pat63* replum was also significantly wider than wild type, with a mean of 574.89 μm, compared to 388.31 μm in wild type (Figure 18B).

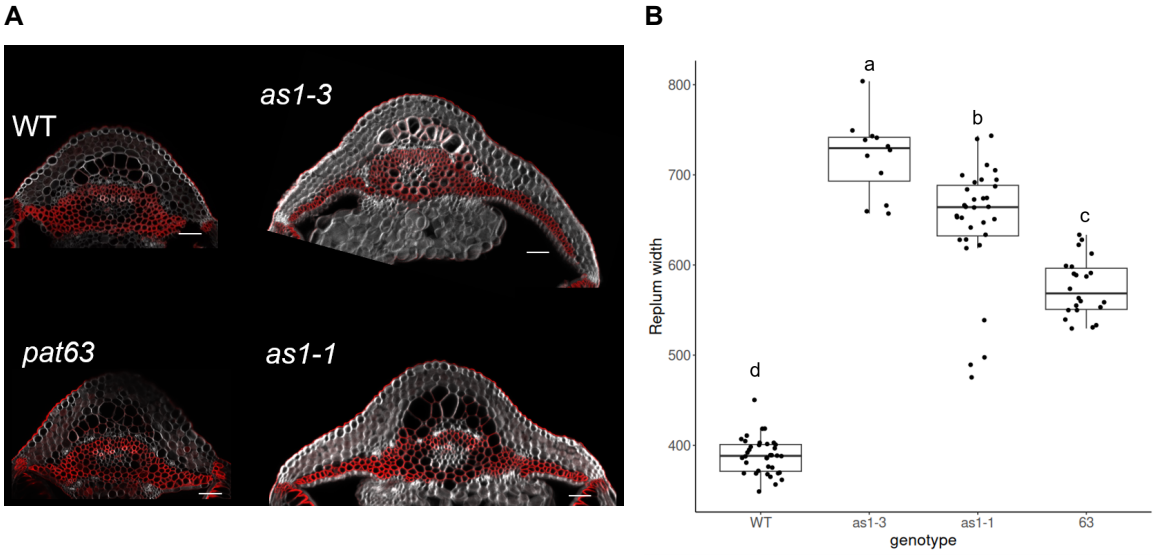

Figure 18. The replum width is enlarged in *as1-3*, *as1-1* and *pat63* compared to wild type. A: Confocal images of a replum of a fruit stage 17b of wild type, *as1-3*, *as1-1* and *pat63*. The morphology of *as1-3* and *as1-1* is through expansion of the replum to the side different from wild type. B: Boxplot of replum width of wild type, *as1-3*, *as1-1* and *pat63*. The replum width means are: wild type 388.31 μm, *as1-3* 720.11 μm, *as1-1* 648.81 μm, *pat63* 574.89 μm. Different letters denote statistically significant differences ($p < 0.05$) between means based on ANOVA (Tukey's HSD). n repla: wild type 36, *as1-3* 12, *as1-1* 32, *pat63* 22.

Fruit length and valve curvature

Another obvious phenotype is the shorter fruit length of *as1-3, as1-1* and *pat63* compared to wild type (Figure 19). The elongated fruit of wild type had a mean length of 20.98 mm, and was significantly different to all the mutant genotypes (Figure 19B). The *pat63* mutant had the shortest fruit with a mean length of 10.36 mm, and was significantly different to all other genotypes (Figure 19B). Both *as1* alleles had shorter fruit that were not significantly different from each other, with mean lengths of 12.25 mm for *as1-3* and 13.01 mm for *as1-1* (Figure 19B). The variation in fruit length was higher for *as1-3* than the other genotypes. These plants had fertility issues and I had to manually pollinate the carpels to generate fruit, which may have resulted in variable seed set and hence variable fruit size. It could well be, that in backcrossed plants these fertility issues are solved and measurements could be repeated.

In order to estimate the explosive coiling of the fruit valves, I measured valve curvature. The radius of the coiled valve approximates the amount of differential contraction in the valve, which is responsible for generating the tension that powers explosion (Hofhuis et al., 2016;

Mosca et al., 2024). I fitted circles to the minimum and maximum curvature of each valve, measured the radius of the circles, and took the inverse of the radius to calculate the curvature (valve curvature = 1/radius). Therefore, the smaller the radius, the greater the curvature and more explosive the valve coiling. Wild type valves had a mean curvature of 2.67 and were significantly different to all the mutant genotypes (Figure 19C. Therefore, wild-type valves had more explosive coiling. *pat63* valves had the smallest curvature with a mean of 0.80, and were significantly different to all other genotypes (Figure 19C). Therefore, *pat63* valves were the least explosive. Both *as1* alleles had less explosive valves than wild type, but were not significantly different from each other, with a mean of 1.46 for *as1-3* and 1.35 for *as1-1* (Figure 19C). Again, *as1-3* valves had more variable values, likely due to the variation in fruit size. In summary, these mutants with short fruit, broad repla and ectopic endocarp*b* lignification, also have valves that coil less explosively than wild type.

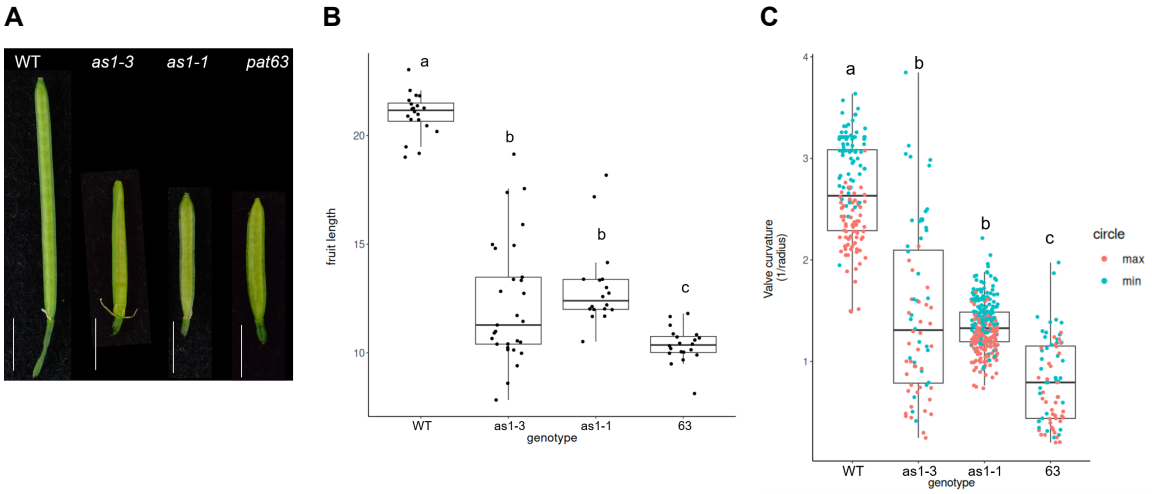

Figure 19. The fruit length and valve curvature are reduced in *as1-3*, *as1-1* and *pat63* compared to wild type. A: Fruit images of stage 17b of wild type, *as1-3*, *as1-1* and *pat63*. B: Boxplot of fruit length of wild type, *as1-3*, *as1-1* and *pat63*. The fruit length means are: wild type 20.98 mm, *as1-3* 12.26 mm, *as1-1* 13.01 mm, *pat63* 10.36 mm. C: Boxplot of valve curvature, calculated by dividing 1 by the radius of the minimum or maximum circle fitting into the curvature. The curvature means are: wild type 2.67, *as1-3* 1.46, *as1-1* 1.35, *pat63* 0.80. Different letters denote statistically significant differences ($p < 0.05$) between means based on ANOVA (Tukey's HSD). n fruit length: wild type 20, *as1-3* 29, *as1-1* 18, *pat63* 20. n valves: wild type 72, *as1-3* 36, *as1-1* 144, *pat63* 38.

3.2.2 Lignin development of *as1-1*

Following this initial phenotypic characterization, I analyzed development of the endocarp*b* SCW in more detail. I compared wild-type development with the development of both thick and thin ectopic lignin in *as1-1* endocarp*b* cells. So far, I had only observed endocarp*b* lignin in mature fruit at stage 17b when the lignification process is complete. To observe different stages of the lignification process, I imaged consecutive fruit of one plant of wild type and one of *as1-1*. Once the oldest fruit exploded, I collected all remaining fruit, representing a developmental series from stage 17b through earlier stages to stage 16, which is before lignification starts. I stained fruit for lignin using Basic Fuchsin and for cellulose using Calcofluor White, and imaged cross-sections under the confocal microscope. In Figure 20, I show exemplary images of each of the different stages.

Lignin first appears in wild-type endocarp*b* cell walls as a thin layer as a U-shape on the adaxial side. The hinges are not yet visible at this stage. The thin lignin layer subsequently thickens, as does the cellulose layer. As the SCW thickens, the hinged pattern is established. The SCW continues to thicken and the hinged pattern becomes clearly visible (Figure 20A).

Development of the endogenous lignin pattern in *as1-1* endocarp*b* cell walls follows a similar progression to wild type. It starts in a thin layer in a U-shape and continues to thicken, forming a hinged pattern. At the earliest appearance of lignin in the endogenous position, I also observed ectopic lignin initiating in an abaxial position (circle, Figure 20B). Development of this ectopic lignin seems to follow the same progression as the endogenous SCW, gradually thickening as the fruit matures. However, I also found ectopic lignin in abaxial positions that seemed to initiate later, since it was not as thick as the endogenous SCW (arrow, Figure 20B). Therefore, ectopic lignin at different stages of thickening were visible in a single fruit, for example in the fruits early stage 17b and stage 17b (arrow, Figure 20B). Interestingly, the thin ectopic lignin in lateral positions initiates later in development, after the endogenous lignin is already thickening (Figure 20B). In summary, the thick ectopic lignin in *as1-1* follows a similar progression to wild type in terms of initiation and thickening, suggesting that it is similarly regulated, but in an ectopic position. In contrast to this, the thin ectopic lignin differs from wild type in the timing of

initiation and lack of thickening.

A

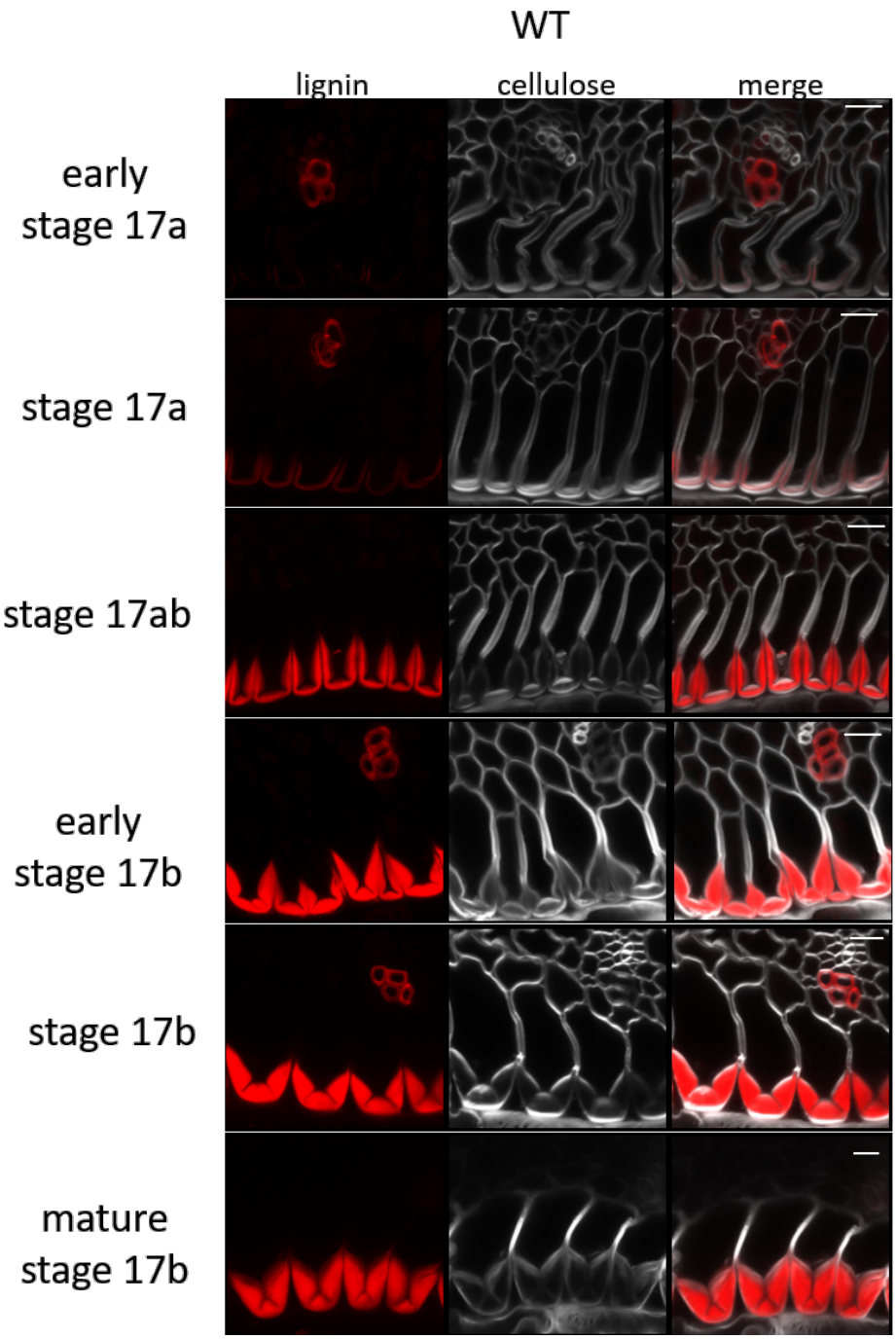

Figure 20

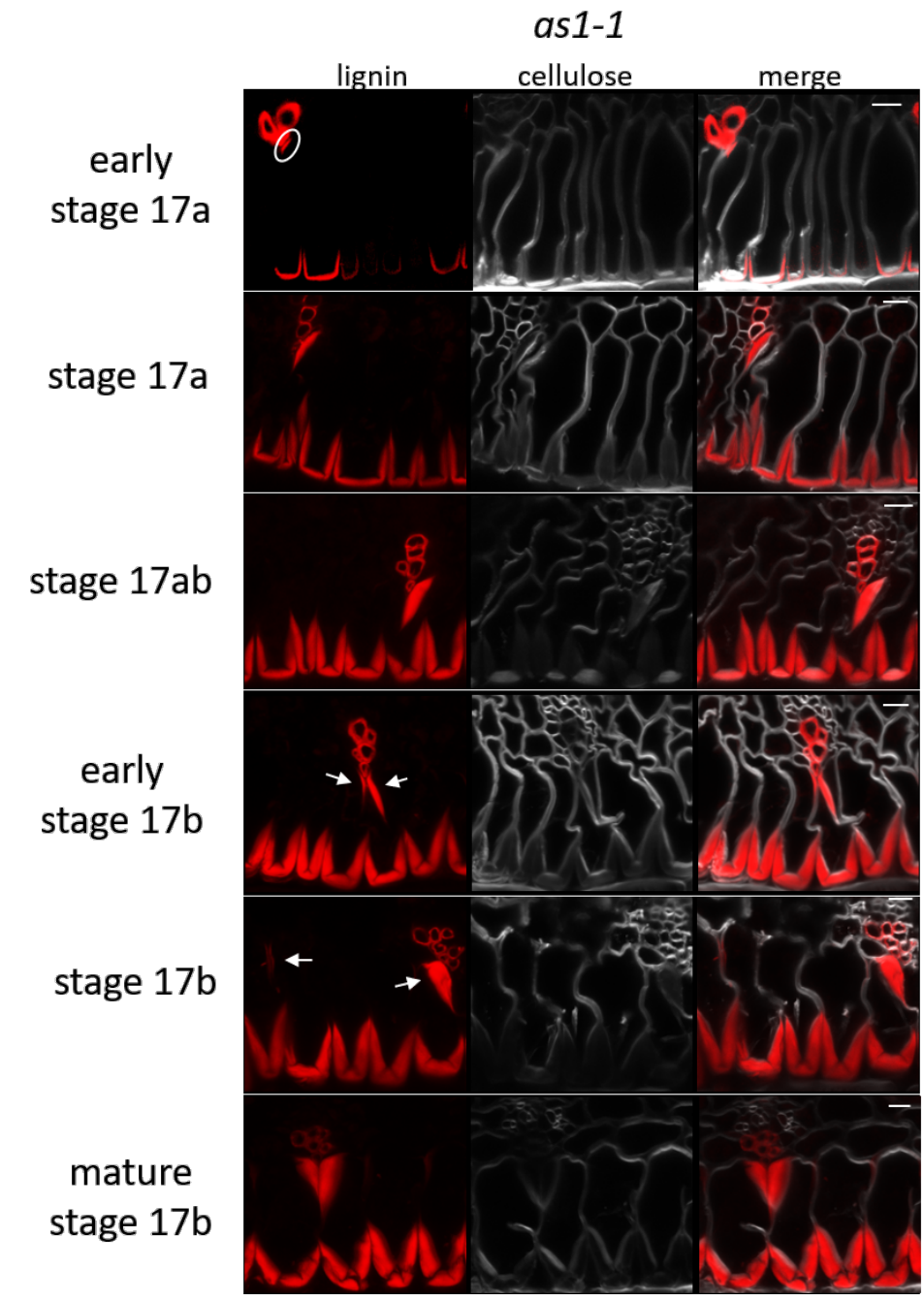

Figure 20. Confocal images of fruit cross-sections from fruit of one plant. Endogenous lignin in wild type (A) and *as-1* (B) develops similar. It initiates in the U-shape and then thickens, forming also the hinges. Abaxial ectopic lignin in *as1-1* initiates with the endogenous lignin (circled), but also later (arrows indicate different initiation stages). Lateral ectopic lignin initiates later than endogenous lignin. Lignin stained with Basic Fuchsin (red), cellulose stained with Calcofluor White (gray). Scale bar 10 μm.

3.2.3 RNA-seq of *as1-1*

To investigate the transcriptome of *as1-1* vs wild-type fruit valves, I performed RNA-sequencing (RNA-seq) of valves removed from stage 17a fruit. At this stage of fruit development, lignification of the endocarp*b* SCW has started in both genotypes (Figure 20).

The tissue harvesting, RNA extractions, sample submission to the MPIPZ Genome Center, and read alignment, and quality control analysis were performed together with Dr. Erin Cullen. RNA was extracted from approximately 22 pooled valves for three biological replicates. Library preparation and RNA sequencing on an Illumina NovaSeq6000 platform was performed by the MPIPZ Genome Center and Novogene. It was a strand-specific transcriptome library, and 2x150bp paired-end sequencing reads. Requested were 6 Gb data per sample. I performed quality control of the reads with FastQC (Bioinformatics), adapter trimming with cutadapt (Martin, 2011), alignment to the *C. hirsuta* reference genome (Gan et al., 2016) with hisat2 (Kim et al., 2019), ordering and indexing of the aligned reads with samtools (Li, 2011), and quantification of reads with htseq (Anders et al., 2014). The read count data of the two genotypes and the three replicates each were merged into one file. I performed differential gene expression analysis with DESeq2 in R (Anders and Huber, 2010).

To assess the quality of my RNA-seq data, I visualized similarity between replicates using principal component analysis (PCA) and hierarchical clustering (Figure 21). These analyses showed that the variance in my data was almost entirely explained by genotype and none of my biological replicates should be considered as outliers.

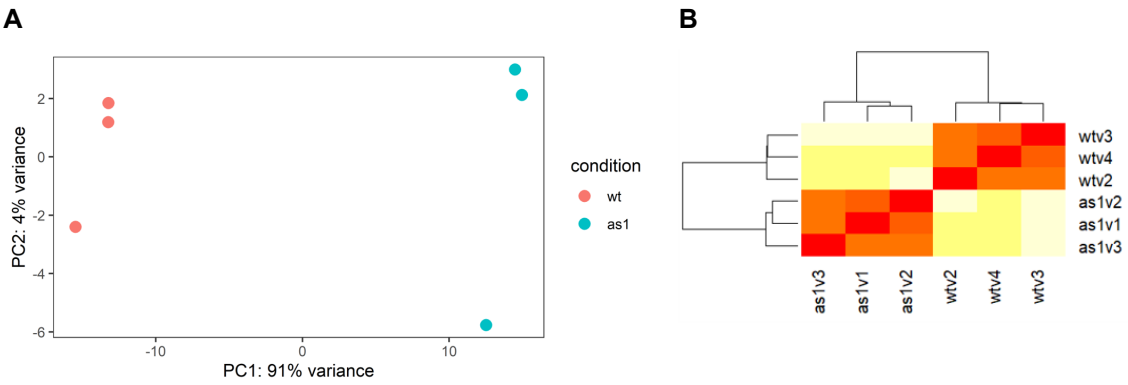

Figure 21. Quality assessment of RNA sequencing data. Principal component analysis (A) and hierarchical clustering (B) show similarity between biological replicates of *as1-1* (as1) and wild type (wt).

I found 2302 differentially expressed genes (DEGs) between wild type and *as1-1* fruit valves when using the criteria of an adjusted p-value < 0.05 and log2 fold change < |1|. Of these DEGs, 1081 genes were upregulated and 1221 genes downregulated in *as1-1*. These results are plotted as log2 fold change in a volcano plot with genes of interest highlighted in red (Figure 22). One of the most highly upregulated DEGs is the *KNOX1* homeobox gene *BP* (Figure 22). Two other *KNOX1* homeobox genes, *KNAT2* and *KNAT6*, were also upregulated DEGs in *as1-1* fruit valves (Figure 22). AS1 acts as a negative regulator of these three *KNOX1* genes: *BP, KNAT2* and *KNAT6*, in lateral organs, such as leaves, in both *A. thaliana* and *C. hirsuta* (Byrne et al., 2000; Ori et al., 2000; Hay and Tsiantis, 2006; Rast-Somssich et al., 2015). Therefore, this result suggests that AS1 likely represses *BP, KNAT2* and *KNAT6* gene expression in *C. hirsuta* fruit valves.

I also found that two key regulators of SCW biosynthesis, *NST3* and *MYB46*, were upregulated DEGs in *as1-1* fruit valves (Figure 22). Other upregulated SCW-related genes included the NAC transcription factor *VND6*, two peroxidases *PER64* and *PRX71*, and two laccases *LAC10* and *LAC16* (Figure 22). Other genes involved in lignin biosynthesis and polymerization were downregulated in *as1-1* valves. Among these DEGs were two laccases, *LAC4* and *LAC17*, which are both required for endocarp*b* SCW lignification in *C. hirsuta* (Pérez-Antón et al., 2022), and two genes involved in the phenylpropanoid pathway, *PAL1* and *C4H* (Figure 22).

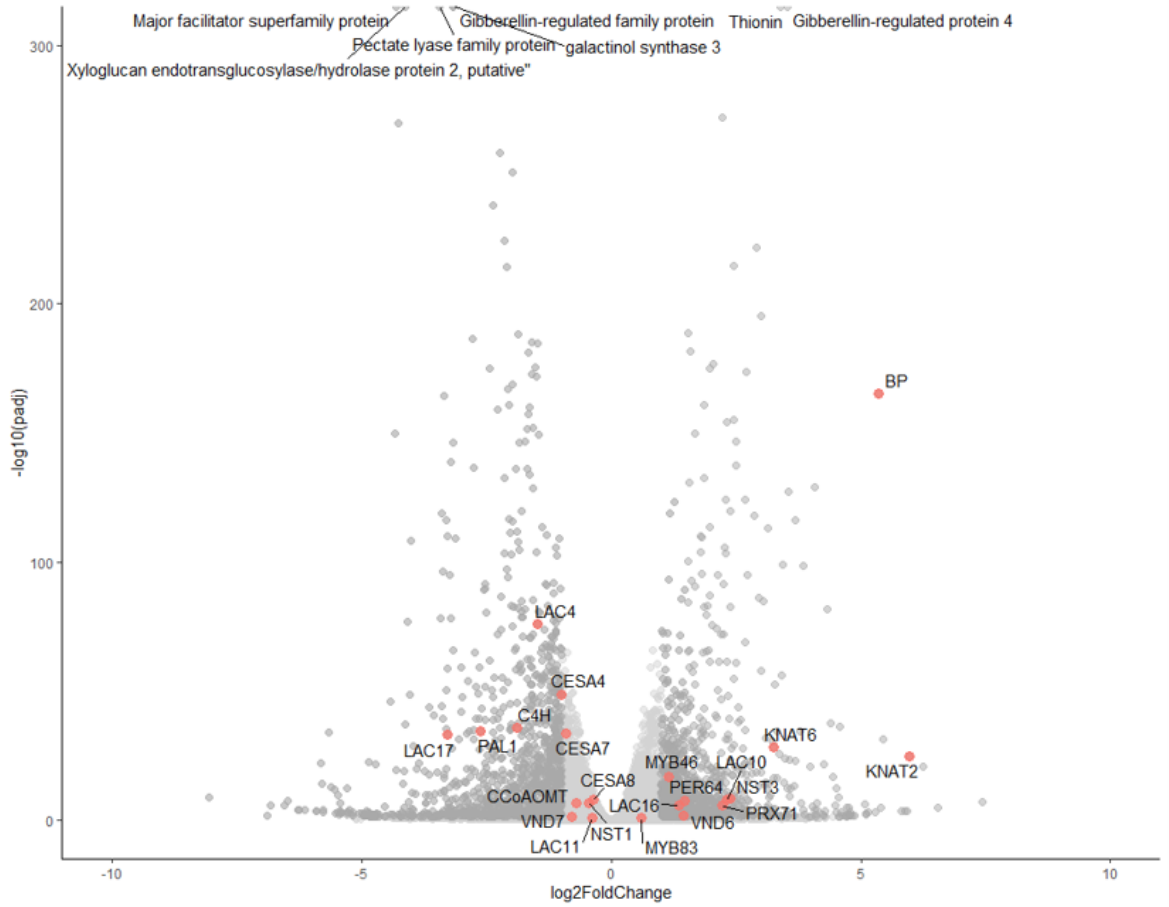

Figure 22. Differential gene expression between wild type and *as1-1*. Volcano plot showing differential expression of genes between *as1-1* and wild type valves as log2 fold change. In dark grey, genes with adjusted p-value < 0.05 and log2 fold change < |1|. Several differentially expressed genes related to lignin biosynthesis or *KNOX1* genes are highlighted in red.

To gain insight into the biological processes affected by differential gene expression in *as1-1* fruit valves, I performed gene ontology (GO) analysis. I used ClusterProfiler (Yu et al., 2012) to plot the GO terms enriched amongst the DEGs upregulated in *as1-1* (Figure 23). For GO analysis, I used genes with *A. thaliana* orthologs identified by reciprocal best BLAST (Gan et al., 2016). I found terms related to cell cycle and microtubules were enriched, as well as cell wall-related terms including pectin, cell wall loosening and cell wall biogenesis (Figure 23). To gain further insight, I plotted the upregulated DEGs associated with the four GO terms highlighted by boxes in Figure 24. Genes associated with the GO term cell wall biogenesis, included *NST3, MYB46, LAC10* and several hemicellulose genes, such as *GALS1, GALS3, AtXTH3* and *AtXTH22* (Figure 24). Genes associated with the GO term pectin, included the

pectin methylesterase genes *PME5* and *PME35* (Figure 24). Genes associated with the GO term cell wall loosening, included 10 expansin genes (Figure 24). Genes associated with the GO term microtubule cytokeleton organization, included tubulins, kinesins and kinases (Figure 24). In summary, the RNA-seq data showed that microtubule and cell wall remodeling processes are upregulated in addition to SCW biosynthesis in *as1-1* fruit valves.

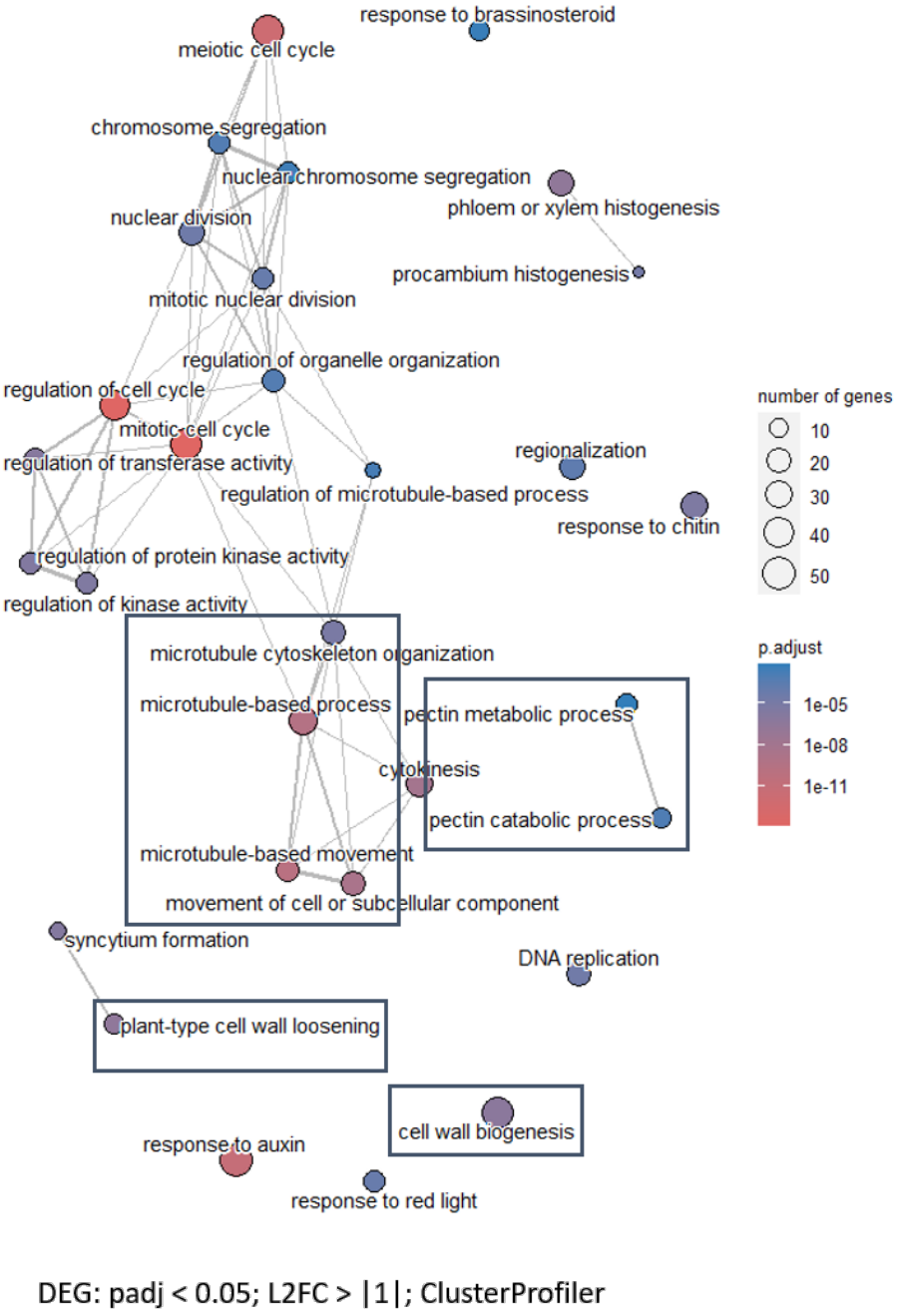

Figure 23. Differential gene expression between wild type and *as1-1*. Gene ontology enrichment map of upregulated genes in *as1-1*. Among them microtubule, pectin and cell wall loosening related processes.

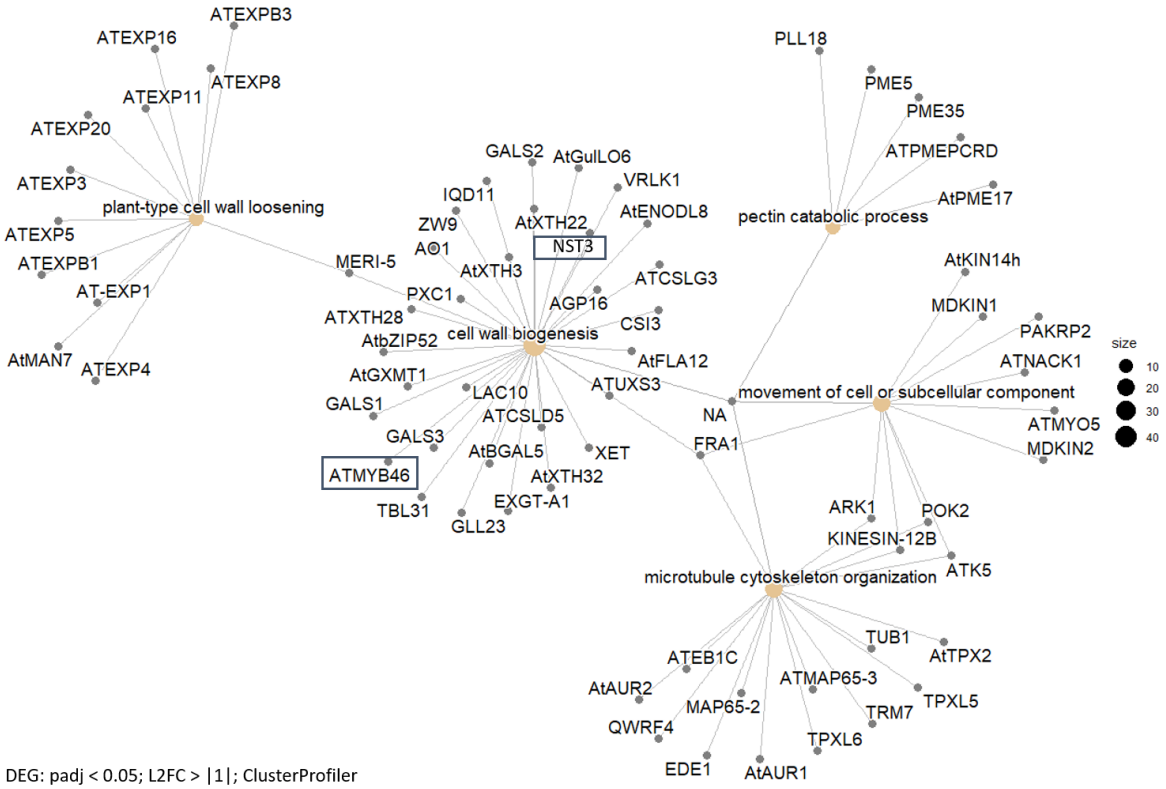

Figure 24. Differential gene expression between wild type and *as1-1*. Network of genes associated with the gene ontology cell wall. Among them the SCW biosynthesis transcription factors *NST3* and *MYB46*.

qRT-PCR validation

To validate whether key genes from the RNA-seq data were upregulated in *as1-1* fruit valves, I used quantitative reverse transcriptase PCR (qRT-PCR) on cDNA synthesized from RNA extracted from stage 17a valves. I analyzed the data using the $\Delta\Delta$Ct method with Clathrin as housekeeping gene (Pfaffl, 2001). I also compared the results from *as1-1*, with *as1-3* and *pat63* fruit valves. I analyzed gene expression of the three *KNOX1* genes, *BP, KNAT2* and *KNAT6*, and the SCW transcription factor genes *NST3* and *MYB46*. In *as1-1* and *as1-3*, transcripts of the three *KNOX1* genes and *NST3* were significantly upregulated compared to wild type (Figure 25). I also validated that *MYB46* transcripts were upregulated in *as1-1*, but not *as1-3* (Figure 25). Interestingly, none of these genes were upregulated in *pat63* fruit valves, only *KNAT6* gene expression was significantly changed and it was downregulated in *pat63* (Figure 25).

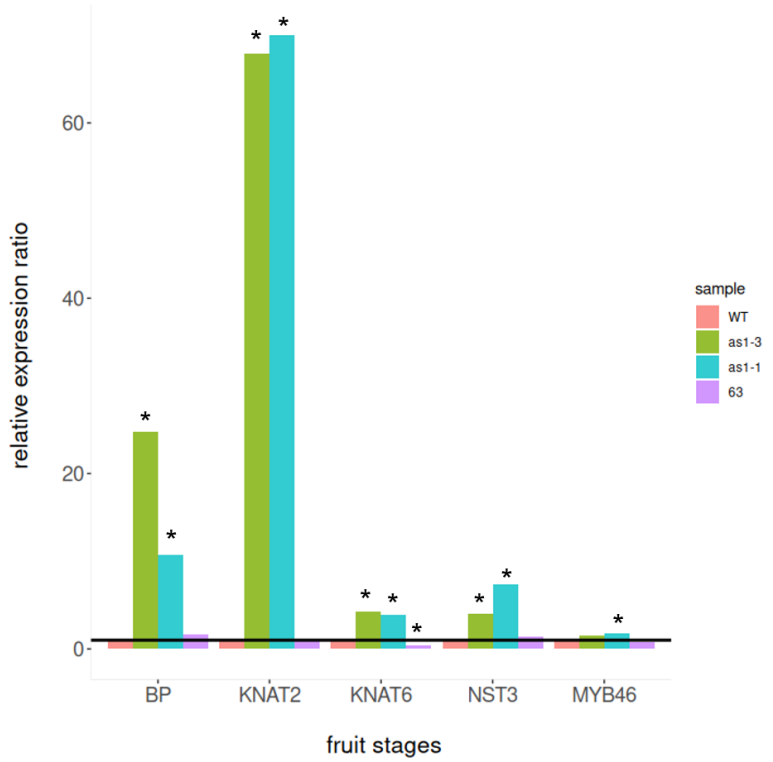

Figure 25. Relative expression levels of wild type, *as1-3*, *as1-1* and *pat63* for the transcripts *BP, KNAT2, KNAT6, NST3,* and *MYB46.*
Significant different expression levels compared to wild type are marked with an asterisks (*). The p-values calculated with a Student's t-test for*BP* *as1-3* 0.0017, *as1-1* 0.0023 and *pat63* 0.155. The p-values for*KNAT2* *as1-3* 0.0032, *as1-1* 0.00096 and *pat63* 0.763. The p-values for*KNAT6* *as1-3* 0.024, *as1-1* 0.036 and *pat63* 0.00006. The p-values for*NST3* *as1-3* 0.0085, *as1-1* 0.0038 and *pat63* 0.251. The p-values for*MYB46* *as1-3* 0.595, *as1-1* 0.009 and *pat63* 0.281. Three biological replicates per genotype, except for *as1-3* only two biological replicates.

3.2.4 Localization of AS1 and BP is complementary in fruit tissue

To investigate the expression and localization patterns of *AS1* and *BP* in the fruit, I used transcriptional and translational reporter lines. For *BP* I used the transgenic lines *pBP::3xVenus* and *pBP::BP:Venus* from Rast-Somssich *et al.* 2015, both in wild type background. The translational reporter for *AS1* was generated by Dr. Yi Wang and transformed into *as1-1* (*pAS1::AS1:Venus;as1-1*) and is therefore a complementation line. I generated the *AS1* transcriptional reporter and transformed it into wild type background (*pAS1::NLS:3xGFP*). I observed expression in the outer epidermal cells of fruit late stage 16.

AS1 is expressed and localized in the valve (Figure 26). While *BP* is expressed and localized in the replum (Figure 26). This complementary localization in the fruit tissue is also reported

in *A. thaliana* fruit (Alonso-Cantabrana et al., 2007) and supports the AS1 function to repress *BP* in the valve.

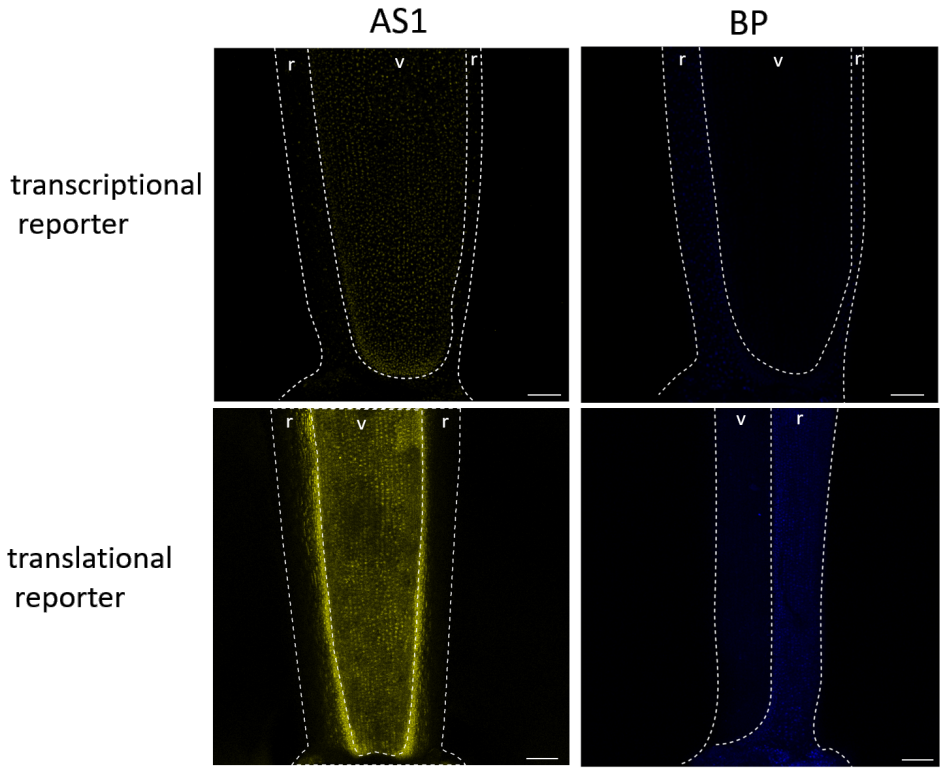

Figure 26. Expression and localization of *AS1* (yellow) and *BP* (blue). *AS1* and *BP* have a complementary expression pattern in the fruit. *AS1* is expressed and localizes in the valve, while *BP* is expressed and localizes in the replum. Confocal images of whole fruit late stage 16. The fruit is outlined by dashed white lines and the valve (v) and replum (r) labeled. Scale bar 100 μm.

I used the complementation line *pAS1::AS1:YFP;as1-1* to observe if *AS1* complements the *as1-1* phenotypes. I observed 4 independent lines, in all was the leaf phenotype fully complemented. However, the ectopic lignin was only partially complemented. I quantified two independent lines (lines 1 and 4), including segregating (T_2 4) and homozygous (T_4 4.1) individuals for line 4. Although all lines had significantly reduced ectopic lignin in endocarp*b* cells compared to *as1-1*, it was still significantly more ectopic lignin than in wild type (Figure 27). The significance was calculated with ANOVA and Tukey post-hoch test using R. This results suggest that the ectopic lignin in endocarp*b* cells is not only caused by loss of *AS1*. A possibility would be that a mutation in the background of *as1-1* modifies the ectopic lignin phenotype. An additional mutation would also explain the differences between the two *as1* alleles.

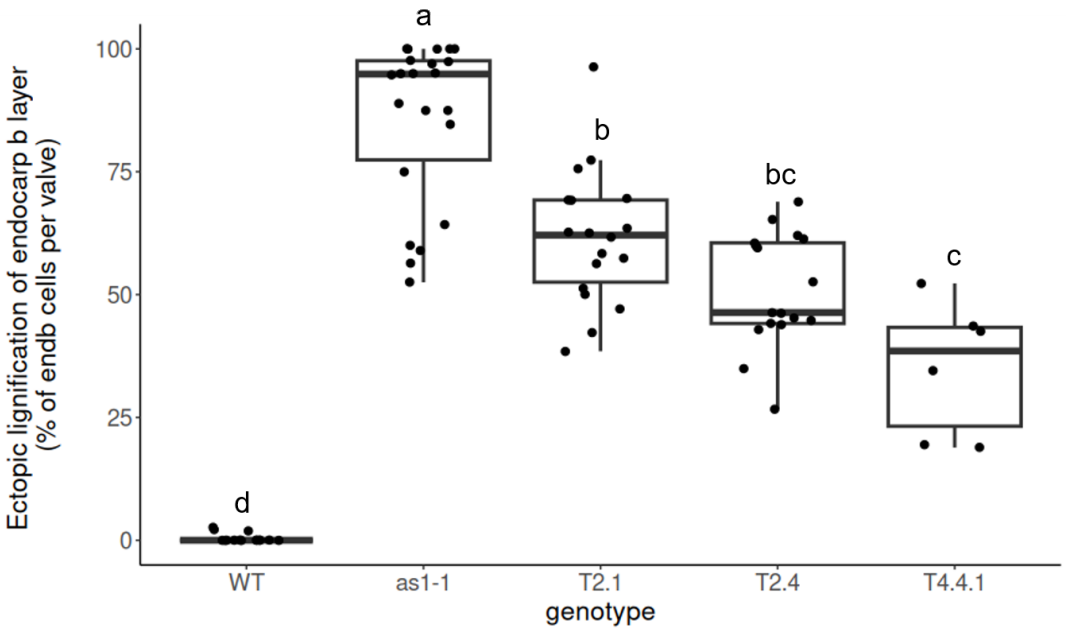

Figure 27. Lignin quantification of *as1-1* and *pAS1::AS1:YFP;as1-1* complementation lines. Quantification of endocarp*b* cells with ectopic lignin divided by endocarp*b* cells. The means are the following: wild type 0.45 %, *as1-1* 85.80 %, T_2 1 61.59 %, T_2 4 50.89 %, T_4 4.1 35.20 %. Different letters denote statistically significant differences ($p < 0.05$) between means based on ANOVA (Tukey's HSD). n valves: wild type 18, *as1-1* 79, T_2 1 18, T_2 4 17, T_4 4.1 6.

3.2.5 Ectopic expression of *BP*

To investigate whether the ectopic expression of *BP* in *as1* fruit valves could contribute to the phenotype of ectopic endocarp*b* lignin, I generated transgenic lines to mis-express *BP* in wild-type fruit valves. To express *BP* in endocarp*b* cells I used the promoter of *PER66* (Pérez-Antón et al., 2022) (*pPER66::gBP:mNeonGreen*), and to express *BP* throughout the valve I used the promoter of *FUL* (Galstyan et al., 2021) (*pFUL::gBP:mNeonGreen*). I observed 15 T_1 lines of *pPER66::gBP:mNG*, of which three had no ectopic lignin, and 12 lines had ectopic lignin in endocarp*b* cells (Figure 28). Most commonly, this was thin ectopic lignin in either lateral positions (four lines) or around the whole cell (7 lines). In five transgenic lines, I observed thick ectopic lignin in abaxial positions, mirroring the endogenous lignin (Figure 28). I observed 16 T_1 lines of *pFUL::gBP:mNG*, of which two had no ectopic lignin, and 14 lines had ectopic lignin in endocarp*b* cells (Figure 28). Two of these lines also had ectopic lignin rarely in small mesocarp cells. In summary, ectopic expression of *BP* is sufficient to cause

ectopic lignin in endocarp*b* cells.

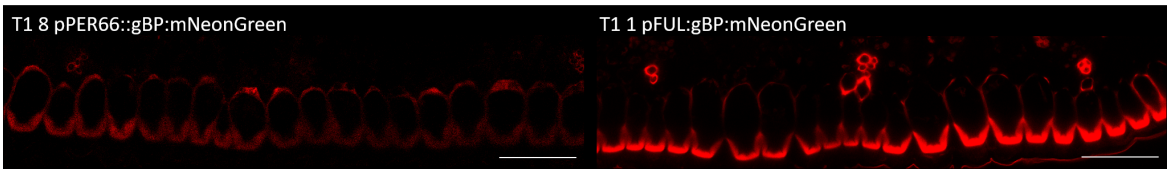

Figure 28. Exemplary confocal images of T_1 lines of *pPER66::gBP:mNeonGreen* and *pFUL::gBP:mNeonGreen*. The depicted images belong to lines with more ectopic lignin compared to other lines. Both have thin whole ectopic lignin. Lignin autofluorescence (*pPER66::gBP:mNeonGreen*) or stained with Basic Fuchsin (*pFUL::gBP:mNeonGreen*) (red). Scale bar 50 μm

3.2.6 Allelism test of *as1-1* and mutant *pat63*

Given the many similarities between the fruit phenotypes of *as1-1* and *pat63*, I performed an allelism test by crossing these two mutants (Figure 29). To check whether *pat63* is a recessive allele, I first crossed *pat63* to wild type and observed segregation in 124 F_2 plants. I observed 91 wild type progeny and 33 had the *pat63* phenotype. This closely fits the expected number of 31 homozygous mutants for a recessive mutation. I used a Chi-square test to support the conclusion that these results fit segregation for a recessive mutant. Therefore, *pat63* is a recessive allele. I then crossed *as1-1* and *pat63* homozygous mutants and observed the F_1 phenotype. A well described phenotype for *as1-1* is its leaf morphology with a compressed rachis and aberrant leaflet positioning (Rast-Somssich et al., 2015) (Figure 29A). In contrast to this, *pat63* leaves are wild type in morphology (Figure 29A). The F_1 progeny of *as1-1* x *pat63* also have wild type-like leaves (Figure 29A). The interpretation from this observation is that the *as1-1* leaf phenotype is complemented, therefore *pat63* is not an allele of the *AS1* gene.
As I showed previously, the fruit length of both *as1-1* and *pat63* is similarly reduced (Figure 19 and Figure 29B). The F_1 progeny of *as1-1* x *pat63* also had short fruit (Figure 29B). This result can be interpreted that *pat63* fails to complement the *as1-1* fruit phenotype, therefore *pat63* is an allele of the *AS1* gene.
Since the ectopic endocarp*b* lignin in *as1-1* and *pat63* is the phenotype that I am interested in, I observed sections of mature fruit of the F_1 progeny of *as1-1* x *pat63* under the confocal (Figure 29C). I found that the F_1 progeny of *as1-1* x *pat63* also had ectopic endocarp*b* lignin

(Figure 29C). This result also suggests that *pat63* is an allele of the *AS1* gene.

The contradictory results from analyzing the leaf and fruit phenotypes in this allelism test are inconclusive. However, one interpretation is that *as1-1* has a second mutation that causes the short fruit and ectopic lignin phenotype, while the mutation in *AS1* causes the leaf phenotype. In this scenario, the background mutation is allelic to *pat63*. This would explain why *pat63* complements the leaf phenotype of *as1-1*, but fails to complement the fruit length and ectopic lignin phenotypes.

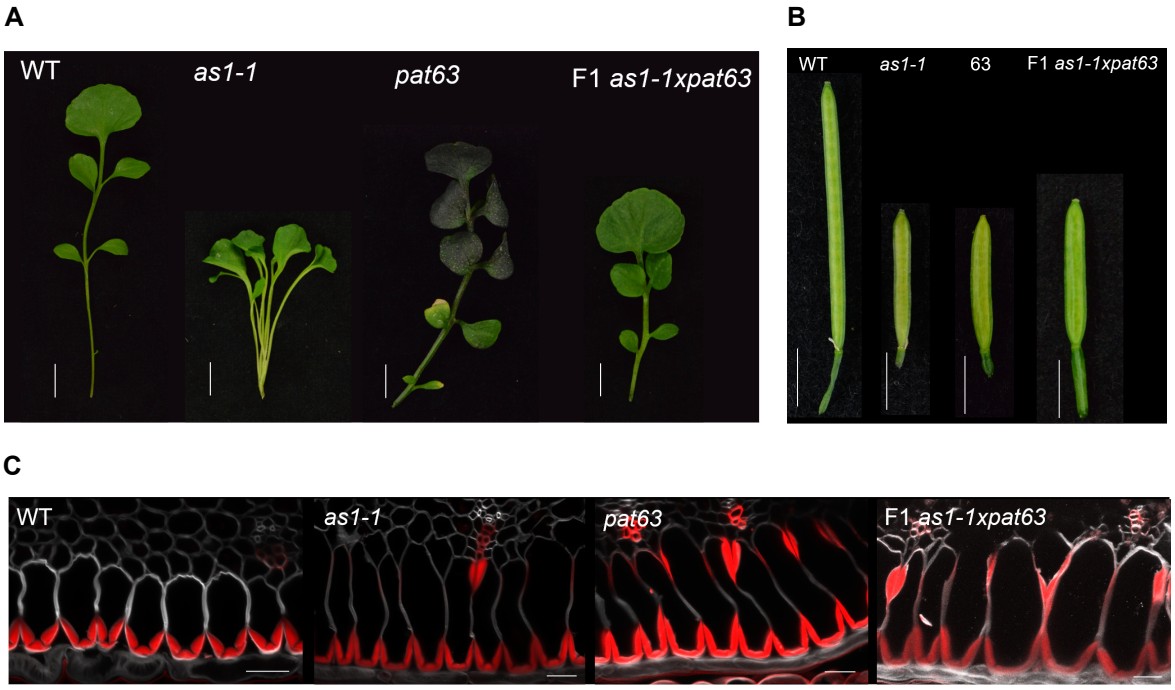

Figure 29. Allelism test of *as1-1* and *pat63* suggests that *as1-1* has a second mutation that is allelic to *pat63*.
A: Leaf phenotypes of wild type, *as1-1*, *pat63*, and F_1 *as1-1 x pat63*. The cross F_1 *as1-1xpat63* does not have the typical *as1* leaf phenotype, but wild type like leaves. Scale bar 1 cm. B: Fruit phenotypes of wild type, *as1-1*, *pat63*, and F_1 *as1-1 x pat63*. F_1 *as1-1 x pat63* fruit resembles *as1-1* and *pat63* fruit. Scale bar 5 mm. C: Confocal images of wild type, *as1-1*, *pat63*, and F_1 *as1-1 x pat63* fruit stage 17b. *as1-1*, *pat63*, and F_1 *as1-1 x pat63* have ectopic lignin in endocar*b* fruit. Lignin stained with Basic Fuchsin (red) and cellulose stained with Calcofluor White (gray). Scale bar 20 μm.

3.2.7 Mapping by sequencing of *pat63*

The results from this chapter indicate that *pat63* has an interesting phenotype that may give insight into the regulation of endocarp*b* SCW pattering in the explosive fruit of *C. hirsuta*.

Moreover, the inconclusive results of the allelism test with *as1-1* means that I need an alternative experimental approach to address whether *pat63* is an allele of *AS1*. For these reasons, I wanted to identify the genetic basis of *pat63*. Therefore, I used a bulked segregant approach called mapping-by-sequencing to genetically map *pat63* using short-read sequencing (Schneeberger, 2014).

This methodology combines genetic linkage (the closer two loci are, the more likely are they inherited together) and bulk segregant analysis with whole-genome re-sequencing. It highlights sequence differences between the mapping population and the reference genome. Different mapping populations can be used, but I chose the F_2 generation of a backcross. To do so, I backcrossed a homozygous *pat63* to *C. hirsuta* Oxford, the mutant background, so that all sequence differences between the mapping population and the reference wild type genome are EMS derived. In the segregating F_2 population the plants with mutant phenotype are identified and plant material collected. The genomic DNA of mutant plants is pooled and their whole genome re-sequenced. Since the plants were selected for the causal mutation we expect to observe an increase of EMS derived single nucleotide polymorphisms (SNPs), around that locus. In contrast, a random allele frequency distribution of EMS derived and wild type SNPs is expected in other regions of the genome (James et al., 2013). Easymap provides an easy and efficient way to analyze next generation sequencing data from mapping-by-sequencing experiments and point out a region in which the causal mutation is located (Lup et al., 2021).

From my backcross of *pat63* to wild type, the F_1 progeny self-fertilized. In the segregating F_2 population, out of 124 F_2 plants, 91 were wild type and 33 had the *pat63* phenotype, as explained in section 3.2.6. I pooled genomic DNA extracted from 32 *pat63* mutants. For short-read sequencing, one genomic DNA library for the mutant pool was prepared and sequenced by Illumina NextSeq2000 sequencing with 2x150 bp paired-end reads at the MPIPZ Genome Center. I used the Easymap software to analyze this bulked segregant sequence data (Lup et al., 2021), using the reference *C. hirsuta* genome as control (Gan et al., 2016). Single nucleotide polymorphisms (SNPs) derived from EMS mutations in the *pat63* sequence reads

were identified. A region on chromosome 6 showed a high frequency of EMS alleles from the *pat63* parent, suggesting that the *pat63* locus is located on chromosome 6. The Easymap software highlighted a region from 8.5 to 12.5 Mb containing the probable location of the *pat63* locus (Figure 30). *AS1* is located on chromosome 4 18.374311 to 18.377717 Mb (Gan et al., 2016). Therefore, *pat63* is not an allele of the *AS1* gene.

Since I identified a large chromosomal region using mapping-by-sequencing, I needed to confirm these mapping results and narrow down a smaller genetic interval containing the *pat63* locus by fine mapping. To do this, I designed cleaved amplified polymorphic sequence (CAPS) markers for EMS derived SNPs on chromosome 6 in the region 4.5 to 12.5 Mb. So far, I could only test one marker on 32 individual *pat63* mutants from the F_2 mapping population used for mapping-by-sequencing. This marker was located around 7.6 Mb on chromosome 6 (7699239 bp). After PCR amplification and restriction enzyme digestion of the amplicon, I was able to identify alleles derived from both the wild type and *pat63* parents (Figure 31). Since two individuals did not have a PCR product, likely due to low DNA concentrations, I had mapping information for 30 individuals. One individual had a heterozygous genotype (#28, Figure 31), indicating a single recombination event between this marker and *pat63*. All other individuals were homozygous for the mutant allele, indicating no recombination. This gives a recombination frequency of 1.67 %, indicating that this marker is closely linked to the *pat63* locus (Figure 31). Therefore, I confirmed that *pat63* is located on chromosome 6 at a position 1.67 cM on either side of a marker at 7.6 Mb. This mapping results provides a starting point for future work to eventually identify the causal gene underlying the *pat63* mutant phenotype.

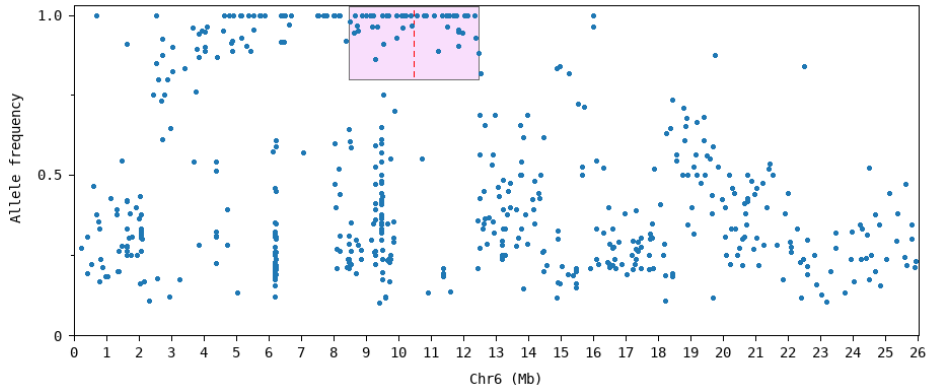

Figure 30. Allele frequency of SNPs identified with easymap (Lup et al., 2021) across chromosome 6 in mapping-by-sequencing experiment. The candidate region for the causal mutation of *pat63* is located on chromosome 6 and highlighted with a box in light pink, from 8.5 to 12.5 Mb.

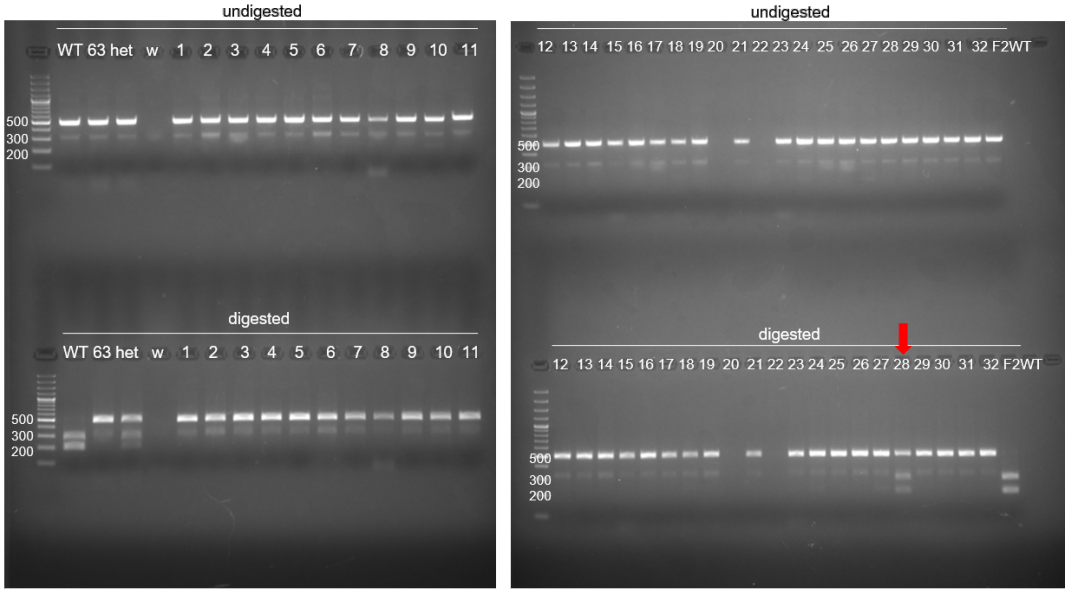

Figure 31. Gel of CAPS primer for SNP at region 7.6 Mb. Amplification product has 499 bp (upper rows). After digestion with MboI (lower rows), wild type is digested into 206 bp and 297 bp fragments. Controls are wild type (WT), homozygous *pat63*, a mix of wild type and *pat63* as heterozygous, and water control (w). Individuals from F_2 *pat66 x Oxf* mapping population with *pat63* phenotype (1-32) were tested. An additional control wild type phenotype (F2WT) is included. Except for #28 which is heterozygous, the other individuals are homozygous for *pat63*. 100 bp Plus DNA ladder.

3.3 Discussion

In this chapter, I analyzed three mutant alleles with thick ectopic lignin, mirroring the endogenous patten of endocarp*b* lignin on the opposite side of the cell. In all of these mutants, explosive coiling of the fruit valves was reduced. Two of these mutants were alleles of the Myb transcription factor-encoding gene *AS1* (*as1-1* and *as1-3*) and the third mutant was *pat63*. I identified many similarities between these mutants. However, I mapped *pat63* to a distinct genome location, showing that it is not an allele of *AS1*. Therefore, I identified and characterized two different regulators of endocarp*b* SCW patterning in *C. hirsuta* fruit.

Both *as1-1* and *pat63* had significantly more ectopic lignin than wild type. *pat63* had more thick ectopic lignin in an abaxial position in the cell, while *as1-1* had more thin ectopic lignin in lateral positions in the cell. Therefore, *AS1* and the gene underlying *pat63* could affect different processes that cause ectopic endocarp*b* lignin in each mutant. Although *as1-3* is a stronger allele than *as1-1* and shows thick ectopic lignin in endocarp*b* cells, this phenotype is not as frequent as in *as1-1*. An allelism test between *as1-1* and *pat63* gave F_1 plants where the *as1-1* leaf phenotype was complemented to wild type, indicating that *pat63* is not an *AS1* allele.

However, fruit phenotypes in the F_1 plants of the cross between *as1-1* and *pat63* were mutant, not wild type, indicating that *pat63* and *as1-1* were allelic. This result also matched the observation that transgenic complementation of *as1-1* with a *pAS1::AS1:YFP* transgene fully complemented the leaf phenotype, but only partially complemented the ectopic endocarp*b* lignin phenotype. One interpretation of these confusing results is that *as1-1* contains a second background mutation that is a *pat63* allele. This can be tested once the gene responsible for the *pat63* mutant phenotype has been identified. For example, the gene mutated in *pat63* can be sequenced in *as1-1* to check whether it is also mutated in the *as1-1* background.

By mapping-by-sequencing and fine-mapping, I mapped the *pat63* locus to chromosome 6, 1.67 cM from a marker at position 7.6 Mb. This position differs from the location of *AS1* on chromosome 4, confirming that *pat63* is not allelic to *AS1*. Future work to further fine-map *pat63* will define a genetic interval containing the gene and is likely to identify candidates for

the causal gene that can be tested by transgenic complementation of *pat63*.

I characterized formation of the lignified SCW in endocarp*b* cells during fruit development in wild type and *as1-1* (which may contain a second mutation in *pat63* as described above). Both the endogenous and ectopic lignin in *as1-1* showed a similar developmental progression to wild type. However, the thin ectopic lignin in lateral positions initiated after the endogenous lignin had already formed. RNA-seq in stage 17a fruit valves of this same genotype showed upregulation of two key SCW biosynthesis genes, *NST3* and *MYB46*, in *as1-1* (Kumar et al., 2015). Interestingly, the three laccases required to polymerize lignin in *C. hirsuta* endocarp*b* cells were not upregulated (Pérez-Antón et al., 2022). This may indicate that the overall amount of lignin is not significantly increased in endocarp*b* cells in *as1-1*, but just differentially deposited. A biochemical analysis to compare the cell wall of *as1-1* vs wild-type valves could test this.

Other genes upregulated in *as1-1* fruit valves were associated with microtubule organization. Microtubule density and alignment is important to guide cellulose synthesis in the primary cell wall and also for patterning in the SCW (Takenaka et al., 2018; Paredez et al., 2006). Expansin genes were also upregulated in *as1-1* fruit valves. Expansins are important for loosening the primary cell wall during growth. Changes in primary cell wall components may also affect SCW formation; for example, changes to cell wall integrity can trigger SCW formation, and cell wall restructuring can allow better connections between the primary and SCW by creating anchoring domains for SCW biosynthesis genes (Kushwah et al., 2020; Bourquin et al., 2002; Francoz et al., 2019). In this way, primary cell wall components could be involved in ectopic lignin formation in the endocarp*b* of *as1-1*.

Three *KNOX1* genes were upregulated in *as1-1* fruit valves. AS1 has the conserved function to downregulate these three *KNOX1* genes: *BP*, *KNAT2* and *KNAT6*, in lateral organs of *A. thaliana* and *C. hirsuta* (Guo et al., 2008; Ikezaki et al., 2010; Hay and Tsiantis, 2006). These three *KNOX1* genes were upregulated in *as1-3*, but not *pat63* fruit valves. The SCW regulator *NST3* was also upregulated in *as1-3*, but not *pat63* valves. This result also suggests that *AS1* and the gene responsible for *pat63* represent different pathways that regulate endocarp*b*

SCW patterning in *C. hirsuta* fruit.

I also confirmed that *BP* mis-expression in the fruit valve was sufficient to cause ectopic endocarp*b* lignin. Transgenic lines expressing *BP* either throughout the valve or more specifically in the endocarp*b*, caused ectopic lignin in endocarp*b* cells. These results suggest that the upregulation of *BP* in *as1* valves could contribute to the ectopic endocarp*b* lignin. However, further genetic analyses are needed to confirm this, such as analyzing the fruit valves of *as1;bp* double mutants.

In this chapter I characterized three mutants with ectopic endocarp*b* lignin, including two *as1* alleles. Expression of the master SCW regulator *NST3* was significantly upregulated in *as1* fruit valves. Therefore, in the next chapter I analyzed the function of *NST3* and its paralog *NST1* in endocarp*b* SCW formation in *C. hirsuta* fruit.

4 The roles of *NST1* and *NST3* in *C. hirsuta*

4.1 Introduction

NST1 and NST3 redundantly regulate the SCW biosynthesis in endocarp*b* cells in *A. thaliana* (Mitsuda and Ohme-Takagi, 2008). In my *as1* mutants, I found a significant upregulation of *NST3*, which could have a role in the ectopic lignin in these mutants. Therefore, I focus in this chapter on the role of *NST3* in endocarp*b* lignification in *C. hirsuta* and the effect of SCW pathway upregulation.

In *A. thaliana*, NST1 and NST3 act often redundantly in SCW formation, as seen in fiber SCW formation (Mitsuda et al., 2007). In Arabidopsis fruit, both genes are expressed in the endocarp*b* layer and in the vascular cells of the replum. Only *NST1* is expressed in the lignified layer of the valve margin. The valve margin consists of two layers, the lignified layer that has lignified SCWs and provides stiffness and the separation layer that secrets cell wall degrading enzymes to loosen the cell wall and allow dehiscence (Ferrandiz, 2002). Loss of *NST1* results in loss of SCW in valve margin cells, but endocarp*b* lignin is deposited. The fruit are indehiscent due to the lack of SCW in the lignified layer. Therefore, SCW in the valve margin is required for dehiscence in *A. thaliana*. No fruit phenotype for *NST3* was found. In the double mutant *nst1;nst3*, however, all SCWs were missing, except for those of the vascular vessels. The fruit were indehiscent, though the valve margin cell types specified properly (Mitsuda and Ohme-Takagi, 2008).

MYB46 is a direct target of NST1 and NST3 and is also regulated by VND6 and VND7. MYB46 also acts as a master switch of SCW biosynthesis (Kumar et al., 2015). Dominant repression of *MYB46* drastically reduces SCW deposition in fibers and vessels, while constitutive expression results in ectopic SCW deposition and stunted growth. This ectopic SCW was deposited in patterns also observed from vessel and fiber cells, such as annular, spiraled, reticulated and pitted. This different patterns were observed in the normally non-lignified cells. Depending on the cell type different patterns were observed (Zhong et al., 2007). MYB46 induces the expression of several transcription factors of the SCW pathway, but also directly activates

biosynthetic genes, like the *CESAs* involved in SCW formation (*CESA4*, *CESA7*, and *CESA8*), genes of the phenylpropanoid pathway, and genes involved in xylan biosynthesis (Kim et al., 2014). MYB46 acts redundantly with MYB83, another direct target of NST1, NST3, VND6, and VND7 (McCarthy et al., 2009).

Overexpression of *MYB46* can lead to ectopic SCW deposition in *A. thaliana*. In *C. hirsuta* it was shown that prolonged dexamethasone-mediated induction of *LAC11* in *C. hirsuta* triple mutant *lac4;lac11;lac17* background rescued the lignification of endocarp*b* cells. Moreover, LAC11 localized to the lateral and abaxial cell walls of endocarp*b* cells and polymerized lignin in these positions. Therefore, ectopic expression of laccases can cause ectopic lignin (Pérez-Antón et al., 2022).

In this chapter, I analyzed single and double mutants of *NST1* and *NST3* in *C. hirsuta*. I also characterized *NST3* and *MYB46* expression. The findings provide insights into SCW patterning in endocarp*b* cells.

4.2 Results

4.2.1 Generation of single and double mutants of *NST1* and *NST3*

In order to understand how *NST1* and *NST3* contribute to fruit lignification in C. hirsuta, I created single and double mutants using CRISPR/Cas9 gene editing. I selected 45 transgenic seeds in the T_1 generation based on seed coat fluorescence (pOLE1::OLE1:RFP marker, (Shimada et al., 2010)) and Sanger sequenced the regions around the sgRNAs in each of these independent transgenic lines. I analyzed the sequence chromatograms using ice.synthego (Synthego) to accurately identify gene edits. Out of the 45 T_1 lines, one was heterozygous for gene edits in *NST1* and *NST3* (line T_1-35). However, this plant had fertility issues and did not produce selfed seed. To propagate this line, I made a cross using wild-type pollen, and also made clonal cuttings of side stems of the plant, which produced some seed. I repeated the Sanger sequence analysis again in fluorescent seed from the selfed progeny of T_1-35 cuttings. In 12 out of 16 T_2-35 plants, I could identify the same gene edits again and also one additional gene edit in *NST3* (Figure 32). In *nst1-1*, an adenine (A) insertion at position 589 bp in the genomic sequence, located in exon 2 of the gene, leads to a frame shift and a premature stop codon at 640 bp, changing the amino acid serine to a stop codon (Figure 32). In *nst3-1*, a four bp deletion, starting at position 446 bp, located in exon 2, causes a frame shift and a premature stop codon at position 738 bp, changing the amino acid valine to a stop codon (Figure 32). Additionally, I identified *nst3-2* which has a thymidine (T) insertion at position 315 bp, causing a frame shift and a premature stop codon at position 331 bp, changing the amino acid serine to a stop codon (Figure 32).

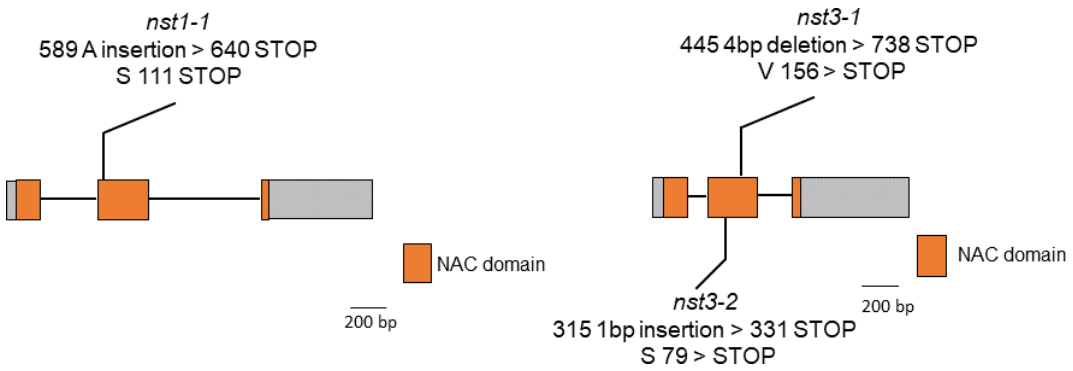

Figure 32. Gene model of *NST1* and *NST3*.
A schematic model of the structure of *NST1* and *NST3* genes and the sites of CRISPR/Cas9 gene edits in *nst1-1*, *nst3-1*, and *nst3-2*. Under each allele name, the first line indicates the nucleotide position of the gene edit, beginning from the start of translation of the genomic sequence. The second line indicates the position in the protein sequence and the amino acid change caused by the gene edit. Boxes represent exons, lines represent introns, and orange boxes represent the coding regions of the NAC DNA-binding domain.

4.2.2 Overall plant phenotype of *nst1*, *nst3* single and *nst1;nst3* double mutants

Phenotypic analysis of the single and double mutants showed differences in stem strength and anther dehiscence. The stems of the single mutants *nst1* and *nst3* stood upright, showing a similar stem strength to wild type plants. While the double mutant *nst1;nst3* had reduced stem strength and the stems were not able to stand upright (Figure 33A). To investigate the underlying cause of the reduced stem strength in *nst1;nst3*, I made cross-sections of the main stems 1 cm above the base. In wild type stems, cells with SCWs are cells in the xylem and interfascicular fibers, that form a ring connecting the xylem (Figure 33B). In *nst1* and *nst3* single mutant stems, the same pattern of lignified cells is visible, although the regular size and spacing of xylem and interfascicular fibers appears altered (Figure 33B). In contast to the single mutants, *nst1;nst3* double mutant stems completely lack lignified interfascicular fibers, but maintain lignified xylem (Figure 33B). Furthermore, *nst1* and *nst1;nst3* double mutants are infertile. The carpels seem to develop similar to wild type, but do not get pollinated, and therefore produce no fruit or seed. Further inspection under the binocular and with SEM imaging showed that the anthers do not open and therefore, no pollen is released (Figure 33C and 33D). Mechanical opening of the anthers to release pollen, or fertilization with wild-type pollen, enabled fruit and seed production in these plants. Therefore, the infertility of *nst1* single and *nst1;nst3* double

mutants is caused by indehiscent anthers that fail to release pollen. The fruit of *nst3* single mutants are indistinguishable from wild type (Figure 35B). Fruit could only be produced for *nst1* and *nst1;nst3* genotypes by manual pollination. I observed that these fruit varied in size, but this could be a result of manual pollination.

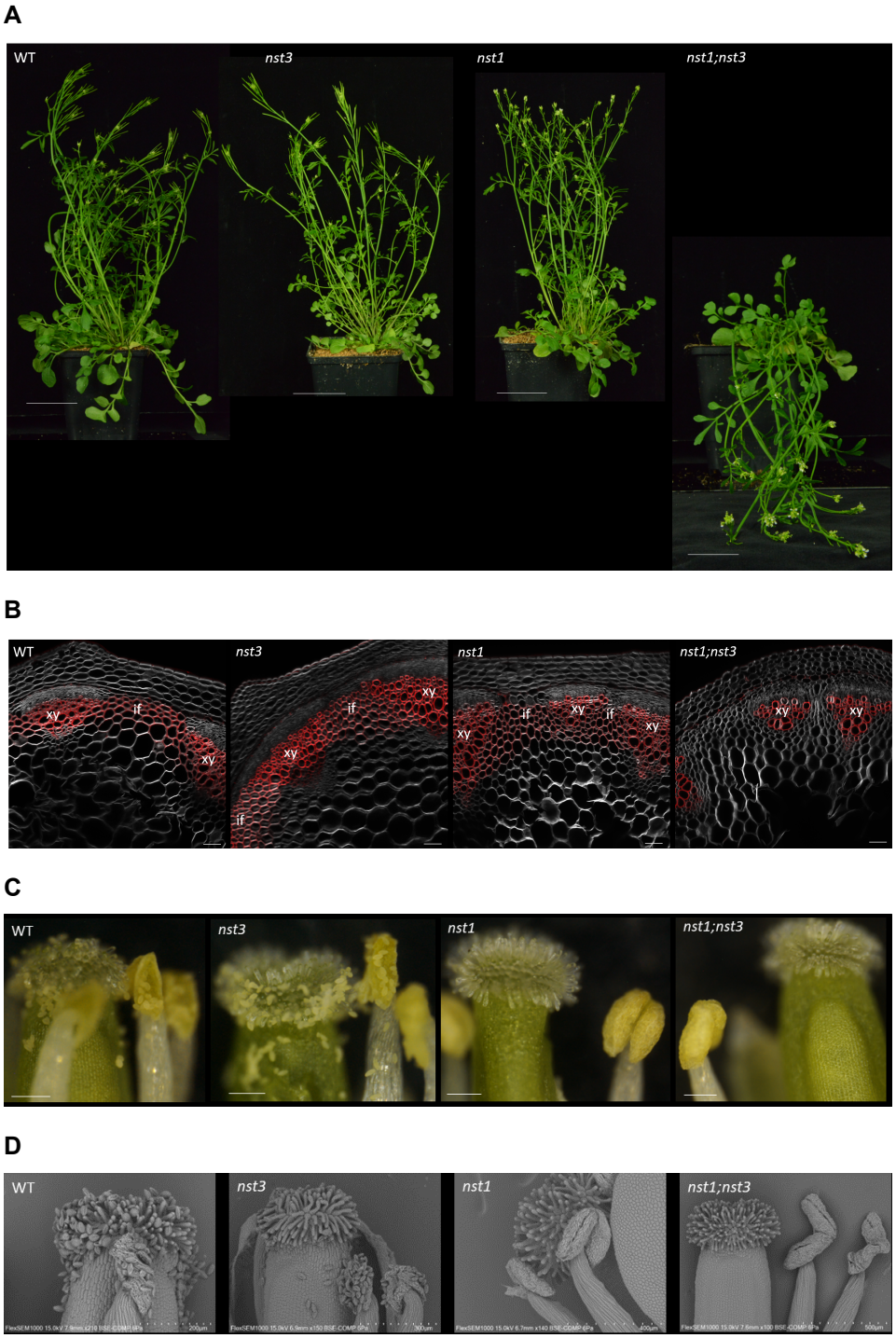

Figure 33. Loss of *NST1* and *NST3* stem results in reduced strength to stand upright. And loss of *NST1* causes sterile plants due to anther indehiscence.
A: Images of the mature plants showing that wild type and the single mutants *nst1* and *nst3* can stand upright, while the double mutant *nst1;nst3* is unable to stand upright. Scale bar 5 cm.
B: Confocal images of stem cross-sections from 1 cm above the base show that in wild type, *nst1*, and *nst3* the xylem (xy) and the interfascicular fibers (if) are lignified, while in *nst1;nst3* only the xylem is lignified. Lignin stained with Basic Fuchsin (red), cellulose stained with Calcofluor White (gray).
C: Images of pistils and anthers shows that wild type and *nst3* anthers are open and dispersing pollen, while *nst1* and *nst1;nst3* anthers are closed and no pollen are visible. Scale bar 100 μm.
D: SEM images of pistils and anthers.

4.2.3 Secondary cell wall (SCW) lignification in *nst1*, *nst3*, and *nst1;nst3* fruit

To investigate the role of *NST1* and *NST3* in fruit lignification, I examined transverse cross-sections of mature fruit at stage 17b in *nst1, nst3* and *nst1;nst3* double mutants, compared to wild type. In all images, lignin is stained with Basic Fuchsin (red) and cellulose stained with Calcofluor White (gray-scale) (Figure 34).

In *nst1* fruit, the amount of lignin in endocarp *b* cells was reduced compared to wild type (Figure 34A). Lignin was deposited in a polar manner on the adaxial side of the cell in a U-shape and very thin lignin around the whole cell wall. No hinge formation was observed by lignin or cellulose staining. Therefore, NST1 has a major role in the biosynthesis and patterning of the endocarp*b* SCW.

In *nst3* fruit, the lignification of endocarp*b* cells was comparable to wild type (Figure 34A). Every cell had a thick, lignified SCW with a hinged pattern, deposited on the adaxial side of the cell. However, the intensity of lignin staining appeared more variable between different SCW layers in *nst3* compared to wild type (Figure 34B). In wild type, lignin staining is sometimes less intense in the newly deposited SCW layers that are still lignifying, but otherwise uniform throughout the SCW (Figure 34A). In contrast to this, less intense lignin staining was observed in older SCW layers in endocarp*b* cells of *nst3* fruit (Figure 34B). Therefore, NST3 contributes to endocarp*b* SCW lignification, but has only a minor role compared to NST1.

In *nst1;nst3* double mutant fruit, the endocarp*b* layer completely lacked any lignin or cellulose thickening (Figure 34A). Only cellulose in the primary cell wall was stained in endocarp*b* cells. This is a stronger defect than I observed in *nst1* single mutants. Therefore, formation of the lignified SCW in endocarp*b* cells of *C. hirsuta* fruit requires the function of both NST1 and NST3 transcription factors.

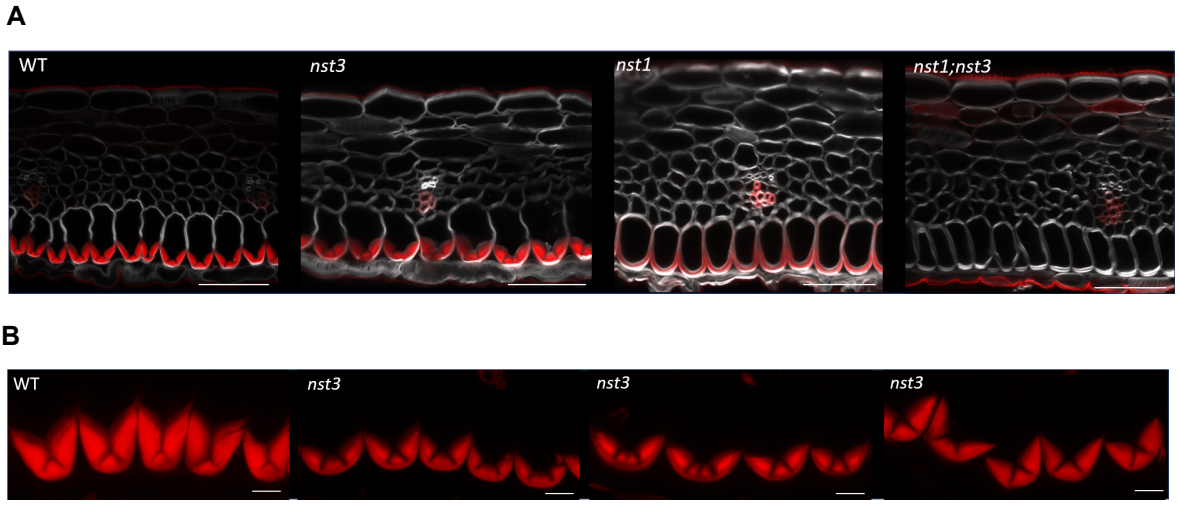

Figure 34. Confocal images of endocarp*b* lignin of *nst1*, *nst3*, and *nst1;nst3* mutants.
A: *nst1* mutants have reduced endocarp *b* lignin. *nst1;nst3* mutants completely lack lignification in endocarp *b* cells. Confocal images of the valve showing lignification in wild type, *nst1*, *nst3*, and *nst1;nst3*. Lignin stained with Basic Fuchsin (red), cellulose stained with Calcofluor White (gray). Scale bar 50 μm.
B: In *nst3* mutants the lignin intensity in the endocarp *b* layer is less uniform compared to wild type. Confocal images of wild type and *nst3* shows that lignin intensity is uniform in wild type, while there are less lignified parts in the pattern in *nst3*. Lignin stained with Basic Fuchsin (red), cellulose stained with Calcofluor White (gray). Scale bar 10 μm.

Lignification of cells at the valve margin are required to form a dehiscence zone in *A. thaliana* fruit. The dehiscence zone consists of a separation layer and a lignified layer and differentiation of these cell types is required for valves to separate from the replum during explosive release. In *nst1* fruit, no SCW thickening occurred at the valve margin (Figure 35A). However, the small cells of the separation layer appear to form at the valve margin similar to wild type (Figure 35A). In *nst3* fruit, both lignified and separation layer cell types form at the valve margin, similar to wild type. In *nst1;nst3* double mutant fruit, the valve margin region had no lignified cells, but the small separation layer cells were formed similar to wild type. Therefore, NST1, but not NST3, is required for cells at the valve margin to lignify and form a dehiscence zone. Given this result, it is interesting that the valves are released from the replum by explosive coiling in all genotypes, including *nst1* and *nst1;nst3* which lack a lignified dehiscence zone (Figure 35B). This suggests that differentiation of a lignified layer is dispensable for valves to release in *C. hirsuta*, and that differentiation of a separation layer may be more important for this process. The replum also contains a large number of lignified cells in *C. hirsuta* fruit. Lignification is not affected in the replum of *nst1* or *nst3* single mutants, but is strongly reduced in *nst1;nst3*

double mutants (Figure 35C). In the replum several cells that appeared to be vessel cells were lignified, but more dispersed in the replum compared to wild type, where they are located closer together. Additionally, some cells were thinly lignified or started lignification in the cell corners. Overall, the formation and patterning of lignified SCWs in the replum is strongly affected by loss of *NST1* and *NST3*, suggesting that these genes act fully redundantly in the replum.

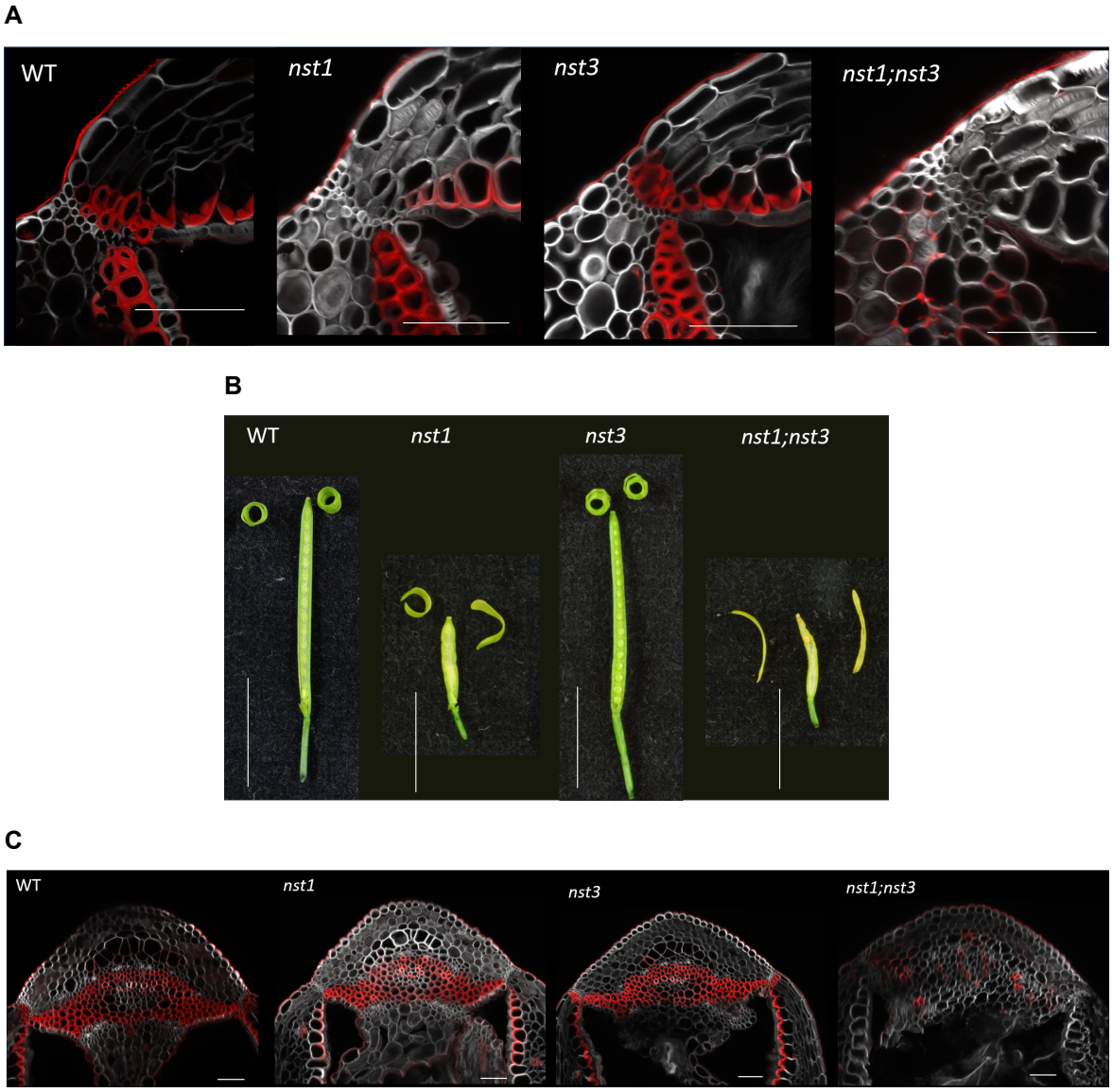

Figure 35. Valve margin and replum lignin of wild type, *nst3*, *nst1*, and *nst1;nst3*. And the dehisced fruit.
A: *nst1* and *nst1;nst3* mutants lack lignin in the valve margin lignified layer. *nst1;nst3* lacks lignification of most cells surrounding vascular vessels in the replum. B: Dehisced fruit and the valves of wild type, *nst1*, *nst3*, and *nst1;nst3*. Scale bar 1 cm C: SCW formation and patterning in *nst1;nst3* replum is affected compared to wild type. Confocal images in A and C: Lignin stained with Basic Fuchsin (red), cellulose stained with Calcofluor White (gray). Scale bar 50 μm.

4.2.4 *NST3* is expressed in lignified and non-lignified cell types of the valve

I investigated *NST3* gene expression and protein localization in *C. hirsuta* fruit. To quantify the amount of *NST3* gene expression, relative to *NST1*, I performed qPCR of *C. hirsuta* wild-type fruit valves at stage 17a. The mean Ct value for *NST3* was 29.30 and the standard devia-

tion between the biological replicates 0.35 (Figure 36A). *NST1* expression was higher, with a mean Ct value of 22.64 with a standard deviation between the biological replicates of 0.09 (Figure 36A). Therefore, *NST3* is expressed in wild-type valves at a lower level than *NST1* in stage 17a fruit. My genetic analyses had also shown that *NST3* played a more minor role than *NST1* in lignification of the fruit endocarp*b* (Figure 34), However, I had found that *NST3*, rather than *NST1*, was significantly upregulated in the *as1* mutant, which has ectopic lignin in the endocarp*b* (Figure 25). Therefore, I further investigated the expression domain of *NST3*.

To analyze *NST3* gene expression, I transformed a transcriptional reporter generated by Wolfram Faigl (pNST3::mCherry:NLS), into wild-type *C. hirsuta*. I observed mCherry expression in 18 T_1 transcriptional reporter lines. Signal was observed in freshly peeled valves in stage 17a fruit, shortly before endocarp*b* lignification starts. In all 18 transcriptional reporter lines *NST3* was expressed in endocar*b* cells, at the vascular bundle, and in small mesocarp cells. Expression in endocarp*b* cells and at vascular bundles is expected, as these are lignified cell types. In the endocarp*a*, signal was observed in nine lines, and in the other nine lines it was observed in less than half the cells (Figure 36B).

To analyze where the NST3 protein is localized in *C. hirsuta* fruit, I used an established translational reporter line generated by Dr. Hugo Hofhuis (*pNST3::gNST3:Venus*). I imaged freshly peeled valves of stage 17a fruit, shortly before endocarp*b* lignification starts. I observed nuclear NST3-V signal in all adaxial cell types of the fruit valve. These cell types include endocarp*a* and *b* cells, and the adjacent small mesocarp cells (Figure 36). The nuclear localization is expected since NST3 is a NAC-domain transcription factor. The localization of NST3 to endocarp*b* cells is also expected, since this is a lignified cell type that is affected by loss of *NST3* (Figure 34). However, the localization of NST3 to epidermal endocarp*a* cells and small mesocarp cells is unexpected since these are non-lignified cell types and are unaffected in *nst3* or *nst1;nst3* double mutants.

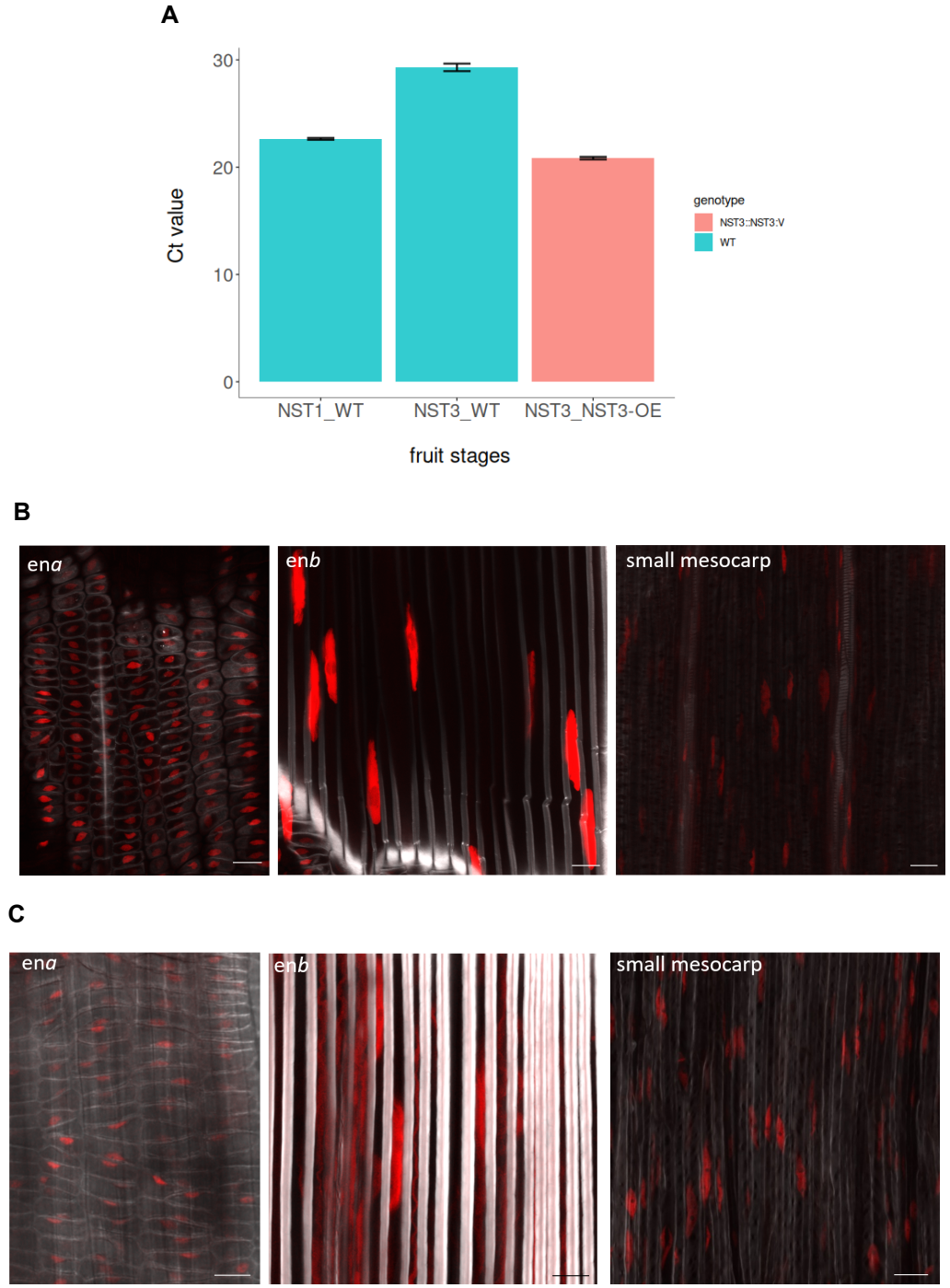

Figure 36. *NST3* is expressed and localizes in the lignified endocarp*b* cells (en*b*), and the non-lignified endocarp*a* cells (en*a*), and small mesocarp cells.
A: Ct values of *NST1* and *NST3* of wild type and *NST3* of *pNST3::gNST3:Venus* valves stage 17a. Wild type *NST1* mean Ct value 22.64, standard deviation between biological replicates 0.09. Wild type *NST3* mean Ct value 29.30, standard deviation between biological replicates 0.35. *pNST3::gNST3:Venus NST3* mean Ct value 20.80, standard deviation between biological replicates 0.12. I analyzed three biological and three technical replicates, each.
B and C: Confocal images of an exemplary T_1 line of *pNST3::mCherry:NLS* (red, B) and *pNST3::gNST3:Venus* (red, C) peeled off valves stage 17a. For endocarp*a* *pNST3::gNST3:Venus* fresh valves with brightfield. For endocarp*b* and small mesocarp peeled of valves stage 17a, fixed and cellulose stained with Calcofluor White (gray). Scale bar 20 μm.

4.2.5 *NST3* upregulation in its own domain is sufficient to cause ectopic lignin in endocarp*b* and small mesocarp cells

To investigate whether NST3 is sufficient to cause lignification, I analyzed the consequences of upregulating *NST3* expression in its own domain. For this experiment, I used the NST3 translational reporter where wild-type *NST3* expression is increased by the *pNST3::gNST3:Venus* transgene. First, I verified by qRT-PCR that *NST3* expression was increased in the fruit valves of *pNST3::gNST3:Venus*, relative to wild type. I found that the mean Ct value for *NST3* in the transgenic line was 20.84 with a standard deviation between the biological replicates of 0.12 . Therefore, *NST3* expression is higher in *pNST3::gNST3:Venus* than wild-type valves in stage 17a fruit (Figure 36A). Next, I analyzed the pattern of lignification in *pNST3::gNST3:Venus* fruit valves by Basic Fuchsin staining. Since NST3 is expressed in both lignified and nonlignified cells, I could test whether these cell types responded similarly or differently to increased NST3 expression. I used transverse cross-sections of stage 17b fruit. The endogenous lignin in endocarp*b* cells was similar to that in wild type (Figure 37). However, I observed additional ectopic lignin around the normally nonlignified part of endocarp*b* cell walls (Figure 37). I also observed lignification of the small mesocarp cells, but not endocarp*a* cells (Figure 37). Therefore, upregulation of *NST3* expression is sufficient to cause ectopic lignin in both lignified and nonlignified cell types.

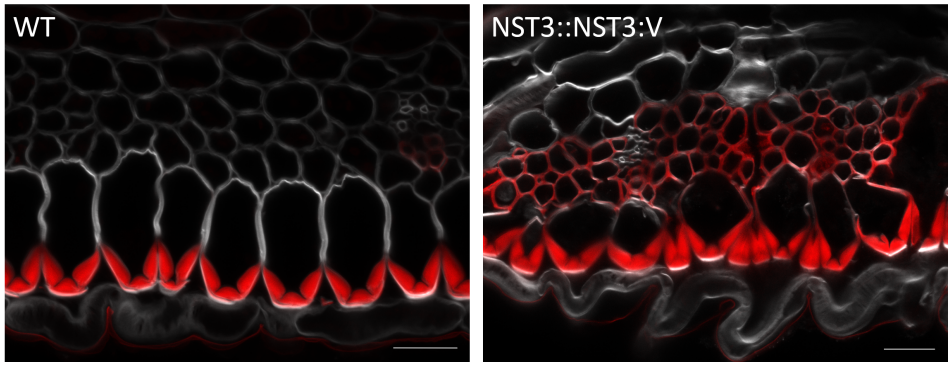

Figure 37. *NST3* upregulation in its own domain is sufficient to cause ectopic lignin in lignified endocarp*b* and non-lignified small mesocarp cells.
Confocal images of wild type (left) and *pNST3::gNST3:Venus* (right) from cross-sections of fruit stage 17b, fixed and lignin stained with Basic Fuchsin (red) and cellulose stained with Calcofluor White (gray). Scale bar 20 μm.

4.2.6 *MYB46* is expressed in endocarp*b* cells in wild type valves

Since the domain of *NST3* expression is broader than just the lignified endocarp*b* layer, I investigated whether or not genes acting downstream of NST3 in the secondary cell wall biosynthetic pathway showed a more restricted pattern of expression. The transcription factor-encoding gene *MYB46* is known to be a direct target of master regulators, such as NST3, in Arabidopsis (Zhong et al., 2007). Once activated, MYB46 regulates further downstream genes in the pathway encoding transcription factors and secondary cell wall effectors (Zhong et al., 2007; Ko et al., 2009; Kim et al., 2012). To analyze where *MYB46* is expressed, I generated a transcriptional reporter (*pMYB46::NLS:3xGFP*) and transformed wild type *C. hirsuta* plants. I selected 14 T_1 lines using the pigmented seed coat resistance marker (Ruby, (He et al., 2020)) and genotyping for the transgene. By imaging freshly peeled valves of stage 17a fruit, I observed GFP signal specifically in endocarp*b* cells in 13 out of 14 lines (Figure 38A). In 10 of these 13 lines I also observed GFP signal in xylem cells in the vascular bundle (Figure 38A). One of the 14 lines was an outlier that had ectopic GFP signal in small mesocarp cells. In summary, *MYB46* expression is more restricted than *NST3*, being limited to lignified cell types - endocarp*b* and xylem - in the fruit valve.

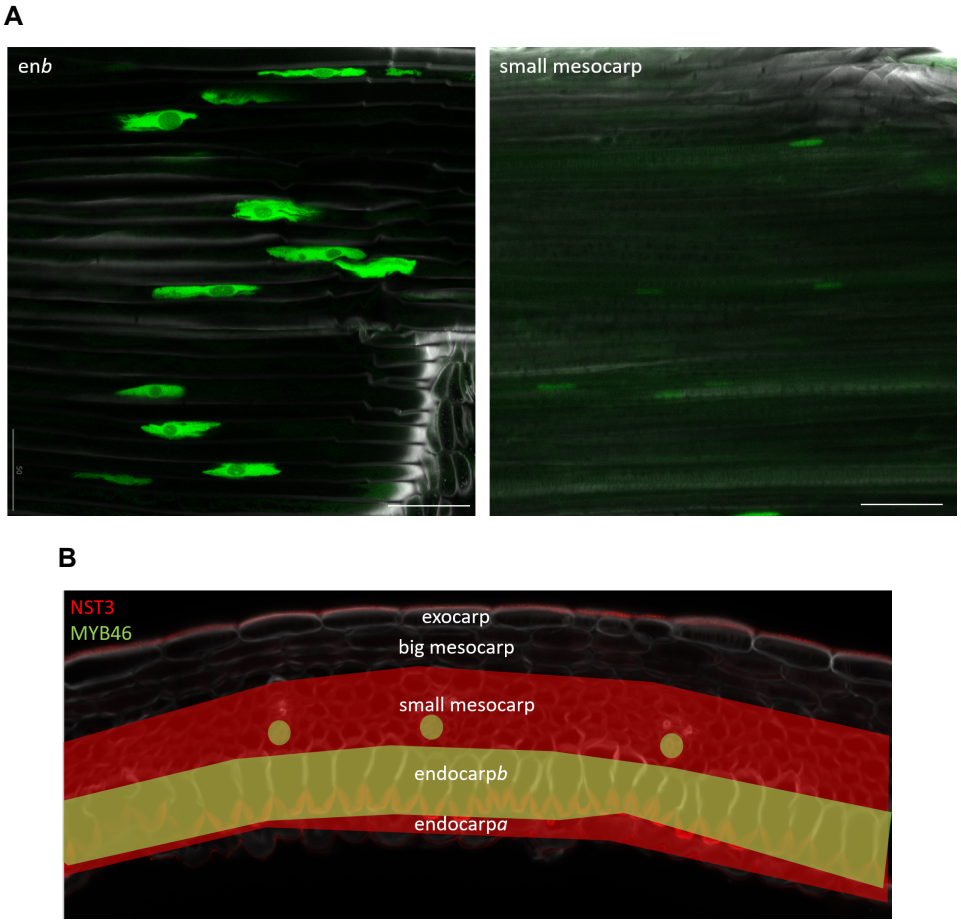

Figure 38. *MYB46* is expressed in lignified cells of the valve, the endocarp *b* cells and at the vascular bundles.
A: Exemplary confocal images of T_1 *pMYB46::NLS:3xGFP* (green) peeled off valves of stage 17a, fixed and cellulose stained with Calcofluor White. Scale bar 20 μm.
B: Schema of *MYB46* (green) and *NST3* (red) expression in the valve. *MYB46* is expressed in the endocarp*b* layer and in vascular bundles. *NST3* is expressed in lignified endocarp*b*, and non-lignified small mesocarp, and endocarp*a*.

4.2.7 Feedforward loop of *MYB46* in endocarp*b* cells

To further investigate how secondary cell wall patterning is regulated in endocarp*b* cells of *C. hirsuta* fruit, I designed a more specific overexpression experiment. I had shown previously that upregulation of NST3 was sufficient to cause ectopic lignification (Figure 37). However, the expression domain of NST3 is broader than just endocarp*b* cells (Figure 36). Therefore, to upregulate secondary cell wall biosynthesis specifically in endocarp*b* cells, I designed a feedforward loop. The idea is to drive the expression of a transcription factor of interest, using the promoter of one of his target genes. In this way, the transcription factor activates its

endogenous targets, but also the transgene promoter, creating a positive feedforward loop of its own upregulation.

To design a feedforward loop in endocarp*b* cells, I took advantage of MYB46 and its known target genes *CESA7* and *LAC11*. Previous work in Arabidopsis had shown that MYB46 binds directly to the promoters of *CESA7* and *LAC11* (Taylor-Teeples et al., 2014; Zhao et al., 2013). Previous work in *C. hirsuta*, had shown that both *CESA7* and *LAC11* are expressed in endocarp*b* cells. *LAC11* encodes a laccase that is required to polymerize lignin in endocarp*b* cells (Pérez-Antón et al., 2022). *CESA7* encodes a subunit of the cellulose synthase complex that is required for cellulose synthesis in endocarp*b* secondary cell walls (Eng). Following the assumption that MYB46 may also regulate *CESA7* and *LAC11* in *C. hirsuta*, I used the promoters of both genes to drive MYB46 expression in a feedforward loop.

I generated *pCESA7::cMYB46:GFP* and *pLAC11::cMYB46:GFP* constructs and transformed wild type *C. hirsuta* plants. I obtained only five T_1 lines for *pCESA7::cMYB46:GFP* because I had low transformation and germination rates. All five plants were sterile dwarves, so I did not proceed any further with these lines (Figure 39A). In contrast, I obtained 15 T_1 lines for *pLAC11::cMYB46:GFP*. These lines showed a range of whole-plant phenotypes, from wild type, for example T_1 1 and T_1 4 (Figure 39B), to dwarfed, for example T_1 15, to seedling arrest, for example T_1 11 (Figure 39C). Except for line T_1 11, I could characterize the fruit of all lines by imaging GFP signal in freshly peeled valves of stage 17a fruit, and imaging endocarp *b* lignification in sectioned fruit stained with Basic Fuchsin at stage 17b.

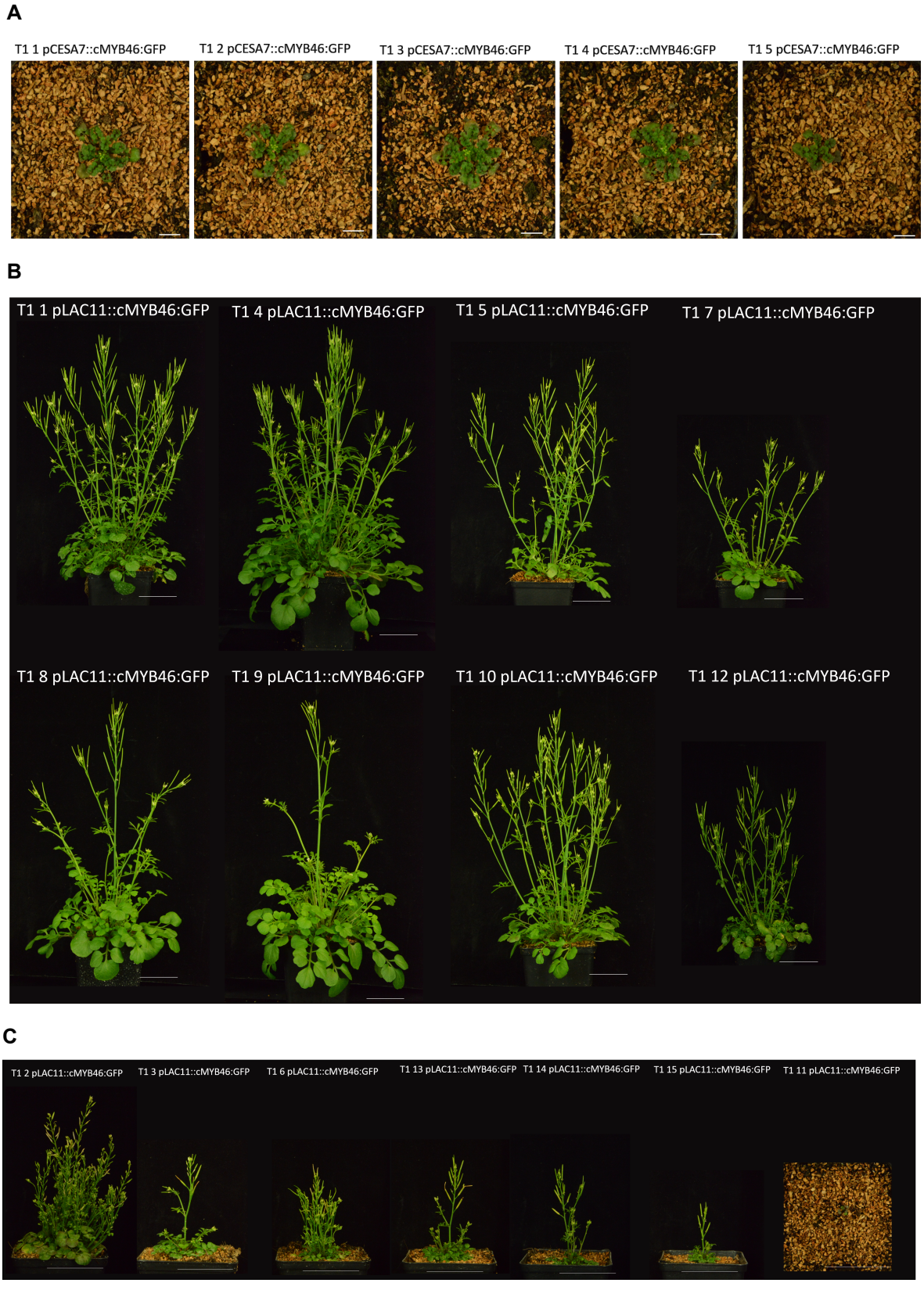

Figure 39. The feedforward lines display different plant phenotypes. A: Five T_1 lines of *pCESA7::cMYB46:GFP*. All are dwarfs and sterile. B: Eight T_1 lines of *pLAC11::cMYB46:GFP* that grew mostly similar to wild type. C: Seven T_1 lines of *pLAC11::cMYB46:GFP* that are dwarfs.
All plants were at least five weeks old, due to different germination time points and growth rates, the stages were not identical. Nikon camera images. Scale bar 5 cm.

Each of the six *pLAC11::cMYB46:GFP* lines with a dwarfed plant stature showed nuclear GFP signal, and therefore MYB46 localization, in endocarp*b* cells, xylem cells in vascular bundles, and also in small mesocarp cells (Figure 40A). Since the expression of *LAC11* is specific to endocarp*b* and xylem cells in the *C. hirsuta* fruit valve (Pérez-Antón et al., 2022), the ectopic expression in small mesocarp cells suggests that these are overexpression lines. For all dwarfed lines, I imaged GFP with the same confocal settings, and found that the signal intensity in endocarp*b* cells was comparable among lines. However, signal intensity in the small mesocarp cells differed between lines; for example, T_1 13 had weak signal in only a few mesocarp cells, whereas T_1 6 had stronger signal in all small mesocarp cells (Figure 40A). Interestingly, the endocarp*b* secondary cell wall pattern in all 6 dwarfed lines was changed from polar to uniform (Figure 40B). I observed secondary cell wall cellulose (stained with Calcofluor White) and lignin (stained with Basic Fuchsin) deposition around the whole cell wall (Figure 40B). Additionally, I observed lignification in cell corners of small mesocarp cells. This lignification varied between lines; for example, T_1 6 had lignin deposition in the majority of small mesocarp cells, whereas few mesocarp cells were lignified in T_1 13 (Figure 40B). The amount of ectopic lignin correlates well with the amount of ectopic GFP signal in small mesocarp cells (Figure 40A, 40B).

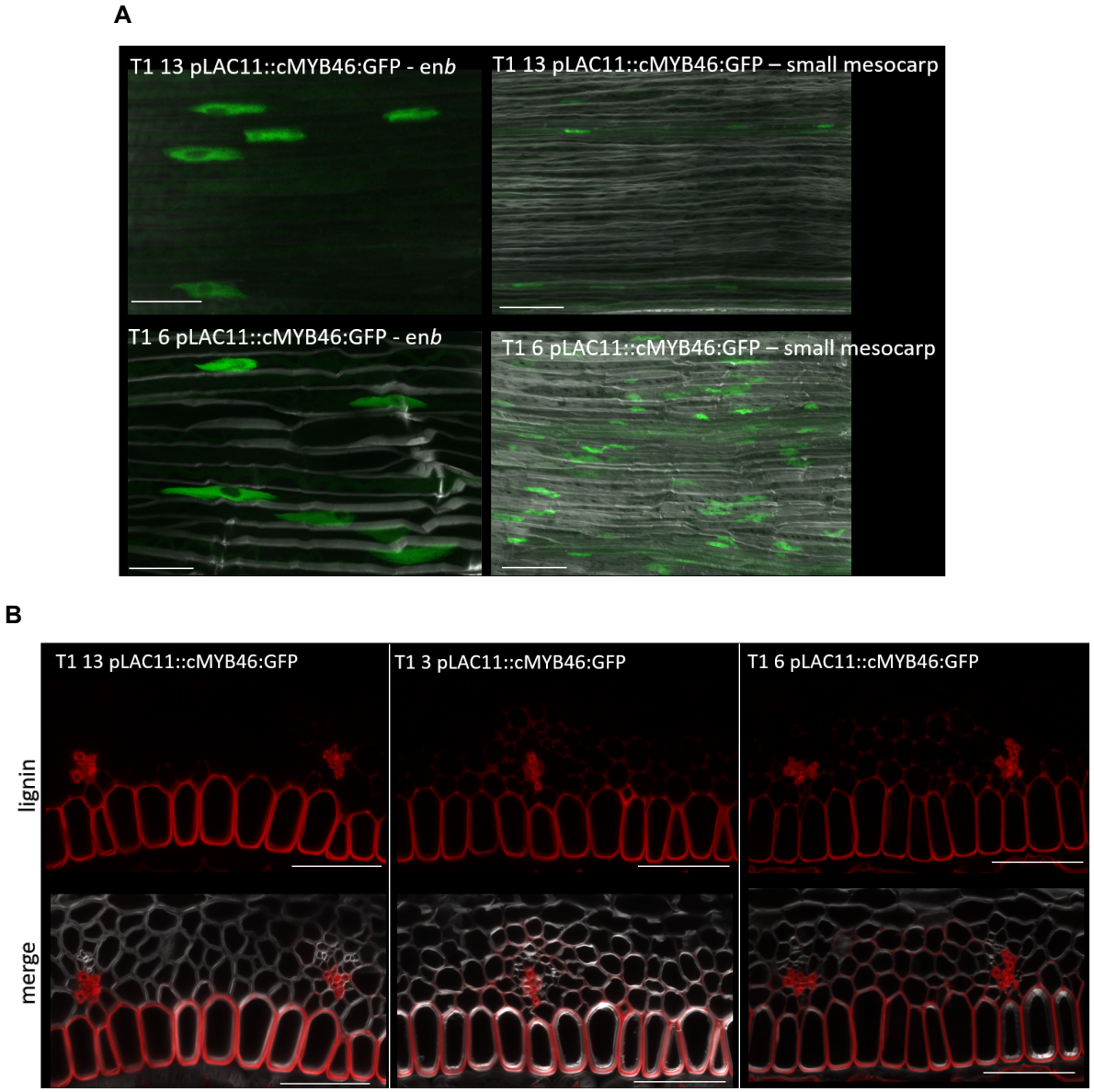

Figure 40. The localization of MYB46 and the lignin pattern in dwarfed feedforward lines. A: MYB46:GFP signal in a peeled off valve stage 17a of two exemplary dwarfed T_1 *pLAC11::cMYB46:GFP* lines. Both have a similar signal in endocarp*b* cells. In the small mesocarp the number of cells with signal differs. B: Exemplary images of sections of fruit stage 17b for dwarfed T_1 *pLAC11::cMYB46:GFP* lines. The endocarp*b* lignin is uniform with some polarity on the adaxial side. Ectopic lignin with varying amount in small mesocarp cells. Upper images show only lignin, bottom images show lignin and cellulose. Confocal images of peeled of valves stage 17a (A), and cross-sections of fruit stage 17b (B), fixed and lignin stained with Basic Fuchsin (red), cellulose stained with Calcofluor White (gray), MYB46:GFP signal (green). Scale bar 50 μm.

The majority of *pLAC11::cMYB46:GFP* T_1 lines (8/15) had a plant stature comparable to wild type (Figure 39B) and showed nuclear GFP signal, and therefore MYB46 localization,

specifically in endocarp*b* cells (Figure 41A). None of these lines had ectopic lignin in small mesocarp cells. The endocarp*b* secondary cell wall pattern varied among the eight plants from polar to uniform (Figure 41). For example, two lines (T_1 9 and T_1 4) had a polar, hinged pattern like wild type, but with thin ectopic lignin around the whole endocarp*b* cell wall (Figure 41B). Line T_1 8 also had a polar pattern, but unlike wild type it lacked the hinged pattern and also had thin ectopic lignin around the whole endocarp*b* cell wall (Figure 41B). The majority of lines (5/8) had a uniform pattern of lignification (Figure 41C). Four lines (T_1 5, 7, 10, 12) had a thick lignified cell wall around the whole endocarp*b* cell, but lignification of the abaxial cell wall was often not complete (Figure 41C). The remaining line, T_1 1, had a fully uniform secondary cell wall pattern (Figure 41C). Therefore, upregulation of MYB46 in its endogenous domain is sufficient to change the endocarp*b* secondary cell wall from a polar, hinged pattern to uniform.

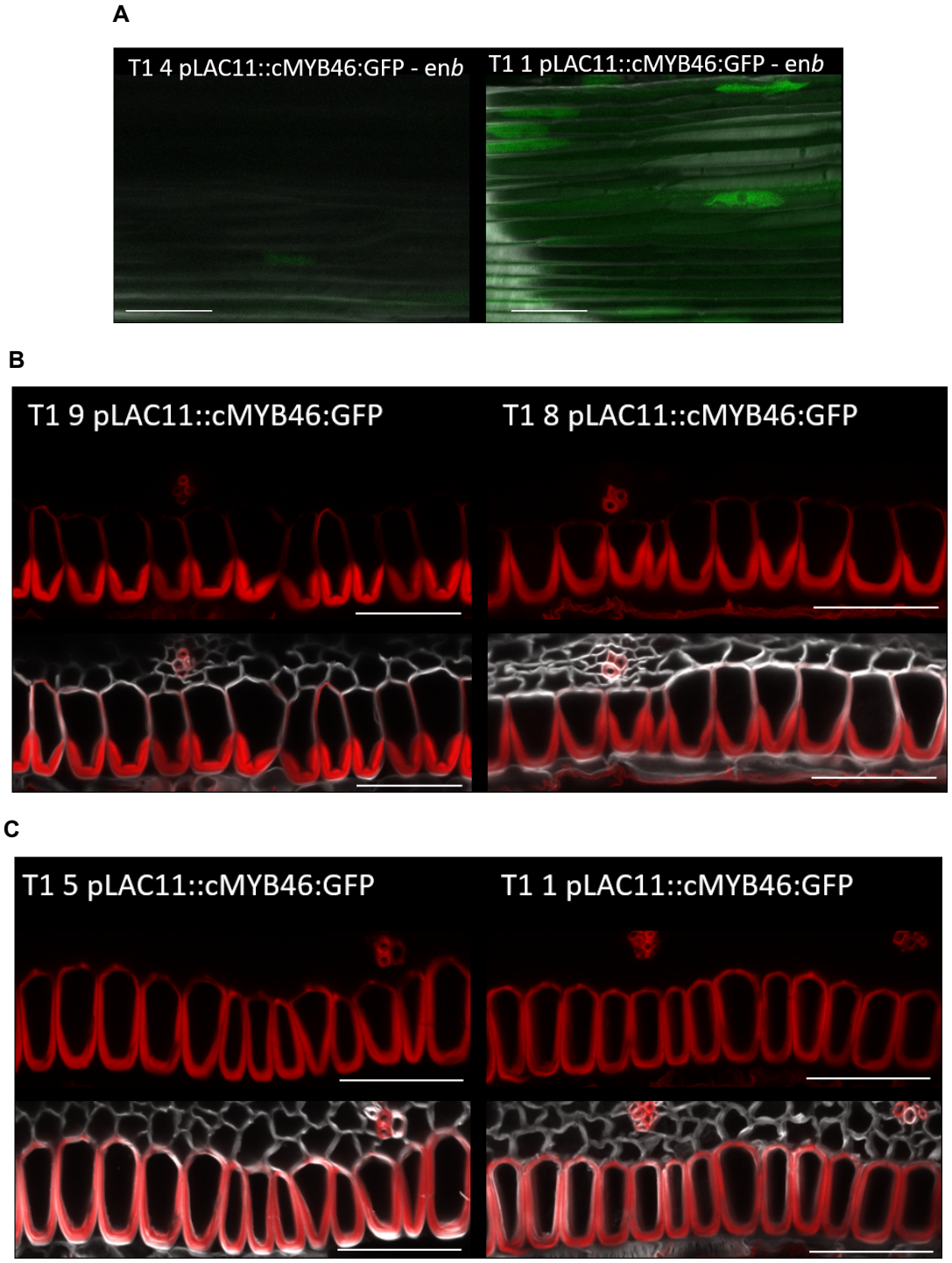

Figure 41. The localization of MYB46 and the lignin pattern in feedforward lines plants similar in stature to wild type. A: MYB46:GFP in signal a peeled off valve stage 17a of two exemplary T_1 *pLAC11::cMYB46:GFP* lines that grew similar to wild type. Signal only in endocarp*b* cells. Intensity of signal varies between the lines. B and C: Exemplary images of sections of fruit stage 17b wild type like T_1 *pLAC11::cMYB46:GFP* lines. The endocarp*b* lignin varies between the lines. From thin ectopic lignin around whole cell with normal endogenous lignin (B, T_1 9) to nearly non-polar lignin with the adaxial side thicker (C, T_1 1). In between lines with endogenous lignin without the hinges and with ectopic lignin around the whole cell (T_1 8) and lignin around the whole cell with polarity on the adaxial side (T_1 5) can be found. Upper images show only lignin, bottom images show lignin and cellulose. Confocal images of peeled of valves stage 17a (A), and cross-sections of fruit stage 17b (B), fixed and lignin stained with Basic Fuchsin (red), cellulose stained with Calcofluor White (gray), MYB46:GFP signal (green). Scale bar 50 μm

4.3 Discussion

By generating loss-of-function alleles for *NST1* and *NST3*, I identified a role for both genes in endocarp*b* SCW deposition in *C. hirsuta*. *nst1;nst3* double mutants had no endocarp*b* SCW, indicating that both genes are required redundantly for this process. *NST1* is more important than *NST3* for endocarp*b* SCW deposition and patterning as *nst1* mutants almost entirely lacked a SCW in the endocarp*b*. These results still need to be confirmed by transgenic complementation. Furthermore, *NST3* is expressed in both lignified and non-lignified cells and its upregulation was sufficient to cause ectopic lignification in these cells. By creating feedforward lines to upregulate the SCW gene *MYB46* in endocarp*b* cells, I found that the SCW pathway has an important input into endocarp*b* SCW patterning.

I successfully generated CRISPR/Cas9 alleles of *NST1* and *NST3* and further studied these mutants. In *A. thaliana*, *NST1* and *NST3* act redundantly in fiber lignification, and thus are important for mechanical support of the stem (Mitsuda et al., 2007). In *C. hirsuta*, only in the double mutant, but not the single mutants, interfascicular fiber lignification in the stem is impaired, while vessel formation, which is regulated by *VND6* and *VND7*, seems to be intact. The loss of interfascicular fiber lignification manifests in the inability of the stem to stand upright. Their role as SCW master regulators and the redundant regulation of interfascicular fiber lignification by *NST1* and *NST3* seems to be conserved between *A. thaliana* and *C. hirsuta* (Mitsuda et al., 2007).

Loss of *NST1* resulted in fertility problems, caused by the indehiscence of anthers and therefore no release of pollen. The carpel could be successfully pollinated with wild type pollen, suggesting that the fertility problems are due to problems with the pollen of *nst1*. In *A. thaliana*, *NST1* is expressed in anthers and stamen filaments, but the anthers have wild-type dehiscence (Mitsuda et al., 2005). The homologous gene *NST2* is also expressed in anthers and *nst1;nst2* double mutants had indehiscent anthers due to the loss of lignification in the anther endocethuim in *A. thaliana* (Mitsuda et al., 2005). This suggests that *NST1* has a larger role in anther dehiscence in *C. hirsuta*, which is shared by *NST2* in *A. thaliana*. To confirm that loss of *NST1* is causal for this phenotype, the mutant should be complemented with wild type

NST1 to observe whether the phenotype is rescued.

In *nst3* the polar SCW pattern in endocarp *b* cells is maintained. However, there are differences in lignin intensity. Variable lignification was also observed in *spl7* and *lac4;lac11/+;lac17* mutants (Pérez-Antón et al., 2022). LAC4, LAC11, and LAC17 are required for endocarp *b* lignification. As multicopper proteins, they require copper which is provided by *SPL7* (Pérez-Antón et al., 2022). SCW is deposited in layers and the different intensities between these layers could indicate changing amounts of lignin polymerization during formation. Therefore, it would be interesting to analyze the distribution of LAC4, LAC11, and LAC17 in *nst3* SCWs.

The endocarp*b* lignification in *nst1* has two major differences compared to wild type. First, there is a reduction in SCW deposition. This suggest that *NST1* is the major regulator for SCW formation in endocarp*b* cells. Second, the hinged pattern is absent, suggesting that reduced activation of the SCW pathway could affect SCW patterning.
Endocarp*b* lignification is completely abolished in *nst1;nst3* double mutants, indicating that the lignifcation observed in *nst1* is due to *NST3*. While the replum is similar to wild type in single *nst1* and *nst3* mutants, lignification of the replum is aberrant in *nst1;nst3* double mutants. Thus, *NST1* and *NST3* act redundantly to lignify cells surrounding the vessels in the replum, similar to the double mutant in *A. thaliana* (Mitsuda and Ohme-Takagi, 2008).

In *nst1* and *nst1;nst3* the lignified layer of the valve margin is non-lignified, but the cells appear similar to wild type, suggesting that the cell identity is unchanged, just no SCW is formed. To confirm this, valve margin markers, like *IND*, could be observed in the *nst1* and *nst1;nst3* mutant background. In *A. thaliana*, *nst1* and *nst1;nst3* mutants have a similar phenotype where the lignification is missing in the valve margin, but the cell identity is maintained (Mitsuda and Ohme-Takagi, 2008). However, these *A. thaliana* mutants have indehiscent fruit due to the lack of lignification. They could be opened by rubbing between the fingers which is different from mutants that lack the valve margin, like *shp1;shp2*, which lack the separation layer that releases cell wall degrading enzymes and lignification layer (Mitsuda and Ohme-Takagi, 2008; Liljegren et al., 2004). In contrast to this, *C. hirsuta nst1* and *nst1;nst3* fruit are

dehiscent. This suggests that the separation layer alone is sufficient for dehiscence along the valve margin in *C. hirsuta*, but not in *A. thaliana*, where the lignification layer is also required.

Transcriptional and translational reporter lines showed that *NST3* is expressed and localized in both lignified and non-lignified cells on the adaxial side of the valve. This seemingly odd result may be explained by the low expression of *NST3* compared to *NST1*, since *NST3* upregulation was sufficient to cause lignification in these non-lignified cells. *MYB46* is a direct target of the SCW master regulators and its expression was limited to lignified cells in the valve. This suggests that the low *NST3* expression in small mesocarp cells is not sufficient to cause *MYB46* expression in these cells.

I constructed feedforward lines to observe strong upregulation of the SCW pathway specifically in lignified cells of the valve. The five T_1 lines under the *CESA7* promoter were all dwarfed and sterile, unfortunately not allowing further observations. However, this shows that the construct was functional, as a phenotype was observed. Pertubation of monolignol biosynthesis, like overexpression of transcription factors involved in lignification, has been shown to lead to dwarfism (Perkins et al., 2020). Since *CESA7* is active in the formation of all SCWs, while *LAC11* is not, this may explain why these lines are more severe.

In the *pLAC11::cMYB46:GFP* lines that grew similar to wild type, I observed a gradual shift from the endogenous polar U-shape pattern with hinges to a uniform pattern. The amount of MYB46:GFP signal correlated with the strength of the shift of the lignin pattern. The dwarved *pLAC11::cMYB46:GFP* lines, with strong GFP signal, all showed a uniform lignin pattern in the endocarp*b* cells. Therefore, the activity of the SCW pathway affects the SCW patterning in the endocarp*b*.

5 General Discussion

Explosive seed dispersal evolved in *C. hirsuta* through cellular innovations in the fruit that underpin the mechanics of rapid valve coiling. One important innovation was a polar pattern of secondary cell wall (SCW) deposition in endocarp*b* cells of the fruit valve (Hofhuis et al., 2016). In my thesis project, I aimed to advance our understanding of the genetic basis of SCW patterning in *C. hirsuta* endocarp*b* cells.

I successfully generated an EMS-mutagenized population in *C. hirsuta* and screened 500 M_2 families for mutants with alterations to the lignified endocarp*b* SCW. I found that the majority of mutants showed ectopic lignin rather than disruption of the polar SCW pattern. Going in to this experiment, I had expected to recover mutants with a uniformly lignified SCW. This is the endocarp*b* SCW pattern observed in *A. thaliana* and other Brassicaceae species with non-explosive fruit (Hofhuis et al., 2016). Therefore, uniform lignification could be expected to represent a default SCW pattern in endocarp*b* cells, and loss of gene function in *C. hirsuta* could be expected to revert to this default pattern. However, my results suggest that this is not the case.

An interesting class of ectopic lignin mutants, were those that mirrored the endogenous SCW on the opposite side of the cell. In all mutants with thick, ectopic lignin, this ectopic SCW was deposited on the abaxial side of endocarp*b* cells, opposite to the endogenous SCW on the adaxial side. The ectopic lignin in these mutants also mirrored the shape of the endogenous SCW thickenings. In some case, thin hinges formed between thickenings, mirroring the endogenous pattern. This mutant phenotype suggests that the polar position of the endocarp*b* SCW is genetically regulated, and loss of gene function results in a partial or full duplication of this pattern on the opposite side of the cell.

At least two plausible mechanisms could explain the polar SCW deposition in endocarp*b* cells (Figure 42). On the one hand, activators could pre-pattern the position where the SCW is deposited (Figure 42A). In ectopic lignin mutants, these regulators could be ectopically activated and recapitulate the endogenous SCW on the opposite side of the cell (Figure 42A).

Cortical microtubules could be involved in this type of patterning mechanism, since the density of microtubules is known to guide cellulose synthase activity to sites of SCW synthesis (Watanabe et al., 2015). However, according to this scenario, ectopic lignin mutants are more likely to represent gain of gene function and, hence, are more likely to be dominant alleles. Whereas, the ectopic lignin mutants that I characterized (*as1* and *pat63*) are recessive alleles. A second possibility is that repressors could pre-pattern the polar SCW by masking the area of the cell where SCW is excluded (Figure 42B). In ectopic lignin mutants, loss of such repressors could allow the endogenous SCW program to be activated on the opposite side of the cell (Figure 42B). This scenario fits the recessive nature of *as1* and *pat63* mutant alleles. It also fits the molecular nature of AS1 as a transcription factor that acts in a repressive complex to negatively regulate the expression of target genes, such as *KNOX1* genes (Guo et al., 2008; Husbands et al., 2015). By further characterizing ectopic lignin mutants, such as *as1* and *pat63*, and identifying the gene underlying the *pat63* phenotype, we are likely to further our understanding of SCW patterning mechanisms.

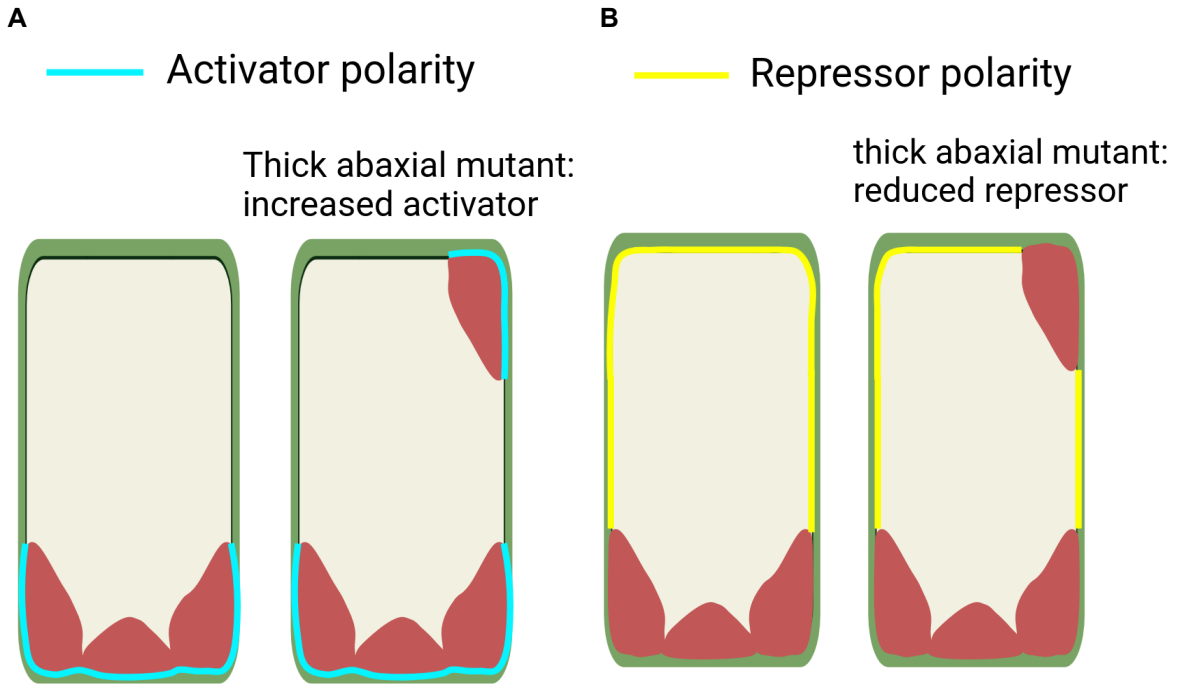

Figure 42. Schematic proposed model of SCW polarity in endocarp*b* cells. Polarity could be maintained via activators (A, blue) or repressors (B, yellow). A: The activators localize to the walls where SCW is deposited. B: The repressors localize to the wall where no SCW is deposited.

To identify genes required for endocarp*b* SCW synthesis, I followed the logic that these genes may be upregulated in the fruit valves of ectopic lignin mutants. For example, *NST3* was upregulated in *as1-1* fruit valves and encodes a master regulator of SCW synthesis. By generating CRISPR/Cas9 loss-of-function alleles of *NST3*, and its paralog *NST1*, I determined that both genes function in endocarp*b* SCW synthesis. Loss of both genes resulted in loss of the endocarp*b* SCW (Figure 43). In *nst1* single mutants, very little SCW was deposited. Interestingly, the reduced SCW in *nst1* was deposited in the normal polar position, but lacked the hinged pattern (Figure 43). This suggests that either a minimal amount of SCW is required for the hinged pattern to elaborate, or that NST1 plays a role in specifying the hinged pattern. To test whether upregulating SCW synthesis affected patterning, I generated *pLAC11::cMYB46:-GFP* feedforward lines. In these plants, the upregulation of SCW synthesis by MYB46 is amplified in endocarp*b* cells. Interestingly, increased MYB46 activity caused the loss of both the polarity and the hinged pattern of SCW deposition (Figure 43). I observed a dose response of MYB46 on SCW patterning: a moderate increase caused thin ectopic lignin and loss of hinge formation, while a strong increase caused a complete switch to a uniform pattern of SCW deposition (Figure 43). Therefore, polar SCW deposition in endocarp*b* cells requires that activity of the SCW pathway is kept in check. Both *NST1/3* loss of function and *MYB46* gain of function suggest that a fine balanced regulation of the SCW pathway is necessary for polar SCW deposition in *C. hirsuta* endocarp*b* cells (Figure 43).

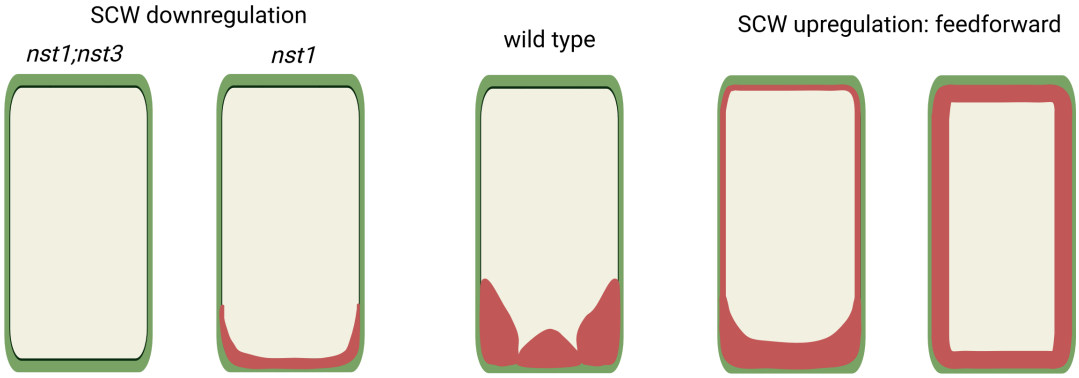

Figure 43. Schematic proposed model of SCW pattern in endocarp*b* cells. Changes in SCW pathway activation affect SCW pattern. Reduced SCW activation, as in *nst1* results in reduced SCW and loss of hinges. Increased SCW activation, as in feedforward lines, results in increased SCW and loss of hinges up to a uniform shape.

The small mesocarp cells that are adjacent to endocarp*b* cells seem to be more susceptible to ectopic deposition of SCW and lignin. In my mutant screen I could observe ectopic lignin in this layer. And dwarfed feedforward lines with leaky expression, also had ectipic *MYB46* expression and SCW in the small mesocarp cells in the fruit. Furthermore, *NST3* is expressed and localizes also to the non-lignified small mesocarp cells besides the lignified endocarp*b* cells. And *NST3* upregulation is sufficient for ectopic lignin in these cells. So far, it is unclear why *NST3* is expressed in the non-lignified small mesocarp cells. Interestingly, the small mesocarp cell layer does not exist in *A. thaliana*.

In my thesis, I observed several mutants affected in the valve margin in *C. hirsuta* fruit. Among them *pat411*, which lacked SCW in the lignified valve margin layer, but had intact cell types of separation layer. *nst1* which also lacked SCW in the lignified layer and had reduced SCW in endocarp*b* cells. And *nst1;nst3* which lacked SCW in the lignified valve margin layer and endocarp*b* cells completely. In all three mutants the separation layer was intact, but the SCW in the lignified layer was missing. All three mutants had dehiscent fruit.
In contrast *pat162* was missing the separation layer and the SCW in lignified layer, and was indehiscent. Therefore, mutants with an intact separation layer are dehiscent, but a mutant lacking this cell type is indehiscent. This difference suggests that the separation layer is more important for fruit dehiscence than the lignification of the lignified layer in *C. hirsuta* fruit. This is in difference to *A. thaliana* in which lack of SCW in the lignified layer caused indehiscent fruit, as it happens in *nst1* (Mitsuda et al., 2007).
Interestingly, when valve margin genes are mis-expressed in *ful* mutants, in *C. hirsuta* ectopic separation layer cells differentiate, while in *A. thaliana* ectopic lignified layer cells differentiate. Therefore, dehiscence in *C. hirsuta* seems to rely on an intact separation layer. While for dehiscence in *A. thaliana* SCW in lignified layer is required.

6 Material and Methods

6.1 Growing conditions and plant material

6.1.1 Plant growing conditions

Plants were grown at the Max Planck Institute for Plant Breeding Research in Cologne, Germany. Plants grown on soil were cultivated in greenhouse chambers with controlled environment in long-day conditions (LD) (days: 20 °C, 16 h; nights: 18 °C, 8 h). *Cardamine hirsuta* seeds were stratified in the dark for 10 days at 4°C before being placed in the light.

6.1.2 Strains and lines used

The strains used in this thesis were: *Cardamine hirsuta* Oxford (herbarium specimen voucher Hay 1 (OXF) described in (Hay and Tsiantis, 2006)). Further alleles and lines used in this thesis and not generated by me are included in Table 2.

Table 2. Mutant allele and transgenic lines used in this study and not generated by me

allele/line	background	Reference
as1-1	*C. hirsuta* wild type Oxford	(Hay and Tsiantis, 2006)
ful-1	*C. hirsuta* wild type Oxford	(Galstyan et al., 2021)
ind-1	*C. hirsuta* wild type Oxford	(Galstyan et al., 2021)
pAS1::gAS1:YFP	*C. hirsuta as1-1*	Generated by Dr. Yi Wang
pBP::gBP:Venus	*C. hirsuta* wild type Oxford	(Rast-Somssich et al., 2015)
pBP::3xVenus	*C. hirsuta* wild type Oxford	(Rast-Somssich et al., 2015)
pNST3::mCherry:NLS	*C. hirsuta* wild type Oxford	Wolfram Faigl
pNST3::gNST3:Venus	*C. hirsuta* wild type Oxford	Dr. Hugo Hofhuis

6.2 Generation of transgenic lines

6.2.1 Bacterial strains

The bacterial strain *Escherichia coli DH10B* was used for plasmid amplification. *Agrobacterium tumefaciens GV3101* strains were used for *C. hirsuta* transformation.

6.2.2 Constructs and cloning strategies

For the generation of all constructs for the transgenic lines, the GreenGate system was used (Lampropoulos et al., 2013). The different entry vector combinations were cloned in the destination vector pGGZwf01. The generated transgenic lines are in table 3 and the primers used for cloning are in table 4.

To generate a transcriptional reporter of *AS1* (*pAS1::NLS:3xGFP*), a 5401 bp promoter sequence was amplified from *C. hirsuta* Oxford genomic DNA.

To generate the lines with ectopic expression of *BP* (*pPER66::gBP:mNeonGreen* and *pFUL::gBP:mNeonGreen*) I amplified the genomic region of *BP*. For the promoter pf *PER66* I used entry vector clones from Dr. Miguel Pérez (Pérez-Antón et al., 2022). For *FUL* promoter a 6183 bp region upstream of the start codon was amplified from *C. hirsuta* Oxford genomic DNA.

To generate a transcriptional reporter of *MYB46* (*pMYB46::NLS:3xGFP*), a 3158 bp promoter sequence was amplified from *C. hirsuta* Oxford genomic DNA.

To generate the feedforward lines *pCESA7::cMYB46:GFP* and *pLAC11::cMYB46:GFP* the promoters generated by Dr. Ryan Eng (Eng) (pCESA7) and by Dr. Miguel Pérez (Pérez-Antón et al., 2022) (pLAC11) were used. To amplify the coding sequence (CDS) of *MYB46*, I used cDNA previously synthesized from *C. hirsuta* extracted RNA.

Table 3. Transgenic lines generated in this study

line	background	Independent lines characterized
pAS1::NLS:3xGFP	*C. hirsuta* wild type Oxford	3
pPER66::gBP:mNeonGreen	*C. hirsuta* wild type Oxford	15
pFUL::gBP:mNeonGreen	*C. hirsuta* wild type Oxford	16
pNST3::3xmCherry:NLS	*C. hirsuta* wild type Oxford	18
pMYB46::NLS:3xGFP	*C. hirsuta* wild type Oxford	14
pCESA7::cMYB46:GFP	*C. hirsuta* wild type Oxford	5
pLAC11::cMYB46:GFP	*C. hirsuta* wild type Oxford	15

Table 4. Primer sequences used for cloning

Usage	Primer name	Primer sequence
cloning of pAS1 Greengate	IS132 pChAS1_pGGA F	AACAGGTCTCAACCTATTTTCTGAAACTCGATTCTAAGATCAGTT
	IS133 pChAS1_fusion1 R	CTACGGTCTCATCTAACAATGACATCCAAACACAGC
	IS134 pChAS1_fusion2 F	AACAGGTCTCATAGATCTCGAAGGACATGCAATATTATG
	IS135 pChAS1_pGGA R	CTACGGTCTCATGTTCTCCTCCTAACAACAACATCACTT
cloning of gBP Greengate	IS86 gBP_pGGC F	AACAGGTCTCAGGCTCCATGGAAGAATATCAGCACAACACCAG
	IS88 gBP_fusion1 R	CTACGGTCTCACCCTGGATGATTCAGTCACAGAC
	IS89 gBP_fusion2 F	AACAGGTCTCAAGGGACCCGGAATTGGATCAATTC
	IS87 gBP_pGGC R	CTACGGTCTCACTGATGGGCCAAGACGATAAGGTCCA
cloning of pFUL Greengate	IS92 pFUL_pGGA F	AACAGGTCTCAACCTCAAAGCGAGAAGTTGCTTTAGAAAAG
	IS93 pFUL_fusion1 R	CTACGGTCTCAGGGACCAGAGAAGGGATACAAG
	IS94 pFUL_fusion2 F	AACAGGTCTCATCCCTCCTTCCACTCTATGTGG
	IS95 pFUL_pGGA R	CTACGGTCTCATGTTATCTCTCTATCTTCAACAAACCCTCA
cloning of pMYB46 Greengate	IS122 pMYB46_pGGA F	AACAGGTCTCAACCTGTTGGATTTACAACTTTGTTGAAAAACATAG
	IS123 pMYB46_fusion1 R	CTACGGTCTCAGACAGACCTAAAATGCAAAAAAAATCAAAG
	IS124 pMYB46_fusion2 F	AACAGGTCTCATGTCTCAAAACCGTTTTCGTCCATG
	IS125 pMYB46_pGGA R	CTACGGTCTCATGTTTGTTTTGTTTTGTTGAGTTAATTTGTTTCTGTTT
cloning of cMYB46 Greengate	IS114 cMYB46_pGGC F	AACAGGTCTCAGGCTCCATGAGAAGACCAGAGGTAGCTATT
	IS115 cMYB46_fusion1 R	CTACGGTCTCAGGACCAAAGTCCCTTCTTCATC
	IS116 cMYB46_fusion1 F	AACAGGTCTCAGTCCCCAGAGGAAGACTCAAA
	IS117 cMYB46_fusion2 R	CTACGGTCTCACTGCGACCACCTGTTGCC
	IS118 cMYB46_fusion2 F	AACAGGTCTCAGCAGATTGCAGCAAGATTGCC
	IS119 cMYB46_pGGC R	CTACGGTCTCACTGATATGCTTTGTTTGAAGTTGAAGTGAAAC

6.2.3 Generation of transgenic plants

Plants were transformed with *Agrobacterium tumefaciens* strain *GV3101* by the floral dip method (Clough and Bent, 1998). T_1 seeds from transformed plants were screened for transgene insertion by using seed coat fluorescent marker or pigmented seed coat resistance marker (RUBY) (He et al., 2020). The following generations were obtained by self-fertilization.

6.3 Generation of mutant alleles

6.3.1 CRISPR/Cas9 mediated mutagenesis of *NST1* and *NST3*

For directed mutagenesis using CRISPR/Cas9, a similar strategy as in (Kamei et al., 2020) was followed, although with several modifications. All possible single guide RNA (sgRNA) positions for the PAM site ”GG” in the *NST1* and *NST3* genomic sequence were identified using CC Top (Stemmer et al., 2015). Two sgRNAs per gene were selected based on location, efficacy, and minimum off-target prediction (Table 5). I used the MultiSite Gateway cloning system and *in silico* created a plasmid with two sgRNAs targeting each gene in pUC57 backbone plasmid and the plasmid was generated by GenScript via mutagenesis of a previously existing Gateway

compatible entry vector. In the plasmid each sgRNA was located downstream of a copy of the *A. thaliana* RNA polIII promoter to drive their expression. This plasmid was cloned together with a plasmid containing the gene encoding an Arabidopsis codon optimized spCas9 protein (Fauser et al., 2014) downstream of an egg cell-specific promoter to drive expression in egg cells and very initial stages of embryo development (Wang et al., 2015). The destination vector was a pPZP200 vector with pFAST-RFP-GW seed coat marker selection (constructed by Dr. Claire Kamei, generated by GenScript). Via the floral dip method (Clough and Bent, 1998) the plasmid was transformed into *C. hirsuta* Oxford.The T_1 seed were selected via the RFP seed coat marker and the regions around the sgRNAs sequenced by Eurofins, subsequently (Prime for sequencing in Table 6, for sequencing primer IS112 and IS96). The results were analyzed with ice.synthego (Synthego). T_2 and T_3 plants were genotyped for homozygous mutations and selected for absence of Cas9.

Table 5. sgRNAs used to knock out *NST1* and *NST3* using CRISPR/Cas9. PAM sites in italics.

	sequence	**strand**
NST1 sgRNA1	AAAATCCGGCCGCAGTGGCT*CGG*	positive
NST1 sgRNA2	TAGACTCGACGACAACACTG*AGG*	negative
NST3 sgRNA1	GTTCGACGCCACAGAACGAT*TGG*	negative
NST3 sgRNA2	GTGTCCGTAGGATTGGACTG*AGG*	negative

Table 6. Primer sequences used for sequencing regions targeted with CRISPR/Cas9

Usage	**Primer name**	**Primer sequence**
NST1 sgRNA1&2	IS112 NST1_I1 F	GTTGCTGTTGTTTGTTCGCA
	IS113 NST1_I2 R	GGGTCAATGACTCCTTAGCAG
NST3 sgRNA1&2	IS96 NST3_E1 F	CAACAAGCTTGAGCCTTGGG
	IS97 NST3_E3 R	TTGTGAAAGTTGGTGGGCCT

6.4 EMS mutagenesis and screen methods

For EMS mutagenesis a similar strategy as in (Hofhuis et al., 2016) was followed, with some modifications. Approximately, 2000 *C. hirsuta* Oxford seed were washed in 0.16 % Tween-20 solution for 15 min. Then five times washed with deionized water for 10 min. Then mutagenized by agitation with 0.3 % EMS (Sigma) in deionized water overnight. Washed extensively

with deionized water. Then seed transferred into 0.1 % agarose and stratified for three days in the dark at 4 °C. The seed were sown on soil and selfed progeny harvested individually for 1127 M_1 plants, and 112 M_1 plant pooled.

Stage 17b fruit, that have undergone lignification, were collected and pooled from multiple individuals of a single M_2 family, hand-cut and lignin autofluorescence observed with Zeiss Axio Imager M2 microscope using dry objectives (20x) and DAPI set. Then the hand-cut sections were stained with Calcofluor White for 1 to 10 min. an d observed under with Zeiss Axio Imager M2 microscope using dry objectives (20x) and DAPI set. When a potentially interesting phenotype was observed within a pool, corresponding plants were collected and observed individually to identify the mutant plant. The selfed progeny of the plant was collected and sometimes backcrossed to wild type.

6.5 Molecular biology methods

6.5.1 Mapping-by-sequencing

The homozygous *pat63* mutant was crossed to wild type *C. hirsuta* Oxford, the F_1 progeny selfed and the F_2 mapping population analyzed for segregation. From plants with mutant phenotype leaf material was collected, freeze dried and used for mapping-by-sequencing. Genomic DNA extraction was performed using the kit Genomic DNA from Plant Nucleo Spin Plant II from Macherey-Nagel. Concentration was measured using Qubit and an equimolar amount was pooled. Genomic DNA was sequenced using the Illumina NextSeq2000 platform with short-read 2x150 bp paired end reads at the MPIPZ Genome Center. 20,000,000 reads were requested for each library, and 23,861,195 total reads were received. For the analysis Easymap was used (Lup et al., 2021) using the reference *C. hirsuta* genome as control (Gan et al., 2016).

6.5.2 Fine mapping

SNPs were tested for their CAPS or dCAPS primer compatibility with dCAPS finder 2.0 (Neff et al., 2002). The primers were designed in geneious prime. The functional, tested primer pair is listed in Table 7.

Table 7. Primer sequences used for fine mapping

Marker name	Primer name	Primer sequence
SNP CAPS (499 bp, MboI wt 206, 297 bp)	Chr6: 7,699,239 bp	F ACCAAAGCGCTCCACAGGTA R GTTTATTGCGTCCCATATCGGC

6.5.3 RNA extraction and cDNA synthesis

RNA was extracted using the Spectrum^{TM} Plant Total RNA kit (Sigma-Aldrich) following the manufacturer's protocol. cDNA synthesis was carried out with the iScript^{TM} cDNA Synthesis kit (BioRad).

6.5.4 qRT-PCR

qRT-PCR was performed with a 2-step program with the DNA-specific dye SYBR Green (Power SYBR green PCR master mix kit; Applied Biosystem) in a QuantStudio 5 PCR machine (Applied Biosystems). Experiments were conducted in triplicate from three biological samples consisting of pooled valves stage 17a. Expression levels were quantified using the comparative Ct method (Pfaffl, 2001) and normalized against the housekeeping gene Clathrin (CARHR174880). Primers used are listed in Table 8.

Table 8. Primer sequences used for qRT-PCR

Usage	Primer name	Primer sequence
BP	IS15 BP-qPCR F	ACTCTTCCCATCAGGATTGTTGA
qRT-PCR	IS16 BP-qPCR R	CCATTCAAGAAGCAATGGAGTT
KNAT2	IS53 KNAT2-qPCR F	TGGCTATCTTGCGCTGCTAC
qRT-PCR	IS54 KNAT2-qPCR R	TGCAAGAGGCCTTTCAGTTT
KNAT6	IS51 KNAT6-qPCR F	CGGAGATCAGAAGAAACGATGA
qRT-PCR	IS52 KNAT6-qPCR R	GCGAGGATACGATGGATGAC
NST3	IS29 NST3-qPCR F	TTCAAGAGGAATGTAGAATCGGT
qRT-PCR	IS30 NST3-qPCR R	TCCTCAGTCCAATCCTACGG
MYB46	IS120 MYB46-qPCR F	GGCAAGGATGTTGGAGCGATGTC
qRT-PCR	IS121 MYB46-qPCR R	GCTGCAATCTGAGACCACCTGTTG
Clathrin	Clathrin-qPCR F	TCGATTGCTTGGTTTGGAAGATAAGA
qRT-PCR	Clathrin-qPCR R	TTCTCTCCCATTGTTGAGATCAACTC

6.5.5 genomic DNA extraction

Extraction of genomic DNA for genotyping and sequencing was performed similarly to (Edwards et al., 1991).

6.5.6 genotyping of transgenic lines and sequencing of genes

For genotyping of transgenic lines gDNA was used. For sequencing of genes either cDNA or gDNA was used. PCR was performed with MangoTaq$_{TM}$ (meridian Bioscience), following the manufacture's protocol. PCR products for sequencing were either cleaned with ExoI and rSAP or with PCR clean-up and Gel extraction kit from Macherey-Nagel and send for sequencing to Eurofins. All primers used for genotyping or sequencing are in Table 9.

Table 9. Primer sequences used for genotyping and sequencing

Usage	Primer name	Primer sequence
FUL	IS35 F	ACTGCGTAAACTCCTCCAGA
sequencing	IS37 R	AGCTTGGTTCTTTCTTGACCT
	IS38 R	GTAGGGCGTAACATCCAAGC
	IS41 F	ACCAAGCTATGTTCGAATCGA
	IS43 F	TCACTGTAGACTCACGCGAA
	IS44 R	AGCTTGGTTCTTTCTTGACCT
IND	IS148 F	ACCGAGAGCTAGACGACAAC
sequencing	IS149 R	TGGCACACCACTACACATCA
AS1	IS63 F	AGGATGGTGAGATGGGAAGA
sequencing	IS55 R	ACGACAACAAAAGAGCTTACGA
BP	IS86 F	AACAGGTCTCAGGCTCCATGGAAGAATATCAGCACAACACCAG
sequencing	IS87 R	CTACGGTCTCACTGATGGGCCAAGACGATAAGGTCCA
pAS1::NLS:3xGFP	IS144 F	TGCCGTCTCTATGGTCTAATCG
genotyping	f327 R	CTCGGGTCTCGATCTCGTCCTCAAGCCCAAGCTGACCCATC
pPER66::gBP:mNeonGreen	IS110 F	ATTCTGTCCAGCTCAGGTGC
genotyping	IS111 R	GATCGGAAGCAAGTCTCGGT
pFUL::gBP:mNeonGreen	IS94 F	AACAGGTCTCATCCCTCCTTCCACTCTATGTGG
genotyping	IS88 R	CTACGGTCTCACCCTGGATGATTCAGTCACAGAC
pNST3::3xmCherry:NLS	f824 F	
genotyping	f569 R	CTCGATCTCGAACTCGTGGC
pMYB46::NLS:3xGFP	IS124 F	AACAGGTCTCATGTCTCAAAACCGTTTTCGTCCATG
genotyping	f268 R	TGAACTTGTGGCCGTTTACGTCGC
pCESA7::cMYB46:GFP	IS118 F	AACAGGTCTCAGCAGATTGCAGCAAGATTGCC
& *pLAC11::cMYB46:GFP*	f327 R	CTCGGGTCTCGATCTCGTCCTCAAGCCCAAGCTGACCCATC

6.5.7 RNA sequencing

For RNA-sequencing of wild-type and *as1-1* fruit valves stage 17a, the valves were dissected and approximately 22 valves pooled for each of the three biological replicates. RNA was extracted using the Spectrum^{TM} Plant Total RNA kit (Sigma-Aldrich) with on-column DNase treatment. The RNA libraries including polyA enrichment with an Illumina HiSeq3000 platform were prepared at the MPIPZ Genome Center. Sequencing was done by NovoGene on a Illumina NovaSeq6000 platform with stranded polyA selection, and 2x150 bp pared-end reads. 6 Gb data per sample were requested. Sample preparation and RNA extraction were performed together with Dr. Erin Cullen.

Analysis was performed with the following tools: quality control of the reads with FastQC (Bioinformatics), adapter trimming with cutadapt (Martin, 2011), alignment to the *C. hirsuta* reference genome (Gan et al., 2016) with hisat2 (Kim et al., 2019), ordering and indexing of the aligned reads with samtools (Li, 2011), and quantification of reads with htseq (Anders et al., 2014). Differential gene expression analysis with DESeq2 in R (Anders and Huber, 2010).

6.6 Microscopy materials and methods

6.6.1 Sectioning

To generate cross-sections, the fruit or stem were embedded in 1.5 mL tubes containing 5% low melt agarose (Hi-Pure Low agarose, biogene Ltd). On a Leica Vibratome VT1000 S, sample sectioning was performed.

6.6.2 Phloroglucinol/HCl staining and Imaging for ectopic lignin quantification

Samples were incubated in 2 % Phloroglucinol dissolved in 95 % ethanol for 10 min, staining solution was removed and samples were treated with 1 N HCl for 1 min. The solution was removed and 1 N HCl solution added. Samples were mounted in 1 HCl solution on slides with a cover slip. Adapted from (Mitsuda et al., 2007).
Light microscopy images of the samples were taken with Zeiss Axio Imager M2 microscope using dry objectives. Images were acquired as single plane images or as Z-stacks. From latter "Extended depth of focus" images were generated with the built-in software ZEN 2 (Zeiss).

6.6.3 Clearing and staining of cross-sections

For fixation, clearing and staining the protocol in (Ursache et al., 2018) was followed. Fixation was performed with 4 % paraformaldehyde for 1 hour. Whole valves were vacuum treated for 30 min up to 1 hour. After fixation samples were cleared with ClearSee solution in darkness with gentle agitation. Samples were stained with 0.2 % Basic Fuchsin (lignin) and 0.1 % Calcofluor White (cellulose). Both were directly prepared in ClearSee and if stained with both, simultaneously stained overnight. If only Calcofluor White was used then staining for 1 hour. Cleared cross-sections were mounted in ClearSee solution for imaging in a CLSM.

6.6.4 Confocal microscopy

Confocal imaging was performed with a CLSM TCS SP8 (Leica) confocal microscope. Used objective include dry objective HC PL FLUOTAR 10x/0.30, and water immersion objectives:

HC Fluotar L 25x/0.95; HC PL APO CS2 40x/1.10; HC PL APO CS2 63x/1.20; HCX PL APO lambda blue 63x/1.20.

All images were acquired with a pinhole of 1 AU. Parameters used for each fluorophore are described in Table 10.

Table 10. Excitation and emission parameter used for the different fluorophores

Fluorophore	Excitation (nm)	Emission (nm)
Lignin autofluorescence	405	440-510
Calcofluor White	405	425-475
Basic Fuchsin	561	600-650
GFP	488	500-520
mNeonGreen	496	510-530
Venus	514	518-535, 517-550
mCherry	561	590-625

References

A. Ali Khan, M. Raess, and M. H. de Angelis. Moving forward with forward genetics: A summary of the infrafrontier forward genetics panel discussion. *F1000Research*, 10:456, June 2021. ISSN 2046-1402. doi: 10.12688/f1000research.25369.1.

H. Alonso-Cantabrana, J. J. Ripoll, I. Ochando, A. Vera, C. Ferrándiz, and A. Martínez-Laborda. Common regulatory networks in leaf and fruit patterning revealed by mutations in thearabidopsis asymmetric leaves1gene. *Development*, 134(14):2663–2671, July 2007. ISSN 0950-1991. doi: 10.1242/dev.02864.

S. Anders and W. Huber. Differential expression analysis for sequence count data. *Genome Biology*, 11(10), Oct. 2010. ISSN 1474-760X. doi: 10.1186/gb-2010-11-10-r106.

S. Anders, P. T. Pyl, and W. Huber. Htseq—a python framework to work with high-throughput sequencing data. *Bioinformatics*, 31(2):166–169, Sept. 2014. ISSN 1367-4803. doi: 10.1093/bioinformatics/btu638.

P. Ballester and C. Ferrándiz. Shattering fruits: variations on a dehiscent theme. *Current Opinion in Plant Biology*, 35:68–75, Feb. 2017. ISSN 1369-5266. doi: 10.1016/j.pbi.2016.11.008.

J. Barros, H. Serk, I. Granlund, and E. Pesquet. The cell biology of lignification in higher plants. *Annals of Botany*, 115(7):1053–1074, apr 2015. doi: 10.1093/aob/mcv046.

B. Bioinformatics. Fastqc. URL http://www.bioinformatics.babraham.ac.uk/projects/fastqc/.

V. Bourquin, N. Nishikubo, H. Abe, H. Brumer, S. Denman, M. Eklund, M. Christiernin, T. T. Teeri, B. Sundberg, and E. J. Mellerowicz. Xyloglucan endotransglycosylases have a function during the formation of secondary cell walls of vascular tissues. *The Plant Cell*, 14(12):3073–3088, Nov. 2002. ISSN 1532-298X. doi: 10.1105/tpc.007773.

M. E. Byrne, R. Barley, M. Curtis, J. M. Arroyo, M. Dunham, A. Hudson, and R. A. Martienssen. Asymmetric leaves1 mediates leaf patterning and stem cell function in arabidopsis. *Nature*, 408(6815):967–971, Dec. 2000. ISSN 1476-4687. doi: 10.1038/35050091.

M. Christiernin, A. B. Ohlsson, T. Berglund, and G. Henriksson. Lignin isolated from primary walls of hybrid aspen cell cultures indicates significant differences in lignin structure between primary and secondary cell wall. *Plant Physiology and Biochemistry*, 43(8):777–785, Aug. 2005. ISSN 0981-9428. doi: 10.1016/j.plaphy.2005.07.007.

S. J. Clough and A. F. Bent. Floral dip: a simplified method foragrobacterium□mediated transformation ofarabidopsis thaliana. *The Plant Journal*, 16(6):735–743, Dec. 1998. ISSN 1365-313X. doi: 10.1046/j.1365-313x.1998.00343.x.

D. J. Cosgrove. Growth of the plant cell wall. *Nature Reviews Molecular Cell Biology*, 6(11): 850–861, Nov. 2005. ISSN 1471-0080. doi: 10.1038/nrm1746.

D. J. Cosgrove. Primary walls in second place. *Nature Plants*, 4(10):748–749, Oct. 2018. ISSN 2055-0278. doi: 10.1038/s41477-018-0278-7.

C. Coulondre and J. H. Miller. Genetic studies of the lac repressor. *Journal of Molecular Biology*, 117(3):525–567, Dec. 1977. ISSN 0022-2836. doi: 10.1016/0022-2836(77)90056-0.

C. Dardick and A. M. Callahan. Evolution of the fruit endocarp: molecular mechanisms underlying adaptations in seed protection and dispersal strategies. *Frontiers in Plant Science*, 5, jun 2014. doi: 10.3389/fpls.2014.00284.

K. Edwards, C. Johnstone, and C. Thompson. A simple and rapid method for the preparation of plant genomic dna for pcr analysis. *Nucleic Acids Research*, 19(6):1349–1349, 1991. ISSN 1362-4962. doi: 10.1093/nar/19.6.1349.

A. Emonet and A. Hay. Development and diversity of lignin patterns. *Plant Physiology*, 190 (1):31–43, June 2022. ISSN 1532-2548. doi: 10.1093/plphys/kiac261.

A. Endler and S. Persson. Cellulose synthases and synthesis in arabidopsis. *Molecular Plant*, 4(2):199–211, Mar. 2011. ISSN 1674-2052. doi: 10.1093/mp/ssq079.

R. Eng. unpublished.

F. Fauser, S. Schiml, and H. Puchta. Both crispr/cas□based nucleases and nickases can be used efficiently for genome engineering in arabidopsis thaliana. *The Plant Journal*, 79(2): 348–359, June 2014. ISSN 1365-313X. doi: 10.1111/tpj.12554.

A. Felipo-Benavent, C. Úrbez, N. Blanco-Touriñán, A. Serrano-Mislata, N. Baumberger, P. Achard, J. Agustí, M. A. Blázquez, and D. Alabadí. Regulation of xylem fiber differentiation by gibberellins through della-knat1 interaction. *Development*, 145(23), Nov. 2018. ISSN 0950-1991. doi: 10.1242/dev.164962.

C. Ferrandiz. Regulation of fruit dehiscence in arabidopsis. *Journal of Experimental Botany*, 53(377):2031–2038, Oct. 2002. ISSN 1460-2431. doi: 10.1093/jxb/erf082.

C. Ferrandiz. Fruit structure and diversity, Jan. 2011.

C. Ferrándiz, S. J. Liljegren, and M. F. Yanofsky. Negative regulation of the shatterproof genes by fruitfull during arabidopsis fruit development. *Science*, 289(5478):436–438, July 2000. ISSN 1095-9203. doi: 10.1126/science.289.5478.436.

C. Ferrándiz, S. Pelaz, and M. F. Yanofsky. Control of carpel and fruit development in arabidopsis. *Annual Review of Biochemistry*, 68(1):321–354, June 1999. ISSN 1545-4509. doi: 10.1146/annurev.biochem.68.1.321.

E. Francoz, P. Ranocha, A. Le Ru, Y. Martinez, I. Fourquaux, A. Jauneau, C. Dunand, and V. Burlat. Pectin demethylesterification generates platforms that anchor peroxidases to remodel plant cell wall domains. *Developmental Cell*, 48(2):261–276.e8, Jan. 2019. ISSN 1534-5807. doi: 10.1016/j.devcel.2018.11.016.

A. Galstyan, P. Sarchet, R. Campos-Martin, M. Adibi, L. A. Nikolov, M. P. Antón, L. Rambaud-Lavigne, X. Gan, and A. Hay. Indehiscent regulates explosive seed dispersal. June 2021. doi: 10.1101/2021.06.11.448014.

X. Gan, A. Hay, M. Kwantes, G. Haberer, A. Hallab, R. D. Ioio, H. Hofhuis, B. Pieper, M. Cartolano, U. Neumann, L. A. Nikolov, B. Song, M. Hajheidari, R. Briskine, E. Kougioumoutzi, D. Vlad, S. Broholm, J. Hein, K. Meksem, D. Lightfoot, K. K. Shimizu, R. Shimizu-Inatsugi, M. Imprialou, D. Kudrna, R. Wing, S. Sato, P. Huijser, D. Filatov, K. F. X. Mayer, R. Mott, and M. Tsiantis. The cardamine hirsuta genome offers insight into the evolution of morphological diversity. *Nature Plants*, 2(11), Oct. 2016. ISSN 2055-0278. doi: 10.1038/nplants.2016.167.

Q. Gu, C. Ferrándiz, M. F. Yanofsky, and R. Martienssen. The fruitfull mads-box gene mediates cell differentiation during arabidopsis fruit development. *Development*, 125(8):1509–1517, Apr. 1998. ISSN 1477-9129. doi: 10.1242/dev.125.8.1509.

M. Guo, J. Thomas, G. Collins, and M. C. Timmermans. Direct repression ofknoxloci by the asymmetric leaves1 complex ofarabidopsis . *The Plant Cell*, 20(1):48–58, Jan. 2008. ISSN 1532-298X. doi: 10.1105/tpc.107.056127.

W. D. Hamilton and R. M. May. Dispersal in stable habitats. *Nature*, 269(5629):578–581, Oct. 1977. ISSN 1476-4687. doi: 10.1038/269578a0.

A. Hay and M. Tsiantis. The genetic basis for differences in leaf form between arabidopsis thaliana and its wild relative cardamine hirsuta. *Nature Genetics*, 38(8):942–947, July 2006. ISSN 1546-1718. doi: 10.1038/ng1835.

Y. He, T. Zhang, H. Sun, H. Zhan, and Y. Zhao. A reporter for noninvasively monitoring gene expression and plant transformation. *Horticulture Research*, 7(1), Sept. 2020. ISSN 2052-7276. doi: 10.1038/s41438-020-00390-1.

H. Hofhuis and A. Hay. Explosive seed dispersal. *New Phytologist*, 216(2):339–342, mar 2017. doi: 10.1111/nph.14541.

H. Hofhuis, D. Moulton, T. Lessinnes, A.-L. Routier-Kierzkowska, R. J. Bomphrey, G. Mosca, H. Reinhardt, P. Sarchet, X. Gan, M. Tsiantis, Y. Ventikos, S. Walker, A. Goriely, R. Smith, and A. Hay. Morphomechanical innovation drives explosive seed dispersal. *Cell*, 166(1): 222–233, jun 2016. doi: 10.1016/j.cell.2016.05.002.

A. Y. Husbands, A. H. Benkovics, F. T. Nogueira, M. Lodha, and M. C. Timmermans. The asymmetric leaves complex employs multiple modes of regulation to affect adaxial-abaxial patterning and leaf complexity. *The Plant Cell*, 27(12):3321–3335, Nov. 2015. ISSN 1040-4651. doi: 10.1105/tpc.15.00454.

M. Ikezaki, M. Kojima, H. Sakakibara, S. Kojima, Y. Ueno, C. Machida, and Y. Machida. Genetic networks regulated byasymmetric leaves1(as1) andas2in leaf development inarabidopsis thaliana:knoxgenes control five morphological events. *The Plant Journal*, 61(1): 70–82, Jan. 2010. ISSN 1365-313X. doi: 10.1111/j.1365-313x.2009.04033.x.

G. V. James, V. Patel, K. J. Nordström, J. R. Klasen, P. A. Salomé, D. Weigel, and K. Schneeberger. User guide for mapping-by-sequencing in arabidopsis. *Genome Biology*, 14(6), June 2013. ISSN 1474-760X. doi: 10.1186/gb-2013-14-6-r61.

C. L. A. Kamei, B. Pieper, S. Laurent, M. Tsiantis, and P. Huijser. Crispr/cas9-mediated mutagenesis of rco in cardamine hirsuta. *Plants*, 9(2):268, Feb. 2020. ISSN 2223-7747. doi: 10.3390/plants9020268.

M. Khan, M. Xu, J. Murmu, P. Tabb, Y. Liu, K. Storey, S. M. McKim, C. J. Douglas, and S. R. Hepworth. Antagonistic interaction of blade-on-petiole1 and 2 with brevipedicellus and pennywise regulates arabidopsis inflorescence architecture . *Plant Physiology*, 158 (2):946–960, Nov. 2011. ISSN 1532-2548. doi: 10.1104/pp.111.188573.

D. Kim, J. M. Paggi, C. Park, C. Bennett, and S. L. Salzberg. Graph-based genome alignment and genotyping with hisat2 and hisat-genotype. *Nature Biotechnology*, 37(8):907–915, Aug. 2019. ISSN 1546-1696. doi: 10.1038/s41587-019-0201-4.

W.-C. Kim, J.-H. Ko, and K.-H. Han. Identification of a cis-acting regulatory motif recognized by myb46, a master transcriptional regulator of secondary wall biosynthesis. *Plant Molecular Biology*, 78(4–5):489–501, Jan. 2012. ISSN 1573-5028. doi: 10.1007/s11103-012-9880-7.

W.-C. Kim, J.-Y. Kim, J.-H. Ko, H. Kang, and K.-H. Han. Identification of direct targets of transcription factor myb46 provides insights into the transcriptional regulation of secondary wall biosynthesis. *Plant Molecular Biology*, 85(6):589–599, May 2014. ISSN 1573-5028. doi: 10.1007/s11103-014-0205-x.

J. Ko, W. Kim, and K. Han. Ectopic expression of myb46 identifies transcriptional regulatory genes involved in secondary wall biosynthesis in arabidopsis. *The Plant Journal*, 60(4): 649–665, Nov. 2009. ISSN 1365-313X. doi: 10.1111/j.1365-313x.2009.03989.x.

M. Kumar, L. Campbell, and S. Turner. Secondary cell walls: biosynthesis and manipulation. *Journal of Experimental Botany*, 67(2):515–531, Dec. 2015. ISSN 1460-2431. doi: 10.1093/jxb/erv533.

S. Kushwah, A. Banasiak, N. Nishikubo, M. Derba-Maceluch, M. Majda, S. Endo, V. Kumar, L. Gomez, A. Gorzsas, S. McQueen-Mason, J. Braam, B. Sundberg, and E. J. Mellerowicz. Arabidopsis xth4 and xth9 contribute to wood cell expansion and secondary wall formation. *Plant Physiology*, 182(4):1946–1965, Jan. 2020. ISSN 1532-2548. doi: 10.1104/pp.19.01529.

A. Lampropoulos, Z. Sutikovic, C. Wenzl, I. Maegele, J. U. Lohmann, and J. Forner. Greengate - a novel, versatile, and efficient cloning system for plant transgenesis. *PLoS ONE*, 8(12): e83043, Dec. 2013. ISSN 1932-6203. doi: 10.1371/journal.pone.0083043.

S. A. Levin, H. C. Muller-Landau, R. Nathan, and J. Chave. The ecology and evolution of seed dispersal: A theoretical perspective. *Annual Review of Ecology, Evolution, and Systematics*, 34(1):575–604, nov 2003. doi: 10.1146/annurev.ecolsys.34.011802.132428.

H. Li. A statistical framework for snp calling, mutation discovery, association mapping and

population genetical parameter estimation from sequencing data. *Bioinformatics*, 27(21): 2987–2993, Sept. 2011. ISSN 1367-4803. doi: 10.1093/bioinformatics/btr509.

D. Liebsch, W. Sunaryo, M. Holmlund, M. Norberg, J. Zhang, H. C. Hall, H. Helizon, X. Jin, Y. Helariutta, O. Nilsson, A. Polle, and U. Fischer. Class i knox transcription factors promote differentiation of cambial derivatives into xylem fibers in the arabidopsis hypocotyl. *Development*, 141(22):4311–4319, Nov. 2014. ISSN 0950-1991. doi: 10.1242/dev.111369.

S. J. Liljegren, A. H. Roeder, S. A. Kempin, K. Gremski, L. Østergaard, S. Guimil, D. K. Reyes, and M. F. Yanofsky. Control of fruit patterning in arabidopsis by indehiscent. *Cell*, 116(6): 843–853, Mar. 2004. ISSN 0092-8674. doi: 10.1016/s0092-8674(04)00217-x.

S. D. Lup, D. Wilson-Sánchez, S. Andreu-Sánchez, and J. L. Micol. Easymap: A user-friendly software package for rapid mapping-by-sequencing of point mutations and large insertions. *Frontiers in Plant Science*, 12, May 2021. ISSN 1664-462X. doi: 10.3389/fpls.2021.655286.

L. R. Lynd. The grand challenge of cellulosic biofuels. *Nature Biotechnology*, 35(10):912–915, Oct. 2017. ISSN 1546-1696. doi: 10.1038/nbt.3976.

M. Martin. Cutadapt removes adapter sequences from high-throughput sequencing reads. *EMBnet.journal*, 17(1):10, May 2011. ISSN 2226-6089. doi: 10.14806/ej.17.1.200.

R. L. McCarthy, R. Zhong, and Z.-H. Ye. Myb83 is a direct target of snd1 and acts redundantly with myb46 in the regulation of secondary cell wall biosynthesis in arabidopsis. *Plant and Cell Physiology*, 50(11):1950–1964, Oct. 2009. ISSN 1471-9053. doi: 10.1093/pcp/pcp139.

G. Mele, N. Ori, Y. Sato, and S. Hake. Theknotted1-like homeobox genebrevipedicellusregulates cell differentiation by modulating metabolic pathways. *Genes and Development*, 17 (17):2088–2093, Jan. 2003. ISSN 1549-5477. doi: 10.1101/gad.1120003.

M. Mesken and J. H. van der Veen. The problem of induced sterility: A comparison between ems and x-rays in arabidopsis thaliana. *Euphytica*, 17(3):363–370, Dec. 1968. ISSN 1573-5060. doi: 10.1007/bf00056237.

N. Mitsuda and M. Ohme-Takagi. Nac transcription factors nst1 and nst3 regulate pod shattering in a partially redundant manner by promoting secondary wall formation after the establishment of tissue identity. *The Plant Journal*, 56(5):768–778, Nov. 2008. ISSN 1365-313X. doi: 10.1111/j.1365-313x.2008.03633.x.

N. Mitsuda, M. Seki, K. Shinozaki, and M. Ohme-Takagi. The nac transcription factors nst1 and nst2 ofarabidopsisregulate secondary wall thickenings and are required for anther dehiscence. *The Plant Cell*, 17(11):2993–3006, Oct. 2005. ISSN 1532-298X. doi: 10.1105/tpc.105.036004.

N. Mitsuda, A. Iwase, H. Yamamoto, M. Yoshida, M. Seki, K. Shinozaki, and M. Ohme-Takagi. Nac transcription factors, nst1 and nst3, are key regulators of the formation of secondary walls in woody tissues ofarabidopsis. *The Plant Cell*, 19(1):270–280, Jan. 2007. ISSN 1532-298X. doi: 10.1105/tpc.106.047043.

G. Mosca, R. C. Eng, M. Adibi, S. Yoshida, B. Lane, L. Bergheim, G. Weber, R. S. Smith, and A. Hay. Growth and tension in explosive fruit. *Current Biology*, 34(5):1010–1022.e4, Mar. 2024. ISSN 0960-9822. doi: 10.1016/j.cub.2024.01.059.

G. Muese, T. Schindler, R. Bergfeld, K. Ruel, G. Jacquet, C. Lapierre, V. Speth, and P. Schopfer. Structure and distribution of lignin in primary and secondary cell walls of maize coleoptiles analyzed by chemical and immunological probes. *Planta*, 201(2):146–159, 1997. ISSN 1432-2048. doi: 10.1007/bf01007699.

S. Naseer, Y. Lee, C. Lapierre, R. Franke, C. Nawrath, and N. Geldner. Casparian strip diffusion barrier in arabidopsis is made of a lignin polymer without suberin. *Proceedings of the National Academy of Sciences*, 109(25):10101–10106, June 2012. ISSN 1091-6490. doi: 10.1073/pnas.1205726109.

R. Nathan. Long-distance dispersal of plants. *Science*, 313(5788):786–788, Aug. 2006. ISSN 1095-9203. doi: 10.1126/science.1124975.

M. M. Neff, E. Turk, and M. Kalishman. Web-based primer design for single nucleotide polymorphism analysis. *Trends in Genetics*, 18(12):613–615, Dec. 2002. ISSN 0168-9525. doi: 10.1016/s0168-9525(02)02820-2.

U. Neumann and A. Hay. Seed coat development in explosively dispersed seeds of cardamine hirsuta. *Annals of Botany*, 126(1):39–59, Dec. 2019. ISSN 1095-8290. doi: 10.1093/aob/mcz190.

N. Ori, Y. Eshed, G. Chuck, J. L. Bowman, and S. Hake. Mechanisms that control knox gene expression in the arabidopsis shoot. *Development*, 127(24):5523–5532, Dec. 2000. ISSN 1477-9129. doi: 10.1242/dev.127.24.5523.

A. R. Paredez, C. R. Somerville, and D. W. Ehrhardt. Visualization of cellulose synthase demonstrates functional association with microtubules. *Science*, 312(5779):1491–1495, June 2006. ISSN 1095-9203. doi: 10.1126/science.1126551.

M. L. Perkins, M. Schuetz, F. Unda, R. A. Smith, R. Sibout, N. J. Hoffmann, D. C. J. Wong, S. D. Castellarin, S. D. Mansfield, and L. Samuels. Dwarfism of high□monolignol arabidopsis plants is rescued by ectopic laccase overexpression. *Plant Direct*, 4(9), Sept. 2020. ISSN 2475-4455. doi: 10.1002/pld3.265.

M. L. Perkins, M. Schuetz, F. Unda, K. T. Chen, M. B. Bally, J. A. Kulkarni, Y. Yan, J. Pico, S. D. Castellarin, S. D. Mansfield, and A. L. Samuels. Monolignol export by diffusion down a polymerization-induced concentration gradient. *The Plant Cell*, 34(5):2080–2095, Feb. 2022. ISSN 1532-298X. doi: 10.1093/plcell/koac051.

M. W. Pfaffl. A new mathematical model for relative quantification in real-time rt-pcr. *Nucleic Acids Research*, 29(9):45e–445, May 2001. ISSN 1362-4962. doi: 10.1093/nar/29.9.e45.

L. Pijl. *Principles of dispersal in higher plants*. Springer, Berlin, 3. rev. and expanded ed. edition, 1982. ISBN 0387112804. Literaturverz. S. 188 - 199.

M. Pérez Antón. *Mechanism of localized lignindeposition in explosive fruit*. PhD thesis, University of Cologne, 2020.

M. Pérez-Antón, I. Schneider, P. Kroll, H. Hofhuis, S. Metzger, M. Pauly, and A. Hay. Explosive seed dispersal depends on spl7 to ensure sufficient copper for localized lignin deposition via laccases. *Proceedings of the National Academy of Sciences*, 119(24), June 2022. ISSN 1091-6490. doi: 10.1073/pnas.2202287119.

M. I. Rast-Somssich, S. Broholm, H. Jenkins, C. Canales, D. Vlad, M. Kwantes, G. Bilsborough, R. Dello Ioio, R. M. Ewing, P. Laufs, P. Huijser, C. Ohno, M. G. Heisler, A. Hay, and M. Tsiantis. Alternate wiring of a knoxi genetic network underlies differences in leaf development of a. thaliana and c. hirsuta. *Genes and Development*, 29(22):2391–2404, Nov. 2015. ISSN 1549-5477. doi: 10.1101/gad.269050.115.

R. Reiss, J. Ihssen, M. Richter, E. Eichhorn, B. Schilling, and L. Thöny-Meyer. Laccase versus laccase-like multi-copper oxidase: A comparative study of similar enzymes with diverse substrate spectra. *PLoS ONE*, 8(6):e65633, jun 2013. doi: 10.1371/journal.pone.0065633.

A. H. Roeder, C. Ferrándiz, and M. F. Yanofsky. The role of the replumless homeodomain protein in patterning the arabidopsis fruit. *Current Biology*, 13(18):1630–1635, Sept. 2003. ISSN 0960-9822. doi: 10.1016/j.cub.2003.08.027.

A. H. K. Roeder and M. F. Yanofsky. Fruit development in arabidopsis. *The Arabidopsis Book*, 4:e0075, Jan. 2006. ISSN 1543-8120. doi: 10.1199/tab.0075.

N. Rojas-Murcia, K. Hématy, Y. Lee, A. Emonet, R. Ursache, S. Fujita, D. De Bellis, and N. Geldner. High-order mutants reveal an essential requirement for peroxidases but not laccases in casparian strip lignification. *Proceedings of the National Academy of Sciences*, 117(46):29166–29177, Nov. 2020. ISSN 1091-6490. doi: 10.1073/pnas.2012728117.

S. Sakamoto, M. Somssich, M. T. Nakata, F. Unda, K. Atsuzawa, Y. Kaneko, T. Wang, A.-M. Bågman, A. Gaudinier, K. Yoshida, S. M. Brady, S. D. Mansfield, S. Persson, and

N. Mitsuda. Complete substitution of a secondary cell wall with a primary cell wall in arabidopsis. *Nature Plants*, 4(10):777–783, Oct. 2018. ISSN 2055-0278. doi: 10.1038/s41477-018-0260-4.

K. Schneeberger. Using next-generation sequencing to isolate mutant genes from forward genetic screens. *Nature Reviews Genetics*, 15(10):662–676, Aug. 2014. ISSN 1471-0064. doi: 10.1038/nrg3745.

S. Scofield, W. Dewitte, and J. A. Murray. Stm sustains stem cell function in thearabidopsisshoot apical meristem and controlsknoxgene expression independently of the transcriptional repressor as1. *Plant Signaling and Behavior*, 9(6):e28934, Apr. 2014. ISSN 1559-2324. doi: 10.4161/psb.28934.

T. L. Shimada, T. Shimada, and I. Hara-Nishimura. A rapid and non-destructive screenable marker, FAST, for identifying transformed seeds ofArabidopsis thaliana. *The Plant Journal*, 61(3):519–528, feb 2010. doi: 10.1111/j.1365-313x.2009.04060.x.

H. M. S. Smith and S. Hake. The interaction of two homeobox genes, brevipedicellus and pennywise, regulates internode patterning in the arabidopsis inflorescence. *The Plant Cell*, 15(8):1717–1727, July 2003. ISSN 1532-298X. doi: 10.1105/tpc.012856.

M. Snyman, T. V. Huynh, M. T. Smith, and S. Xu. The genome-wide rate and spectrum of ems-induced heritable mutations in the microcrustacean daphnia: on the prospect of forward genetics. *Heredity*, 127(6):535–545, Oct. 2021. ISSN 1365-2540. doi: 10.1038/s41437-021-00478-x.

M. Stemmer, T. Thumberger, M. del Sol Keyer, J. Wittbrodt, and J. L. Mateo. Cctop: An intuitive, flexible and reliable crispr/cas9 target prediction tool. *PLOS ONE*, 10(4):e0124633, Apr. 2015. ISSN 1932-6203. doi: 10.1371/journal.pone.0124633.

Synthego. Ice analysis. URL https://ice.synthego.com/#/.

Y. Takenaka, Y. Watanabe, M. Schuetz, F. Unda, J. L. Hill, P. Phookaew, A. Yoneda, S. D. Mansfield, L. Samuels, M. Ohtani, and T. Demura. Patterned deposition of xylan and lignin is independent from that of the secondary wall cellulose of arabidopsis xylem vessels. *The Plant Cell*, 30(11):2663–2676, Oct. 2018. ISSN 1532-298X. doi: 10.1105/tpc.18.00292.

M. Taylor-Teeples, L. Lin, M. de Lucas, G. Turco, T. W. Toal, A. Gaudinier, N. F. Young, G. M. Trabucco, M. T. Veling, R. Lamothe, P. P. Handakumbura, G. Xiong, C. Wang, J. Corwin, A. Tsoukalas, L. Zhang, D. Ware, M. Pauly, D. J. Kliebenstein, K. Dehesh, I. Tagkopoulos, G. Breton, J. L. Pruneda-Paz, S. E. Ahnert, S. A. Kay, S. P. Hazen, and S. M. Brady. An arabidopsis gene regulatory network for secondary cell wall synthesis. *Nature*, 517(7536): 571–575, Dec. 2014. ISSN 1476-4687. doi: 10.1038/nature14099.

R. Ursache, T. G. Andersen, P. Marhavý, and N. Geldner. A protocol for combining fluorescent proteins with histological stains for diverse cell wall components. *The Plant Journal*, 93(2): 399–412, Jan. 2018. ISSN 1365-313X. doi: 10.1111/tpj.13784.

S. P. Venglat, T. Dumonceaux, K. Rozwadowski, L. Parnell, V. Babic, W. Keller, R. Martienssen, G. Selvaraj, and R. Datla. The homeobox gene brevipedicellus is a key regulator of inflorescence architecture in arabidopsis. *Proceedings of the National Academy of Sciences*, 99(7):4730–4735, Mar. 2002. ISSN 1091-6490. doi: 10.1073/pnas.072626099.

Z.-P. Wang, H.-L. Xing, L. Dong, H.-Y. Zhang, C.-Y. Han, X.-C. Wang, and Q.-J. Chen. Egg cell-specific promoter-controlled crispr/cas9 efficiently generates homozygous mutants for multiple target genes in arabidopsis in a single generation. *Genome Biology*, 16(1), July 2015. ISSN 1474-760X. doi: 10.1186/s13059-015-0715-0.

Y. Watanabe, M. J. Meents, L. M. McDonnell, S. Barkwill, A. Sampathkumar, H. N. Cartwright, T. Demura, D. W. Ehrhardt, A. Samuels, and S. D. Mansfield. Visualization of cellulose synthases in arabidopsis secondary cell walls. *Science*, 350(6257):198–203, Oct. 2015. ISSN 1095-9203. doi: 10.1126/science.aac7446.

N. Woerlen, G. Allam, A. Popescu, L. Corrigan, V. Pautot, and S. R. Hepworth. Repression

of blade-on-petiole genes by knox homeodomain protein brevipedicellus is essential for differentiation of secondary xylem in arabidopsis root. *Planta*, 245(6):1079–1090, Feb. 2017. ISSN 1432-2048. doi: 10.1007/s00425-017-2663-2.

L. Xu, Y. Xu, A. Dong, Y. Sun, L. Pi, Y. Xu, and H. Huang. Novelas1andas2defects in leaf adaxial-abaxial polarity reveal the requirement forasymmetric leaves1and2anderectafunctions in specifying leaf adaxial identity. *Development*, 130(17): 4097–4107, Sept. 2003. ISSN 0950-1991. doi: 10.1242/dev.00622.

G. Yu, L.-G. Wang, Y. Han, and Q.-Y. He. clusterprofiler: an r package for comparing biological themes among gene clusters. *OMICS: A Journal of Integrative Biology*, 16(5):284–287, May 2012. ISSN 1557-8100. doi: 10.1089/omi.2011.0118.

Q. Zhao, J. Nakashima, F. Chen, Y. Yin, C. Fu, J. Yun, H. Shao, X. Wang, Z.-Y. Wang, and R. A. Dixon. LACCASE is necessary and nonredundant with PEROXIDASE for lignin polymerization during vascular development in arabidopsis. *The Plant Cell*, 25(10):3976–3987, oct 2013. doi: 10.1105/tpc.113.117770.

R. Zhong, E. A. Richardson, and Z.-H. Ye. The myb46 transcription factor is a direct target of snd1 and regulates secondary wall biosynthesis in arabidopsis. *The Plant Cell*, 19(9): 2776–2792, Sept. 2007. ISSN 1532-298X. doi: 10.1105/tpc.107.053678.

List of Abbreviations

A. thaliana	*Arabidopsis thaliana*
AS1/2	ASYMMETRIC LEAVES1/2
bHLH	basic helix-loop-helix
BP	BREVIPEDICELLUS
bp	base pair
CAPS	cleaved amplified polymorphic sequences
CESA4/7/8	cellulose synthase 4/7/8
C. hirsuta	*Cardamine hirsuta*
CDS	coding sequence
CLSM	Confocal laser scanning microscropy
cM	centi Morgan
DEG	differentially expressed genes
DNA	desoxyribonucleic acid
EMS	ethyl methanesulfonate
FAST	fluorescence-accumulating seed technology
FUL	FRUITFULL
F1, F2	generation of crossed seed
GFP	green fluorescent protein
GO	gene ontology
IND	INDEHISCENT

indel	Insertion-Deletion
KNOX	Knotted1-like homeobox
KNAT2/6	KNOTTED1-LIKE in ARABIDOPSIS THALIANA 2/6
LAC4/11/17	LACCASE4/11/17
Mb	Mega base
ML	monolignols
MYB46	MYB DOMAIN PROTEIN 46
M1, M2	generation of mutagenized seed
NST1/3	NAC SECONDARY WALL THICKENING PROMOTING FACTOR 1/3
PAM	Protospacer adjacent motif
pat	*lignin pattern*
PCR	Polymerase chain reaction
PCW	primary cell wall
PCA	principal component analysis
RNA	ribonucleic acid
RNA-seq	RNA sequencing
RPL	REPLUMLESS
SAM	shoot apical meristem
SCW	secondary cell wall
SEM	scanning electron microscopy

sgRNA	single guide RNA
SHP1/2	SHATTERPROOF1/2
SNPs	single nucleotide polymorphisms
SPL7	SQUAMOSA promoter binding protein-like 7
T1, T2	generation of transformed seed
VND6/7	VASCULAR-RELATED NAC-DOMAIN PROTEIN 6/7
WT	wild type

Declaration

Erklärung zur Dissertation

gemäß der Promotionsordnung vom 12. März 2020

„Hiermit versichere ich an Eides statt, dass ich die vorliegende Dissertation selbstständig und ohne die Benutzung anderer als der angegebenen Hilfsmittel und Literatur angefertigt habe. Alle Stellen, die wörtlich oder sinngemäß aus veröffentlichten und nicht veröffentlichten Werken dem Wortlaut oder dem Sinn nach entnommen wurden, sind als solche kenntlich gemacht. Ich versichere an Eides statt, dass diese Dissertation noch keiner anderen Fakultät oder Universität zur Prüfung vorgelegen hat; dass sie - abgesehen von unten angegebenen Teilpublikationen und eingebundenen Artikeln und Manuskripten - noch nicht veröffentlicht worden ist sowie, dass ich eine Veröffentlichung der Dissertation vor Abschluss der Promotion nicht ohne Genehmigung des Promotionsausschusses vornehmen werde. Die Bestimmungen dieser Ordnung sind mir bekannt. Darüber hinaus erkläre ich hiermit, dass ich die Ordnung zur Sicherung guter wissenschaftlicher Praxis und zum Umgang mit wissenschaftlichem Fehlverhalten der Universität zu Köln gelesen und sie bei der Durchführung der Dissertation zugrundeliegenden Arbeiten und der schriftlich verfassten Dissertation beachtet habe und verpflichte mich hiermit, die dort genannten Vorgaben bei allen wissenschaftlichen Tätigkeiten zu beachten und umzusetzen. Ich versichere, dass die eingereichte elektronische Fassung der eingereichten Druckfassung vollständig entspricht."

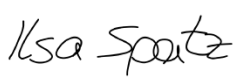

Köln, 01.07.2024, Ilsa Spatz